TABLE OF CONTENTS

LIST OF FIGURES

LIST OF TABLES

Chapter 1   Introduction

1.1 Analog fiber-optic link

Optical communication systems have been the mainstream information transmission system in past decades and are still dominant today thanks to the invention and development of broad band semiconductor lasers, low loss fibers, fast photodetectors and other high quality optoelectronic components. The fiber-optic link has many advantages which include tremendous available bandwidth (~200 THz), very low transmission loss and immunity to electrical disturbance etc; all of this makes a fiber-optic link the preferred transmission solution in many applications [1].

The digital fiber-optic link has a major role in present optical communication systems. Fiber optic transmission of digital data for long haul and metro access is widely used in the communication industry. Normally, in a digital transmission system, the signal is sampled and digitized first, then the digital format signal is transmitted via a series of optical pulses in which the high and low power levels represent either the number 1 or 0. However, RF or microwave signals often need to be transmitted, distributed and processed directly without going through the costly digital encoding process. The analog optical transmission system aims to reproduce an identical version of the input signal at the output. Since the original type of any signal is actually an analog signal, it is often more cost efficient to transmit the data in its native format. Additionally, the analog

optical link offers more bandwidth efficiency and thus allows a higher data transmission rate [2].

In Fig 1.1, a typical analog fiber-optic link diagram is shown, which is similar to a traditional analog microwave transmission system in terms of the input and output ends. It contains a modulated optical source at the sending end, which is modulated in an analog manner. The optical fiber provides a transmission medium in which the modulated optical signals can be transmitted and distributed. These modulated optical signals are detected and demodulated at the receiving end to recover the RF signals.

One important application of the analog optical link technique is in commercial communication systems such as cable-TV video distribution [3]. Older cable TV system use a long cascade of electronic amplifiers that result in noise build-up and poor reception near the fringes of the system coverage. Since the optical loss for fibers is very low, analog fiber-optic links can provide the low cost network for distribution of RF signals to
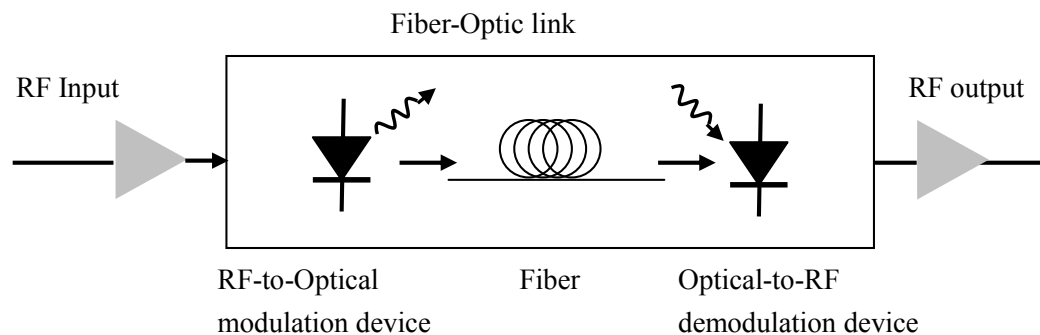
Fig. 1.1 The schematic of basic components of a analog fiber-optic link.

end users by decreasing the number of electronic repeaters. An RF signal is directly distributed from a system head to local neighborhoods via a star configuration of fiber optic cables. Then the signal is converted back to analog electronics over a conventional coaxial cable and delivered to end subscribers.

In the high frequency regime, an analog fiber-optic link offers an attractive alternative to electrical systems too. The traditional microwave and millimeter wave transmission systems, using coaxial cables and metallic waveguides, have extremely large attenuation and consequently, are complex and expensive. Conversely optical fibers have a small size, low weight, and more importantly, are immune to electromagnetic interference such as lighting and electrical charges. Applications of analog optical links include the up-link cellular remote antenna and phased array radar system [4]. By using fiber as a transmission waveguide, both the design of new sites, and physical expansion of the network are much easier. This technique, also referred as fiber-to-the-antenna (FTTA) is employed by the wireless communication company to replace the coaxial cable between the radio base station (RBS) and the antenna. Additionally, an available 200 THz bandwidth of optical fiber also offers an advantage. It is easy to mix traffic in the same fiber by allocating different sub-carriers to different traffic. The analog video signal and data transmission can all be carried on the same fiber. A dense wavelength division multiplexed (DWDM) analog fiber-optic system was demonstrated that distributes RF over fiber up to 3 GHz. This system can provide new services such as PCS, broad band wireless internet and digital video [5].

1.2 Optical transmitter

The optical transmitter is one of the most researched subjects in fiber optical communications. To enhance the transmission capability of a fiber-optic link, a high performance optical source or transmitter is required.   The characteristics of the transmitter often determine the maximum length of a fiber link and the data rate that is achievable. The main component of a transmitter is a semiconductor diode laser (LD). In present fiber-optic link systems, the typical operation wavelength of the semiconductor laser is 1310 nm and 1550 nm, which correspond to the dispersion and absorption minimum of optical fibers, respectively. The RF (10KHz-300MHz) and microwave (300 MHz to 300 GHz) signals can be modulated on to the laser. Analog modulation optical

Direct modulation   External modulation
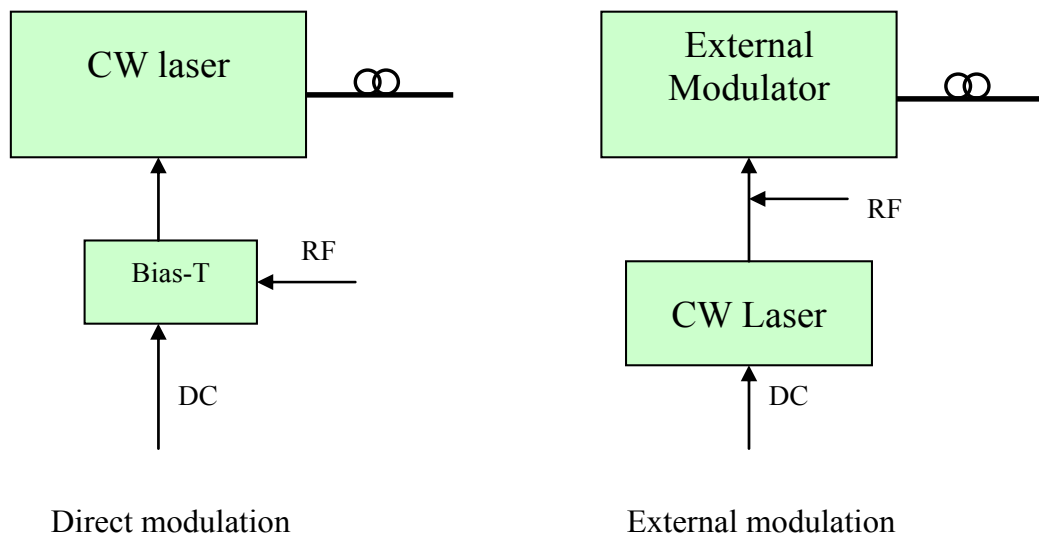
Fig. 1.2 Illustration of (a) direct and (b) external modulation of transmitter in fiber-optic links

transmitters can be achieved either by using an external modulator or by direct modulation of the semiconductor laser [6]. In Fig 1.2, the diagram of direct and external modulation in a fiber-optic link is shown.

Direct modulation can be realized by directly varying the laser drive current with the information signal to produce a varying optical output power. The system is relatively simple and low cost. When using a directly modulated laser diode for a high-speed transmission system, the modulation frequency can not be larger than the relaxation frequency of the laser, which is a function of both the stimulated lifetime and the photon lifetime. Moreover, analog modulation of a laser diodes is carried out by making the drive current above threshold proportional to the information signal, so a linear relation between the light output and the current input is required, but this linear relation cannot be achieved in semiconductor lasers. The intrinsic non-linear coupling between an electron and photon of semiconductor lasers results in undesired signal degradation. Another limitation on direct modulation laser diodes is the electron-photon conversion efficiency [7]. Typical values for end-to-end RF loss are in the range of -20 dB to -30 dB due principally to the efficiency of RF-light conversion. An electrical amplifier is usually used to compensate for loss and boost the signal-to-noise ratio for weak signals.

The limitations of direct modulation described above can be overcome by external modulation. The external modulator, which can either be a separate device or an integral part of the package, has high linearity, high optical power, low chirp and low noise. However, it also suffers from high cost and power consumption. In this work, We will

focus on improving the modulation bandwidth and efficiency of directly modulated low dimensional confined semiconductor lasers, called quantum dot (QD) lasers. In the next section, the development and current status of QDs will be reviewed first.

1.3 Introduction to quantum dot or dash semiconductor lasers

1.3.1 A Brief History of Quantum Dot Semiconductor Lasers

The first successful semiconductor lasers with GaAs and GaAsP alloys were demonstrated by several groups in 1962 [8, 9]. These lasers were homostructure devices that had no any carrier confinement mechanism and could only be operated under pulse conditions and very low temperature. With the development of new growth and processing techniques, the performance of semiconductor laser has been improved significantly over the past forty years. In one of the revolutionary steps, heterostructure lasers were demonstrated by Alferov and Hayashiand *et. al* in the late 60s and 70s [10, 11, 12, 13]. The threshold current density was dramatically reduced from more than 10^4 A/cm^2 to the order of $10^2 \sim 10^3$ A/cm^2 by applying a layer of one semiconductor material (active layer) sandwiched between two layers of another material that has a wider band gap. The large-scale commercial application of laser diodes became possible since then.

As the thickness of active layer drops below 10 nm, the distribution of available energy states for electrons and holes confined in the active layer changes from quasi-continuous to discrete. This is the so called quantum effect. The idea that the quantum effect could be used in semiconductor lasers was first suggested by Henry and

Dingle in early 1975 [14]. It wasn't until the late 1970s and early 1980s that Dupuis and

Tsang *et. al*. demonstrated the earliest quantum well (QW) lasers grown by metal-organic

chemical vapor deposition (MOCVD) and molecular-beam epitaxy (MBE) techniques,

respectively [15, 16].   Over the past twenty years, QW lasers have been fully developed

with further threshold current reduction and larger power range coverage. Quantum size

effect also can be used to change the energy gap in order to cover a wider wavelength

range (from visible to IR) by varying III-V alloy composition and QW thickness. [17, 18,

19]. The success of QW lasers inspired more efforts to explore semiconductor materials

with multi-dimensional carrier confinement. Quantum dots (QD) are the semiconductor

nanostructures that act as artificial atoms by confining electrons and holes in three

dimensions. Arakawa and Asada *et. al* [20, 21] predicted in the early 1980s that QD

lasers should exhibit performance that is less temperature-dependent and has less

threshold current density than existing semiconductor lasers. These theoretical models

were based on lattice-matched heterostructures and an equilibrium carrier distribution.

However, the challenge in realizing quantum dot lasers with superior operation to that

shown by quantum well lasers is that of forming high quality, uniform quantum dots in

the active layer. Initially, the most widely followed approach to forming quantum dots

was through electron beam lithography of suitably small featured patterns (~300 Å) and

subsequent dry-etch transfer of dots into the substrate material. The problem that plagued

these quantum dot arrays was their exceedingly low optical efficiency: high

surface-to-volume ratios of these nanostructures and associated high surface

recombination rates, together with damage introduced during the fabrication itself, precluded the successful formation of a quantum dot laser. The best quantum-box laser, developed with *lattice-matched* heterostructures, demonstrated laser operation with an unpractical threshold current density of 7.5 kA cm^2 in pulsed operation at a low temperature of only 77K [22]. At the beginning of the 1990s, it was realized that the strain relaxation on step or facet edges may result in the formation of high density and ordered arrays of quantum dots for lattice-mismatched materials [23, 24, 25]. The first self-assembled QD laser was demonstrated in 1994, with fully quantized energy levels in both bands and a strongly inhomogeneous broadened gain spectrum [26]. Since then the field has seen steady progress, the performance of self-assembled QD lasers have now reached or surpassed those of the well-established quantum-well lasers. [27, 28, 29]

1.3.2. Epitaxy and quantum dot formation

Self-assembled QD growth is realized from lattice mismatched combinations of semiconductor materials and the most common mode used for growth is the Stranski-Krastanow (S-K) mode. If the deposited semiconductor is slightly mismatched to the substrate, the deposited film will be strained, so that its in-plane lattice constant fits the lattice constant of the substrate. Growth will continue pseudomorphically until the accumulated elastic strain energy is high enough to form dislocations. In S-K mode, the growth of a pseudomorphic 2D layer is followed by reorganization of the surface material in which 3D islands are formed. Fig 1.3 is an illustration of 2-D wetting layer and 3-D

island formation in S-K mode that is responsible for forming the InAs QDs on a GaAs substrate.

InAs Deposition

GaAs substrate

Wetting layer ~ 1.0 monolayer

GaAs substrate

Dot nucleation ~1.5 monolayer

50-100 nm spacing

15-20 nm

GaAs substrate

Fully formed dots ~2.0-2.5 monolayer
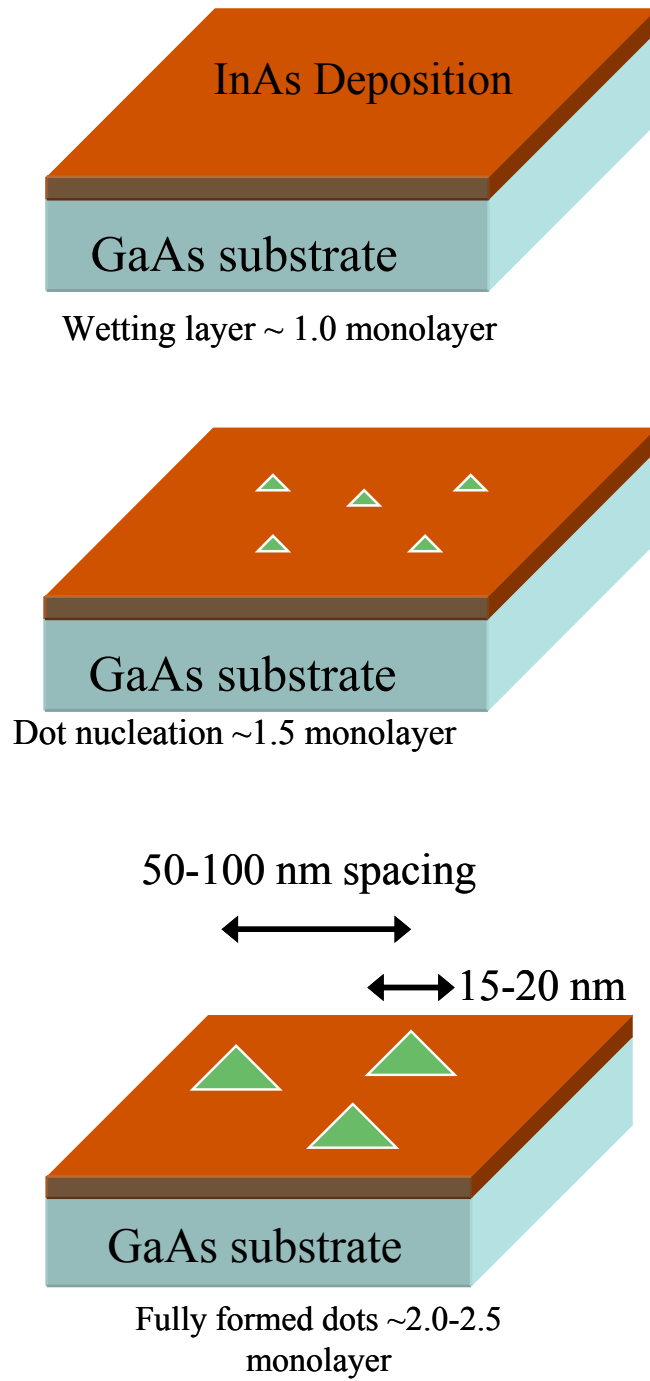
Figure 1.3 Self-assembly growth technique for InAs quantum dots by S-K mode

1.3.3 Quantum Dot Advantages

Due to the three dimensional confinement of the carriers in QDs with dimensions comparable to or below the exciton's Bohr radius, the density of states consists of a series of atomic-like delta functions, which lays the foundation upon which many QD advantages are built. Fig. 1.4 illustrates the density of states functions for bulk, quantum well, quantum wire, and quantum dot active regions. For QDs, the state density is a δ-function in energy, which is dramatically different from either bulk (continuous) or QW (step function). For the real QD materials, the density of states has a line broadening caused by fluctuations in the quantum dot sizes. The fundamental advantages of QD lasers include an ultra-low threshold current, temperature-insensitive operation, high material gain and differential gain, a decreased linewidth enhancement factor, an ultra-broad bandwidth, easily saturated gain and absorption, and a larger tuning range of the lasing wavelength.

Ultra-low threshold current   A reduction in the threshold current density can be attributed to the small scaling of the active region and reduced density of states. There is less material to populate with electron-hole pairs in order to establish population inversion. Also the atom-like density of states function leads to lower transparency current because the number of noncontributing lower energy states that need to be filled is further reduced [30, 31]. In 1999, Liu *et. al* demonstrated the QD laser with threshold current density of 26 A/cm^2 using a dots-in-a-well (DWELL) structure [32]. The

threshold current density below 20A/cm^2 is demonstrated by Park *et. al.* [33].
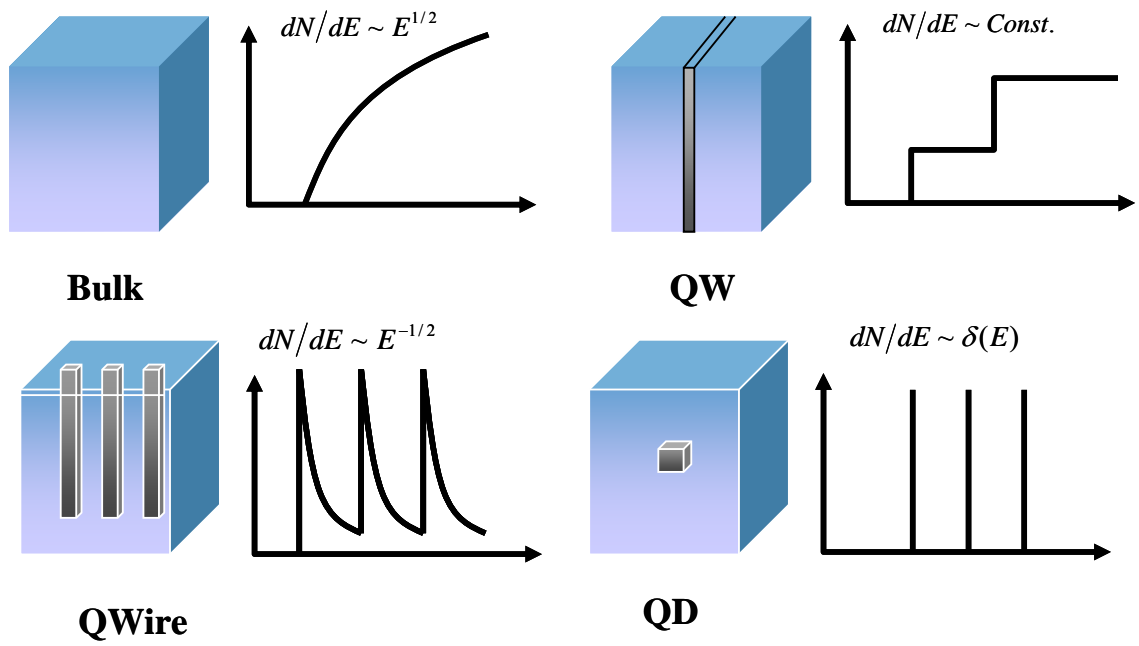
Fig. 1.4 The density of states functions for bulk, quantum well, quantum wire, and quantum dot active regions.

Temperature insensitive threshold, high T_0 Due to their well separated energy levels, the QD laser is expected to be operated with high characteristic temperature T_0. However, this has been achieved only in narrow temperature ranges and typically below room temperature [26, 34]. The P-type doping technique in the QD active region was proposed by Shchekin and Deppe to compensate the closely spaced hole levels. Using this approach, an InAs/GaAs QD laser in the 1310 nm range with 213 K T_0 and an InAs/InP 1500 nm QD laser with 210 K T_0 have been reported [35, 36] separately. A value of T_0=363K at room temperature is realized by tunnel injection QD lasers at a wavelength of 980 nm [37].

Small linewidth enhancement factor The symmetry inherent in the QD density of states function is manifested by the symmetry in the gain spectrum, which is important because it predicts that the zero dispersion point of refractive index aligns with the gain peak. The resulting benefit is that the linewidth enhancement factor (LEF), which is a key parameter in the characterization of semiconductor lasers, is predicted to be zero, leading to chirp-free operation. The common ways used to measure LEF are based on the analysis of the amplified spontaneous emission (ASE) [38], on the FM/AM response ratio under small signal current modulation [39] and pump-probe experiments [40]. The published value of LEF can vary a significant amount depending on which measurement techniques are used. Experiments have reported a great variety of values for the LEF ranging from 0 to 50 [38, 41-43].

Easily saturated gain and absorption Due to the limited number of available

states, the gain of QD lasers is easily saturated by increasing the number of injected carriers. These characteristics result in QDs being an ideal material system for mode-locked lasers (MLL) and super-luminescent light emitting diodes (SLEDs) [44 ,45]. The strong gain saturation with carrier density is also the main motivation to explore gain-lever effect using QD materials, which will be discussed in Chapter 3.

1.4 Improving modulation performance of QD lasers

1.4.1 p-doped QD lasers

The QD lasers have generally been demonstrated with the performance over or matching those of QW devices. However, there has always been some theoretical question about the ultimate high-speed performance of direct-modulation QD lasers. First, the inhomogenous linewidth, associated with an approximately 10% inhomogeneity in size and fluctuation in shape and composition broadening, severely limits the performance of QD lasers. Second, the capture/relaxation time of carriers in QD's is predicted to be much longer than in QW's because of the "phonon bottleneck" effect. The excited and ground states are not typically separated by phonon energies, thus only multi-phonon assisted relaxation events are permitted, which are typically much slower [46]. Even though some fast mechanisms were proposed, such as electron-hole scattering [47] and Auger process [48], and it has been proven that the "phonon bottleneck" effect is not significant at room temperature and high current bias condition, $1 - 10$ ps phonon-scattering relaxation time

still hinders the high-speed modulation of QD lasers. The third limitation is contributed to the so called "hot carrier" effect. In the self-assembled QDs grown by S-K mode, the number of wetting layer/barrier states is much larger than the number of available dot states, thus the injected electrons predominantly reside in the wetting layer and barrier states. The relaxation process from the 2-D wetting layer states to the lasing state in QDs is very slow [49]. The reduction of the electron-hole scattering rate and wetting layer carrier occupation leads to severe gain saturation and limits the achievable modulation bandwidth of QD lasers. Two techniques have been proposed to overcome the hot carrier effect: tunneling injection (TI) [50] and p-doping in the QD active medium [51].In the tunneling injection scheme, "cold" electrons are injected into the ground state of the QD by direct or phonon-assisted tunneling from an adjacent QW layer. Since the injection rate is comparable with the stimulated recombination rate, a quasi-Fermi distribution of carriers can be maintained. The p-doping technique is based on the theory that the hole levels are closely spaced in energy so that there is a thermal broadening of the hole's distribution amongst the many available states. This thermal broadening results in the depletion of the ground state hole distribution at elevated temperatures. The p-doped layer act as a supplier of extra holes, thus, the hole population in the ground state is compensated with fewer injected electron-hole pairs from the electrical contact. However, even though a slight bandwidth enhancement is reported by p-doped QD lasers over the un-doped conventional QD lasers [52], the prediction has not yet been shown as pointed out in Ref [49].

1.4.2 Gain-lever effect

As we discussed in section 1, one of the limitations of directly-modulated lasers in analog fiber optic links is low efficiency of the electron-photon conversion. The typical values for end-to-end RF loss are in the range -20 dB to -30 dB, which means much higher microwave power is required for full optical modulation [53, 54]. An additional electrical amplifier may be needed for signal boost, and system cost will increase as well. Therefore, improving modulation efficiency of lasers is a key to reducing the link loss in fiber-optic systems. The two-section laser based on the gain-lever effect was proposed in the late 1980s to accomplish high modulation efficiency in intensity modulation (IM) and frequency modulation (FM), and even broad wavelength tunability [54-56]. The gain-lever effect is based on the sublinear relationship between gain and carrier density in semiconductor lasers. A gain lever laser consists of two electrically isolated sections, which are biased asymmetrically. One section is biased at a low gain level and is RF modulated. Another section is biased at a high gain level. When the device is biased above threshold, the sum of the gain of two sections is clamped at a constant value. If one section increases in optical gain by increasing the bias, the gain of the other section must be decreased to keep the total gain of two sections constant. Correspondingly, the differential gains of the two sections are different under this asymmetrically biased condition. In the normal gain lever case, since the modulation efficiency enhancement is proportional to the ratio of the differential gains of the two sections, the operation point

should be chosen where the differential gain of the modulation section is larger than that of gain section. The idea of the gain lever effect was first proposed by Vahala *et. al.* in 1989 [57]. Subsequently, the gain-lever effect was applied to both the ridge waveguide and distributed feedback (DFB) QW lasers. A 22 dB modulation efficiency enhancement was demonstrated by Moore and Lau using an electrically-pumped two-section QW laser [54]. By interchanging the bias points of the two sections of the gain-lever laser, the inverted gain-lever laser showed 22 GHz/mA FM efficiency [55]. The gain-lever effect also can be used in DFB lasers to improve the tuning behavior and obtain better control of the power-current relations [58]. However, the existing literature only explored QW gain-lever devices and lacks discussion on the possibility of bandwidth enhancement using the gain-lever laser. Due to the delta-function like density of states, QD lasers, which have stronger gain saturation characteristic and larger differential gain, are expected to demonstrate a bigger gain-lever effect. The modulation efficiency and bandwidth enhancement brought by gain-lever QD lasers will be presented in this work.

1.4.3 The injection-locked laser

For analog fiber-optic transmissions, the application of injection-locked lasers has been demonstrated in radio-over-fiber [59], mm-wave generation [60] and optical switching [61]. An optical injection-locking system consists of two sources, which are usually called a master and slave laser. The output light from the master laser, which is

typically a narrow linewidth DFB laser, is injected into the slave laser. When the optical frequencies of the two lasers are close enough, the phase locking phenomenon can occur. The CW operation behavior and modulation characteristic of the slave laser can be significantly changed such as reduced linewidth, enhanced relaxation frequency and modulation bandwidth, suppressed mode hopping, reduced chirp and relative intensity noise. The research on injection-locking between two semiconductor lasers was launched by Kobayashi *et al.* in the early 1980s [62]. Since then, many advantages of injection-locked lasers have been demonstrated including modulation bandwidth enhancement, chirp reduction, nonlinear distortion reduction, and relative intensity noise reduction [63-66]. The 2.7X bandwidth enhancement was reported using a 1550 nm VCSEL as a slave laser [65]. Jin *et. al* demonstrated bandwidth enhancement on injection-locked Fabry-Perot (F-P) QW lasers [66].

In this work, the analog modulation characteristics of injection-locked quantum dash lasers are discussed for the first time. It is realized that both the gain-lever and injection locking lasers are actually a coupled oscillator system and share the same frequency response function under certain assumptions. A clearer physical view of the modulation characteristics of the injection-locked laser is provided, which has been blurred previously by a complicated set of fitting parameters in the frequency response function.

1.5 Organization of dissertation

This dissertation describes the direct modulation characteristics of single and two-section QD lasers and injection-locked quantum dash lasers.

Chapter 2 discusses the static performance and modulation frequency response of un-doped and p-doped InAs/GaAs QD lasers with different doping levels. It is shown that p-doping in the QD active region increases not only the ground state gain, but also the internal loss. The undesired increase in internal losses induces gain saturation and gain compression, thus degrading the high-speed performance of p-doped QD lasers. We found that the modulation bandwidth and relaxation frequency decrease monotonically with the p-doping level.

In chapter 3, the modulation response of gain-lever quantum dot lasers will be studied. The modulation efficiency enhancement, which is desired for analog fiber optic links, was achieved by taking advantage of the gain-lever effect in both p-doped and un-doped QD lasers with a two-section configuration. Due to the stronger gain saturation, the un-doped device shows a higher gain-lever effect over the p-doped device. The new relative response function was derived under the high photon density approximation. A 1.7X 3-dB bandwidth improvement is theoretically predicted by the new model and realized in un-doped QD gain-lever laser.   It is also demonstrated for the first time that in gain-lever lasers, the 3-dB bandwidth can be 3X higher than the relaxation frequency instead of 1.55X in typical single section lasers.

Chapter 4 describes the modulation characteristics of injection-locked F-P quantum dash lasers. The bandwidth enhancement is observed by varying the injection power and changing the detuning. It is found that the side mode locking variation has no significant impact on modulation response so that the power injection ratio should refer to the total slave power, not the individual modes. The new finding in this chapter is a new equation to describe the modulation response of the injection-locked laser, which is inspired by the gain lever model under high photon density approximation. The two key parameters for injection-locked laser: the frequency detuning and injection power ratio are included in a single parameter in the gain-lever model which represents the effective damping rate of the master laser. The analytical expression of the relaxation frequency is derived too. The maximum achievable 3-dB bandwidth at a certain power level is predicted for the first time.

References

[1] G. P. Agrawal, "Fiber-optical Communication Systems", 3rd edition, John Wiley & Sons, New York, 2002.

[2] S. C. Chang, "RF Photonic Technology in Optical Fiber Links", 1st edition, Cambridge University Press, pp. XV-1, 2002

[3] T. E. Darcie, G. E. Bodeep, " Lightwave Subcarrier CATV Transimission Systems", *IEEE Trans. Microwave Theory and Techniques*, vol. 38 (5), pp.524-533, 1990

[4] C. H. Cox, "Analog Fiber-Optic links with Intrinsic Gain". *Microwave Journal*, vol. 35, no. 9, pp. 90-93, 1992

[5] A. Paolella, K. Lafond, J. Borlando, M. Aviles, "Dense wavelength division multiplexing photonic transport for wireless access systems", *Optical Fiber Communication Conference and Exhibit*, vol. 17, no. 22, pp. 768-769, 2002

[6] A. Yariv, "Optical Electronics", *3rd Edition, Holt Saunders*, 1985.

[7] C. H. Cox, G. E. Betts, and L. M. Johnson, "An analytic and experimental comparison of direct and external modulation in analog fiber-optic links," *IEEE Trans. Microwave Theory Tech.,* vol. 38, pp. 501-509, 1990.

[8] N. R. Hall, G. E. Fenner, J. D. Kingsley, T. J. Soltys, and R. O. Carlson. "Coherent Light Emission From GaAs Junctions". *Physical Review Letters*, vol 9, no 9, pp. 366–369, 1962.

[9] N. Holonyak, Jr. and S. F. Bevacqua, "Coherent (visible) light emission from Ga(As$_{1-x}$P$_x$) junctions", *Appl. Phys. Lett.*, vol 82, no. 1, 1962.

[10] Z. I. Alferov, V. M. Andreev, V. I. Korol'kov, E. L. Portnoi, and D.N. Tret'yakov, "Injection properties of n-Al Ga As-p-GaAs hetero-junctions", *Fiz. Tekh. Poluprovodn.*, vol. 2, pp. 1016 1017, 1968. *Sov.Phys.-Semicond.*, vol. 2, p. 843-844, 1969.

[11] Z. I. Alferov, V. M. Andreev, D. Z. Garbuzov, Yu. V. Zhilyaev, E. P. Morozov, E. L. Portnoi, and V. G. Trofim, "Effect of heterostructure parameters on the laser threshold current and the realization of continuous generation at room temperature," *Sov. Phys. Semicond.,* vol 4, pp. 1573-1575, 1970

[12] I. Hayashi, M. B. Panish, P. W. Foy and S. Sumski, " Junction lasers which operate continuously at room temperature," *Appl. Phys. Lett.,* vol. 17, pp. 109-111, 1970

[13] R. D. Dupuis, and P. D. Dapkus, "Very low threshold Ga$_{1-x}$Al$_x$As-GaAs double-heterostructure lasers grown by metalorganic chemical vapor deposition," *Appl. Phys. Lett.,* vol. 32, pp. 473-475, 1978

[14] R. Dingle, W. Wiegmann, and C. H. Henry, "Quantum States of Confined Carriers in Very Thin Al$_x$Ga$_{1-x}$As-GaAs-Al$_x$Ga$_{1-x}$As Heterostructures", *Phys. Rev. Lett.* vol. 33, pp. 827 – 830, 1974

[15] R. D. Dupuis, P. D. Dapkus, N. Holonyak Jr., E. A. Rezek, R. Chin, "Room Temperature operation of quantum-well Ga1-xAlxAs-GaAs laser diodes grown by metalorganic chemical vapor deposition", *Appl. Phys. Lett.* vol. 32, pp. 295-297, 1978

[16] W. T. Tsang, "Extremely low threshold (AlGa)As modified multiquantum well

heterostructure lasers grown by molecular-beam epitaxy", *Appl. Phys. Lett.* vol. 39, pp. 786-788, 1981.

[17] W. T. Tsang, "Extremely low threshold (AlGa)As graded-index waveguide separateconfinement heterostructure lasers grown by molecular-beam epitaxy", *Appl. Phys. Lett.* vol. 40, pp. 217-219, 1982

[18] N. Chand, E. E. Becker, J. P. Van der Ziel, S. N. G. Chu, and N. K. Dutta, "Excellent uniformity and very low (less-than-50A/cm2) threshold current density strained InGaAs quantum-well diode-lasers on GaAs substrate "*Appl. Phys. Lett.* vol. 58, pp. 1704-1706, 1991

[19] N. Holonyak, Jr., "Quantum-well and superlattice lasers" Fundamental effects," in Proceedings of the Third (1982) Workshop on the Physics of Submicron Structures, H. Grubin, K. Hess, G. I. Iafrate, and D. K. Ferry, Eds. *New York: Plenum,* pp. 1-18, 1984

[20] Arakawa, and H. Sakaki, "Multidimensional quantum well laser and temperature dependence of its threshold current", *Appl. Phys Lett.*, vol. 40, no.11, pp. 939-941, 1982

[21] M. Asada, Y. Miyamoto, Y. Suematsu, "Gain and The Threshold of 3-Dimensional Quantum-Box Lasers", *IEEE Journal of Quantum Electronics*, vol.22, no.9, p.1915-1921, 1986

[22] H. Hirayama, K. Matsunaga, M. Asada and Y. Suematsu, "Lasing Action of Ga $Ga_{0.67}In_{0.33}As$/GaInAsP/InP Tensile-Strianed Quantum-Box Laser", *Electronics Letters*, vol.30, no.2, p.142-143 1994.

[23] D. Leonard, S. Fafard, K. Pond, Y. H. Zhang, J. L. Merz, and P. M. Petroff,

"Structural And Optical-Properties Of Self-Assembled Ingaas Quantum Dots," *Journal Of Vacuum Science & Technology B*, vol. 12, no. 4, pp. 2516-2520, 1994.

[24] D. Bimberg, M. Grundmann, N. N. Ledentsov, S. S. Ruvimov, P. Werner, U. Richter, J. Heydenreich, V. M. Ustinov, P. S. Kopev, and Z. I. Alferov, "Self-organization processes in MBE-grown quantum dot structures," *Thin Solid Films*, vol. 267, no. 1-2, pp. 32-36, 1995.

[25] Petroff, P. M. And Denbaars, S. P., "MBE And MOCVD Growth And Properties Of Self-Assembling Quantum-Dot Arrays In Iii-V Semiconductor Structures," *Superlattices And Microstructures*, vol. 15, no. 1, pp. 15-21, 1994.

[26] N. Kirstaedter, N. N. Ledentsov,, M.Grundmann,, D.Bimberg,, V. M.Ustinov,, S. S. Ruvimov, M. V. Maximov,, P. S. Kopev, Z. I.Alferov, Richter, U., Werner, P., U. Gosele, And J. Heydenreich, "Low-Threshold, Large T_0 Injection-Laser Emission From (InGa)As Quantum Dots," *Electronics Letters*, vol. 30, no. 17, pp. 1416-1417, 1994.

[27] A. Stintz, G. T. Liu, H. Li, L. F. Lester, and K. J. Malloy, "Low Threshold Current Density 1.3μm InAs quantum dot lasers with the Dots-in-a-Well (DWELL) structure", *IEEE Photon. Technol. Lett.* vol. 13, 2000

[28] D. Bimberg, "Quantum dots for lasers, amplifiers and computing", *J. Phys. D: Appl. Phys.* vol. 38, pp. 2055–2058, 2005.

[29] S. Schneider, P. Borri, W. Langbein, U. Woggon, R.L. Sellin, D. Ouyang, D. Bimberg, "Linewidth enhancement factor in InGaAs quantum-dot amplifiers ", *IEEE J.*

Quantum Electronics , vol.40, no.10, pp. 1423-1429, 2004.

[30] N. N. Ledentsov, V. A. Shchukin, M. Grundmann, N. Kirstaedter, J. Böhrer, O. Schmidt, D. Bimberg, V. M. Ustinov, A. Yu. Egorov, A. E. Zhukov, P. S. Kop'ev, S. V. Zaitsev, N. Yu. Gordeev, Zh. I. Alferov, A. I. Borovkov, A. O. Kosogov, S. S. Ruvimov, P. Werner, U. Gösele, and J. Heydenreich, "Direct formation of vertically coupled quantum dots in Stranski-Krastanow growth", *Phys. Rev*. B, vol 54, pp. 8743-8750, 1996

[31] D.L. Huffaker, G. Park, Z. Zou, O.B. Shchekin,, and D. G. Deppe, "1.3 μm room temperature GaAs-based quantum-dot Laser," *Appl. Phys. Lett.*, vol. 73 no**.** 18, pp. 2564-2566, 1998

[32] G. T. Liu, A. Stintz, H. Li, K. J. Malloy, and L. F. Lester, " Extremely Low Room-Temperature Threshold Current Density Diode Lasers Using InAs Dots in an In$_{.15}$Ga$_{.85}$As Quantum Well", *Electronics Letters*, Vol. 35, 1163-1165, 1999

[33] G. Park, O. B. Shchekin, D. L. Huffaker, D. G. Deppe: "Low-Threshold Oxide confined 1.3μm Quantum-Dot Laser ", *IEEE Photonics Technology Letters,* Vol. 13, pp. 230-232, 2000

[34] K. Mukai, Y. Nakata, K. Otsubo, M. Sugawara, N. Yokoyama, and H. Ishikawa, "High characteristic temperature of near-1.3-μm InGaAs/GaAs quantum-dot lasers at room temperature," *Applied Physics Letters* , Vol. 76, pp. 3349-3351, 2001

[35] OB. Shchekin, J. Ahn, DG. Deppe, "High temperature performance of self-organised quantum dot laser with stacked p-doped active region", *Electronics Letters*, vol. 38, no.14, p.712-713, 2002

[36] Y. Li, T. J. Rotter, Y. C. Xin, A. Stinz, A. Martinez, K. J. Malloy and L. F. Lester, "High Characteristic Temperature of p-doped InAs Quantum Dots-in-a-Well Lasers on InP Substrate", *Proc. Conf. Lasers Electro-Opt.*, Paper CThX6, 2006,

[37] S. Pradhan, S. Ghosh, and P. Bhattacharya, "Temperature dependent steady-state characteristics of high-performance tunnel injection quantum dot lasers," *Electron. Lett.*, vol. 38, pp. 1449, 2002.

[38] T. C. Newell, D. J. Bossert, A. Stintz, B. Fuchs, K. J. Malloy, and L. F. Lester, "Gain and linewidth enhancement factor in InAs quantum-dot laser diodes," *IEEE Photonics Technology Letters*, vol. 11, pp. 1527-1529, 1999.

[39] C. Harder, K. Vahala, and A. Yariv, "Measurement of the linewidth enhancement factor a of semiconductor lasers," *Appl. Phys. Lett*. vol. 42, pp. 328-330, 1983

[40] S. Schneider, P. Borri, W. Langbein, U. Woggon, R. L. Sellin, D. Ouyang, and D. Bimberg, "Linewidth enhancement factor in InGaAs quantum-dot lasers," *IEEE J. Quantum Electron*. vol. 40, pp. 1423-1429, 2004.

[41] J. Muszalski, J. Houlihan, G. Huyet, and B. Corbett, "Measurement of linewidth enhancement factor in selfassembled quantum dot semiconductor lasers emitting at 1310nm," *Electron. Lett.* vol. 40, pp. 428-430, 2004.

[42] A. A. Ukhanov, A. Stintz, P. G. Eliseev, and K. J. Malloy, "Comparison of the carrier induced refractive index, gain, and linewidth enhancement factor in quantum dot and quantum well lasers," *Appl. Phys. Lett*. vol. 84, pp. 1058-1060, 2004.

[43]. B. Dagens, A. Markus, J.X. Chen, J.-G. Provost, D. Make, O. Le Gouezigou, J.

Landreau, A. Fiore and B. Thedrez, "Giant linewidth enhancement factor and purely frequency modulated emission from quantum dot laser", *Electron. Lett.* vol. 41, pp. 323-324, 2005.

[44] Huang, X. D., Stintz, A., Li, H., Lester, L. F., Cheng, J., and Malloy, K. J., "Passive mode-locking in 1.3μm two-section InAs quantum dot lasers," *Applied Physics Letters*, vol. 78, no. 19, pp. 2825-2827, 2001.

[45] Y. C Xin, A. Martinez, T. Saiz, A. J. Moscho, Y. Li, T. A. Nilsen, A. L. Gray, L. F. Lester, "1.3-μm quantum-dot multisection superluminescent diodes with extremely broad bandwidth", *IEEE Photonics Technology Letters*, vol.19, no.5-8, pp.501-503, 2007

[46] M. Sugawara, K. Mukai, and H. Shoji, "Effect of phonon bottleneck on quantum-dot laser performance," *Applied Physics Letters*. vol. 71, pp. 2791-2793, 1997.

[47] T. S. Sosnowski, T. B. Norris, H. Jiang, J. Singh, K. Kamath, and P. Bhattacharya, "Rapid carrier relaxation in $In_{0.4}Ga_{0.6}As$/GaAs quantum dots characterized by differential transmission spectroscopy," *Physical Review B,* Vol. 57, R9423-R9426, 1998.

[48]. H. Su, L. F. Lester, "Dynamic properties of quantum dot distributed feedback lasers: high speed, linewidth and chirp", *Journal of Physics D-Applied Physics*, vol.38, no.13, pp.2112-2118, 2005

[49] Urayama J, Norris T B, Jiang H, Singh J and Bhattacharya P, "Temperature dependent carrier dynamics in self-assembled InGaAs quantum dots", *Appl. Phys. Lett.* Vol. 80 **,** pp**.** 2162-2164, 2002.

[50] S Fathpour, Z Mi and P Bhattacharya, "High-speed quantum dot lasers", *J. Phys. D:*

Appl. Phys. Vol. 38**,** pp. 2103–2111, 2005

[51] D. G. Deppe, H. Huang, and O. B. Shchekin, "Modulation characteristics of quantum-dot lasers: The influence of P-type doping and the electronic density of states on obtaining high speed," *IEEE Journal of Quantum Electronics*, vol. 38, no. 12, pp. 1587-1593, 2002.

[52] S. Fathpour, ZT. Mi, P. Bhattacharya, "Small-signal modulation characteristics of p-doped 1.1- and 1.3-mu m quantum-dot lasers", *IEEE Photonics Technology Letters*; vol.17, no.11, pp.2250-2252, 2005

[53] C. P. Seltzer, L. D. Westbrook, H. J. Wicks, "The Gain-Lever effect in InGaAsP/InP Multiple-Quantum Well Lasers", *Journal of Lightwave Technology*, vol.13, no.2, pp.283-289, 1995.

[54] N. Moore, K. Y. Lau, Ultrahigh efficiency Microwave signal transmission using tandem-contact single quantum well GaAlAs lasers, *Applied Physics Letters*, vol.55, no.10, p.936-938, 1989.

[55] K. Y. Lau, "The inverted gain-levered semiconductor-laser direct modulation with enhanced frequency-modulation and suppressed intensity modulation"**,** *IEEE Photonics Technology Letters*; vol. 3, no.8, pp.703-705, 1991

[56] W. M. Yee and K. A. Shore, "Enhanced Wavelength Tunability in Asymmetric Gain-Levered Quantum-Well Semiconductor Lasers", *Journal of Lightwave Technology*, vol.13, no.4, pp.588-591, 1995

[57] K. J. Vahala, M. A. Newkirk, and T. R. Chen, "The optical gain lever: a novel gain

mechanism in the direct modulation of QW semiconductor lasers," *Appl. Phys. Lett.,* Vol. 54, pp. 2506, 1989

[58] Giora Griffel, Robert J. Lang, and Amnon Yariv, "Two-Section Gain-Levered Tunable DistributedFeedback Laser with Active Tuning Section", *IEEE Journal of Quantum Electronics*, vol. 30, no. 1, 1994.

[59] A. Kaszubowska, P. Anandarajah, and L. P. Barry, "Improved performance of a hybrid radio/fiber system using a directly modulated laser transmitter with external injection," *IEEE Photonics Technology Letters*, vol. 14, pp. 233-235, 2002.

[60] M. Al-Mumin, W. Xinhong, M. Weiming, S. A. Pappert, and L. Guifang, "Optical generation and sideband injection locking of tunable 11-120 GHz microwave/millimetre signals," *Electronics Letters*, vol. 36, pp. 1547-1548, 2000.

[61] K. Weich, E. Patzak, and J. Horer, "Fast all-optical switching using two-section injection-locked semiconductor lasers," *Electronics Letters*, vol. 30, pp. 493-4, 1994.

[62] S. Kobayashi, S. Kimura, "Injection locking characteristics of an AlGaAs semiconductor-laser", *IEEE Journal of Quant. Electro.*, vol. 16, no. 9, pp. 915-917, 1980

[63] C. Lin, J. K. Andersen, and F. Mengel, "Frequency chirp reduction in a 2.2 Gbit/s directly modulated InGaAsP semiconductor laser by CW injection," *Electron. Lett.*, vol. 21, pp. 80-81, 1985.

[64] T. B. Simpson, J. M. Liu, and A. Gavrielides, "Bandwidth enhancement and broadband noise reduction in injection-locked semiconductor lasers," *IEEE Photon. Technol. Lett.*, vol. 7, no. 7, pp. 709-711, 1995.

[65] X. J. Meng, T. Chau, D. T. K. Tong, and M. C. Wu, "Suppression of second harmonic distortion in directly modulated distributed feedback lasers by external light injection," *Electron. Lett.*, vol. 34, no. 21, pp. 2040-2041, 1998.

[66] C.-H. Chang, L. Chrostowski, and C. J. Chang-Hasnain, "Injection locking of VCSELs," *IEEE J. Sel. Topics Quantum Electron.*, vol. 9, pp. 1386-93, Sep./Oct. 2003.

[67] S. K. Hwang, J. M. Liu, J. K. White, "35-GHz intrinsic bandwidth for direct modulation in 1.3-µm semiconductor lasers subject to strong injection locking", *IEEE Photon. Technol. Lett.*, vol. 16, no. 4, pp. 972-974, 2004

[66] X.-M. Jin, S.-L. Chuang, "Bandwidth enhancement of Fabry-Perot quantum-well lasers by injection-locking", *Solid-State Electronics*, vol. 50 pp. 1141–1149, 2006

Chapter 2 Modulation Bandwidth of p-doped Single Section Quamtum Dot lasers

2.1. Introduction

Self-assembled quantum dot (QD) semiconductor lasers have been considered as a potential candidate for high-speed devices due to their unique three-dimensional carrier confinement [1, 2]. In planar quantum well materials, the density of state is a step-wise continuous function. The electron and holes occupy a wide range of energy levels. Since the lasing spectrum is relative narrow, the probability is small for the electron and holes to occupy those states that couple to lasing mode. In contrast, for quantum dot materials, which have a delta-function-like density of states, the spontaneous emission linewidth and the gain spectra are theoretically much narrower, so the QD lasers can achieve very high differential gain, which is one of the key parameters for creating high-speed semiconductor lasers.

However, the conventional separate confinement heterostructure (SCH) InAs and InGaAs QD lasers have not shown significant modulation bandwidth enhancement yet [3, 4]. The first factor that limits the modulation performance of QD lasers is inhomogeneous linewidth broadening, stemming from the stochastic size distribution of the self-assembled dots. The linewidth of photoluminescence is one of indicator of uniformity of the dot's size. The narrowest photoluminescence reported to date is 19 meV

[5], which is considerably wider than the linewidth limit of 5-8 meV due to homogeneous lifetime broadening [6]. A larger variation in dot size results in lower peak modal gain as well as differential gain in real QD lasers. The second limitation comes from the large density of states of the wetting layer and barriers [6, 7]. In the Stranski–Krastanow growth mode, a self-assembled QD layer is formed on top of a wetting layer. The accessible states in the wetting layer can be as much as two orders magnitude greater than that in the QDs. The injected carriers will predominately occupy the states in the wetting layer, where the energy of the state is high. The relaxation time for those carriers from the upper energy state to the lasing state is longer. This "hot carrier" effect influences the performance of QD lasers by increasing the threshold current density, compressing the gain and damping the frequency response. As result, the modulation bandwidth of conventional SCH QD lasers is limited to about 6-7 GHz at room temperature. [3].

Two promising techniques have been demonstrated to solve the hot carrier effect discussed above: Tunneling injection (TI) and p-doping of dots. Bhattacharya *et al*. [8] proposed the tunnel injection technique in QD lasers by applying a QW layer adjacent to a QD layer as an injector well. The "cold" carriers were injected into QD ground state by direct or phonon-assistant tunneling process, then removed at relatively the same rate by stimulated emission, so the carrier distribution will be maintained close to a quasi-Fermi distribution and carrier hot-carrier effect can be by-passed. A 23 GHz 3-dB bandwidth was achieved for 980 nm TI-QD lasers [8].

The P-doping technique in the QD active region was proposed by Shchekin and

Deppe to compensate the closely spaced hole level [7]. The extra holes avoid the gain saturation with carrier density so that the maximum ground state gain and differential gain is increased. The characteristic temperature and modulation bandwidth of QD lasers can be improved significantly by p-doping. A T_0 as high as 210 K was demonstrated in the InAs/InP 1500 nm QD lasers [9] and 213 K for InAs/GaAs QD lasers in the 1310 nm range was reported by Shchekin *et. al* [10]. A modulation bandwidth of 30 GHz was theoretically predicted using a p-doped QD device [11]. Sugawara [12] *et. al.* demonstrated a temperature-insensitive 10 Gb/ s operation within 20–70 °C using a 10-layer stack p-type QD active region that had a direct modulation bandwidth of 7.7 GHz at room temperature. Fathpour *et al.* [13] reported a 3 dB bandwidth of 8 GHz for a *p*-doped device at 1.3 μm under pulse conditions, but compared with the un-doped QD device the bandwidth enhancement is only few GHz in the p-doped device. Therefore, at the experimental level, the prediction has not yet been shown as pointed out in Ref [11]. Besides, the studies on literature were limited on p-doped materials with low dot density, and the gain enhancement has been achieved by p-doping at low dot density. But more interesting case is high dot density QDs with high-doping level. This is the main topic of this chapter.

2.2. Modulation response equation for single section QD lasers

Modulation response is the measure of any system response at the output to a signal of

varying frequency at its input. The carrier relaxation and spectral hole burning have a greater influence on the dynamic property of QD lasers. In QD lasers, the discrete energy does benefit the linewidth and differential gain, but it slows down the carrier relaxation process. Different approaches have been proposed to investigate carrier dynamics in QD lasers. [15-17]. In our dots-in-a-well (DWELL) SCH structure, the intraband relaxation is assumed fast enough so that quasi-equilibrium can be kept. The slower relaxation process such as carrier transport from the QW into the QD's state can be treated as a parasitic RC time constant. According to this simplification, a set of three rate equations model, which was derived initially for QW lasers, can be applied to describe the small-signal modulation response of QD lasers [4, 18]:

$$\frac{dN_B}{dt} = \frac{J}{ed} - \frac{N_B}{\tau_s} - \frac{N_B}{\tau_c} + \frac{N_W}{\tau_e} \qquad (2.1a)$$

$$\frac{dN_W}{dt} = \frac{N_B}{\tau_c} - \frac{N_W}{\tau_e} - \frac{N_W}{\tau_s} - \frac{v_g G(N)S}{1+\varepsilon S} \qquad (2.1b)$$

$$\frac{dS}{dt} = \frac{\Gamma v_g G(N)S}{1+\varepsilon S} - \frac{S}{\tau_p} \qquad (2.1c)$$

where N_B and N_W are the carrier density in the quantum well confined region and barrier respectively, τ_s is the carrier recombination lifetime, τ_p is the photon lifetime, Γ is the optical confinement factor, v_g is the group velocity, G is the material gain that is a function of carrier density, S is the photon density, ε is the non-linear gain compression coefficient, τ_e is the active region escape time and τ_c is the carrier transport time, which

includes the capture time and various parasitic effects, such as the equivalent RC constants of the packaging, since they are indistinguishable from the transport effect in the experimental measurement. The small signal analysis gives the relative modulation response as:

$$|M(f)|^2 = \left| \frac{s(f)/i(f)}{s(0)/i(0)} \right| \propto \frac{1}{1+(2\pi f \tau_c)^2} \frac{f_r^{\,4}}{\left[(f_r^{\,2} - f^2) + (\frac{\gamma}{2\pi})^2 f^2 \right]} \qquad (2.2)$$

Where s is the photon density, i is injected current density, f_r is relaxation frequency, γ is the damping rate. The low-pass filter term arising from τ_c produces a low frequency roll-off in the response curve. The relationship between f_r and γ defines the so called K factor as:

$$\gamma = K f_r^{\,2} + \frac{1}{\tau_{eff}} \qquad (2.3)$$

And

$$f_r^{\,2} = \frac{V_g (g_0/\chi) S}{4\pi^2 \tau_p (1 + \varepsilon S)} \qquad (2.4)$$

$$G = \frac{G_0}{1 + \varepsilon S} \equiv \frac{G_0}{1 + P/P_{sat}} \qquad (2.5)$$

where τ_{eff} is the effective carrier lifetime, a_0 is the differential gain without gain compression, and $\chi = 1 + \tau_e/\tau_c$ is the modification factor due to the carrier transport with τ_e the carrier escape time. The gain compression coefficient, ε, can be calculated using Eqn.

(2.4) if f_r and S can be experimentally obtained. P is the output power measured at the facet of the device. The introduction of P_{sat} is for convenience to estimate at what output power the gain compression becomes significant.

p$^+$-GaAs contact layer, p doped 3×10^{19} cm^{-3}, 60 nm
Graded Al$_{0.66->0}$Ga$_{0.34->1}$As, p doped 2×10^{19} cm^{-3}, 40 mm
Al$_{0.66}$Ga$_{0.34}$As Cladding, p-doped, 3×10^{17} -5×10^{18} cm^{-3}, 1300 nm
Graded Al$_{0->0.66}$Ga$_{1->0.34}$As, Un-doped 10 nm
GaAs, Un-doped 5 nm
GaAs, Un-doped 5 nm
GaAs, P-doped 5 nm
GaAs, Un-doped 5 nm
InAs/InGaAs, Undoped 7.8 nm , DWELL
GaAs. Un-doped 5 nm
Graded Al$_{0.66->0}$Ga$_{0.34->1}$As, Un-doped 10 nm
Al$_{0.66}$Ga$_{0.34}$As Cladding, n-doped, 3×10^{17} -3×10^{18} cm^{-3}, 1300 nm
Graded Al$_{0.66->0}$Ga$_{0.34->1}$As, n doped 3×10^{18} cm^{-3}, 40 nm
n-GaAs buffer layer, -doped 5×10^{18} cm^{-3}, 300 nm
n-GaAs substrate

6X

Fig 2.1   Layer structure of the p-type quantum dot device with variable doping density

2. 3 Wafer growth and device fabrication

To compare the improvement of the p-doping technique, one un-doped QD wafer (# 632) and three p-doped QD wafers with different doping level: 20 holes/QD (619), 30 holes/QD (618) and 40 holes/QD (620) were grown during the same campaign. The 1.22 μm InAs/InGaAs DWELL laser structure, which is shown in Fig. 2.1 was grown on an n+-doped GaAs substrate. The active region consists of 6 DWELL stacks of self assembled InAs QDs in a 7.8-nm wide, compressively strained InGaAs quantum well (QW) separated by 15 nm GaAs barriers. The dot density is 2.5×10^{11} cm^{-2} for all four wafer samples. For the p-doped wafer, there is a δ-doped layer added in the barrier 5 nm above each QW with different sheet densities of beryllium. The total GaAs/InGaAs waveguide thickness is about 137 nm. The cladding layer on the p-side is 1300-nm thick p-doped $Al_{0.66}Ga_{0.34}As$. The cladding on the n-side is 1300-nm thick n-doped $Al_{0.66}Ga_{0.34}As$. The laser structure has been capped with a 60-nm thick heavily p-doped GaAs layer.

2.4. Static performance of the un-doped and p-doped lasers

To examine the static operating parameters of un-doped and p-doped lasers, 50-um-wide broad area lasers were fabricated out of these wafers. The samples were cleaved to different cavity lengths ranging from 0.5-mm to 2-mm. The cavity-dependent light-current (*L-I*) characteristics were measured under pulse conditions (500-ns pulse

width and 1% duty cycle). The internal loss and injection efficiency can be derived from the plot of the inverse of external quantum efficiency versus cavity length. The results are listed in Table 2.1. It is well known that p-type doping can increase the maximum gain, G_{max}, of the QD laser as shown in the third column of Table 2.1. But the p-doped devices have larger internal losses compared to the un-doped lasers, due to free-carrier absorption and the internal loss increases with doping level. The injection efficiency does not experience much change between un-doped and p-doped devices, because the diode laser structure is same for these devices.

Table 2.1. Static performance of un-doped and p-doped lasers

Wafer #	Broad area lasers			1.2mm long RWGs			
	α_i	η_i	G_{max}	G_{th}	i_{th}	SE	T_0
un-doped	2	65	15	12	8	0.54	57
20 h/dot	7.5	56	22	17.5	25	0.36	48
30 h/dot	8.7	63	24	18.7	31	0.28	48
40 h/dot	10	60	25	20	32	0.32	32

The 3.5-μm-wide ridge waveguide (RWG) lasers were then fabricated from these wafers to perform dynamic characterization. First, the sample was dry-etched to form 3.5-μm wide ridges using a BCl_3 inductively-coupled plasma (ICP) etch. Then BCB dielectric processing was applied for planarization and to isolate the p-type metal and the etched upper cladding layer. The p-type metal is Ti/Pt/Au with a thickness of 50nm/50nm/250nm. After lapping and polishing of the substrate, Au/Ge/Ni/Au n-type metallization was deposited, and the sample was annealed at 380°C for 1 minute. This

temperature is lower than the optimal value for annealing the time contact but is necessary to avoid delamination of the BCB material from the ridge waveguide. Finally, the sample was cleaved to 1.2-mm long laser diode bars for further testing.

The static performance measurements for RWG lasers were performed too under pulsed conditions of 0.5 us and 1% duty cycle. The L-I characteristics for four devices are plotted in Fig. 2.2. The slope efficiency (SE), the threshold modal gain and threshold current density (at 20^0C) were extracted from the data in this figure and are listed in Table 1. The slope efficiency of the un-doped laser is larger than those of the p-doped lasers. This can be attributed to the larger internal loss for p-doped material. For the lowest hole concentration device, the value of SE is 0.36 W/A, which is similar to the value reported by Fathpour et.al.[12]. This indicates our p-doped QD material is of high quality. Generally, as the doping level increases, the slope efficiency goes down. A slightly lower SE value in device 618 is due to the 10% measurement accuracy. The characteristic temperatures, which are included in Table.1, are extracted by measuring the threshold current from 20^0C-80^0C under CW operation. The value of 57 K is fairly typical for un-doped QD devices with same structure. All p-doped lasers show lower T_0 compared to the un-doped laser. The lowest T_0 occurs when the doping level is highest. This trend is contrary to most previous reports that p-doped devices have higher T_0 value [9, 10]. Large internal loss and non-linear gain compression arising from the heavy doping could be contributing to this unusual behavior, more detailed discussions are presented in the following part of this chapter.
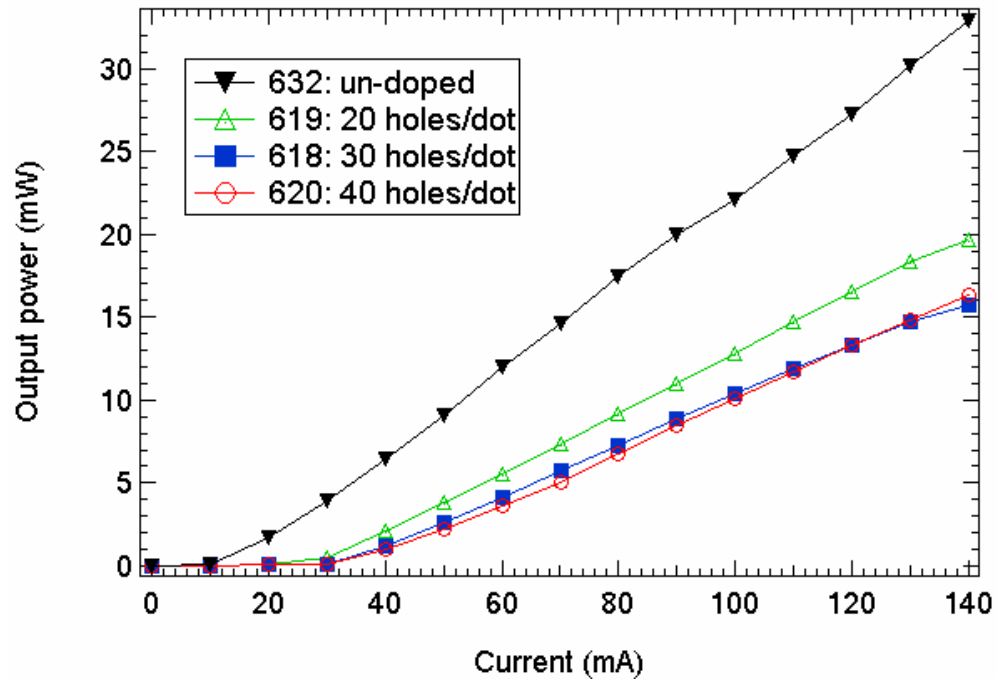
Fig. 2.2 The L-I curve of ridge waveguide lasers fabricated from p-doped and un-doped

QD wafters.

2.5. Small signal modulation response of the 1.2 mm devices.

To prepare for high-speed testing, each RWG device was soldered using indium on a Au-coated copper heat-sink and an "on-wafer" RF probe was used. As shown in Fig 2.3, the signal-ground configuration was achieved by mounting another chip adjacent to the device with the same thickness to minimize the parasitic capacitance and inductance. DC and small-signal microwave signals were provided from port 1 of an HP8722D vector network analyzer. The output of the laser diode was coupled into a tapered fiber (the coupling efficiency is about 10%) then collected by a Newport high-speed photodetector (40 GHz bandwidth)，which was connected to port 2 of the HP8722D. The measurements were performed on the four lasers by using the same RF calibration to ensure consistency. The modulation response from each device is shown in Fig. 2.4. Because of a low frequency roll-off in the detector response, the frequency range of study covers from 700 MHz to 20 GHz. Based on Eqn [2.2-2.4], the modulation characteristic parameters, such as relaxation frequency, f_r and the K factor were extracted from Fig. 2.4 and are summarized in Table 2.

Table 2.2. Dynamic performance of the un-doped and p-doped lasers

Wafer	max f_r	mod. eff.	$f_{-3\,dB}$	K-factor	P_{sat}
Unit	GHz	GHz/mA$^{1/2}$	GHz	ns	mW
undoped	5.3	0.54	5.2	1.42	90
20 h/dot	4.6	0.51	4.6	1.14	62.7
30 h/dot	3.8	0.48	4.2	1.04	53.2
40 h/dot	3.6	0.46	4.4	1.01	18.4

From Port 1
of 8722D

S   G
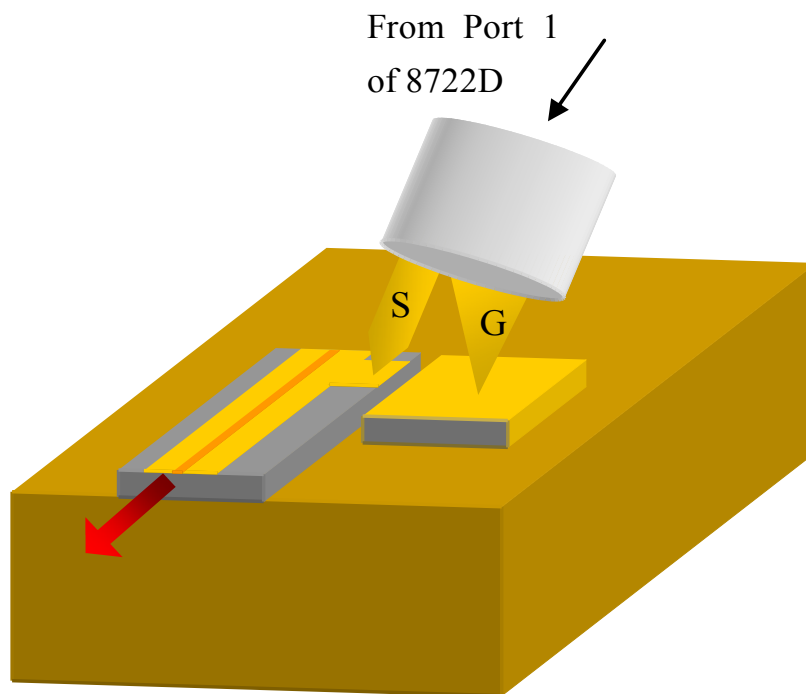
Fig 2.3 Signal-Ground configuration for Hi-speed testing. The adjacent metallic chip moves the ground so that it is coplanar with the surface of laser anode contact.
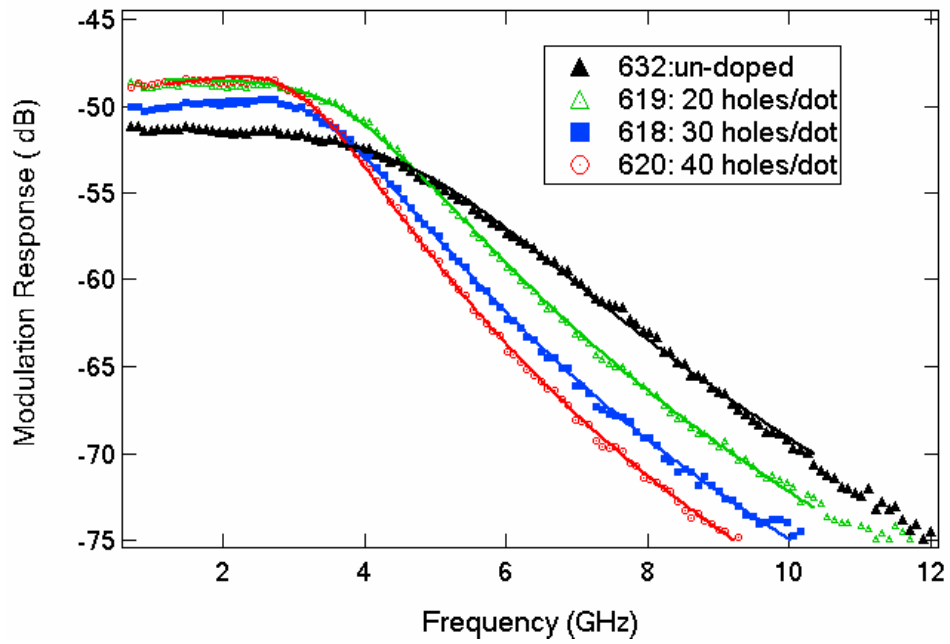
Fig 2.4 Modulation response of 1.2 mm-long un-doped and p-doped QD RWG lasers.

The normalized current（I-I_{th}）$^{1/2}$ is 8.5.

The relaxation frequency, f_r, versus the square-root of the current above threshold ($I-I_{th})^{1/2}$ is plotted in Fig. 2.5 for the four different lasers. The maximum relaxation frequency obtained at a normalized bias current of 10 decreases monotonically with the p-doping level from 5.3 GHz (un-doped) to 3.6 GHz (40 h/dot). In the low bias range, the f_r increases linearly with root normalized current as expected. The relaxation frequency is saturated when the root normalized current exceeds 7. From Fig. 2.2, it is confirmed that heating effect can be neglected in our measurement since there is no roll off in the L-I curves until about 140 mA. The ground state lasing is also confirmed across the whole current range. This trend in f_r arises from gain compression factors in QD lasers indicated by Eqn (2.4)

The slope of f_r versus $(I-I_{th})^{1/2}$ curve is defined as the modulation efficiency of RF-modulated laser diodes, and is proportional to the square root of the product of threshold gain and differential gain. In the linear regime $((I-I_{th})^{1/2}$ up to 6 mA$^{1/2}$), the highest modulation efficiencies obtained among the lasers decrease monotonically with p-doping from 0.54 GHz/mA$^{1/2}$ (undoped), to 0.46 GHz/mA$^{1/2}$ (40 holes/dot) but still higher than previously reported results indicating excellent material quality[12]. Since the injection efficiencies are very similar for both un-doped and p-doped devices, the differential gain must be decreasing with the p-doping level to explain this trend. It is conjectured that the increased internal loss with increased p doping more than offsets, the larger maximum ground state gain and, consequently, causes gain saturation. To achieve the same normalized current, the driving currents of p-doped lasers are much higher than

that of un-doped laser. The effect of carrier heating becomes severe at high bias condition and enhances nonlinear gain saturation too [19]. To obtain a perspective on the non-linear gain saturation in p-doped lasers, the evolution of the squared relaxation frequency versus the output power is plotted in Fig. 2.6 The saturation power P_{sat} that is listed in Table 2 can be extracted by curve-fitting these results with Eqns (2.4)-(2.5). The fitting function was shown in the figure as an inset. It can be seen that the non-linear regime is more pronounced when the p-type doping level is high. The P_{sat} decreases from 90 mW for the undoped wafer to 18.4 mW, indicating that the relaxation frequency of the p-doped device saturates rapidly compared with the un-doped device. This also can be proof that a high doping level may deteriorate modulation bandwidth of QD lasers. In Ref [12], Fathpour *et .al* reported a consistent result that p-doping technique can only provide a limited improvement on QD laser's bandwidth after comparing the modulation response between p-doped and un-doped 1.1um QD device. However, they attributed this result to a larger fraction of holes occupying the QD wetting layer states instead of the lasing states in the QD. Our results indicate that for large QD densities, this slight improvement with p-doping actually reverses and becomes a detriment to the high speed performance
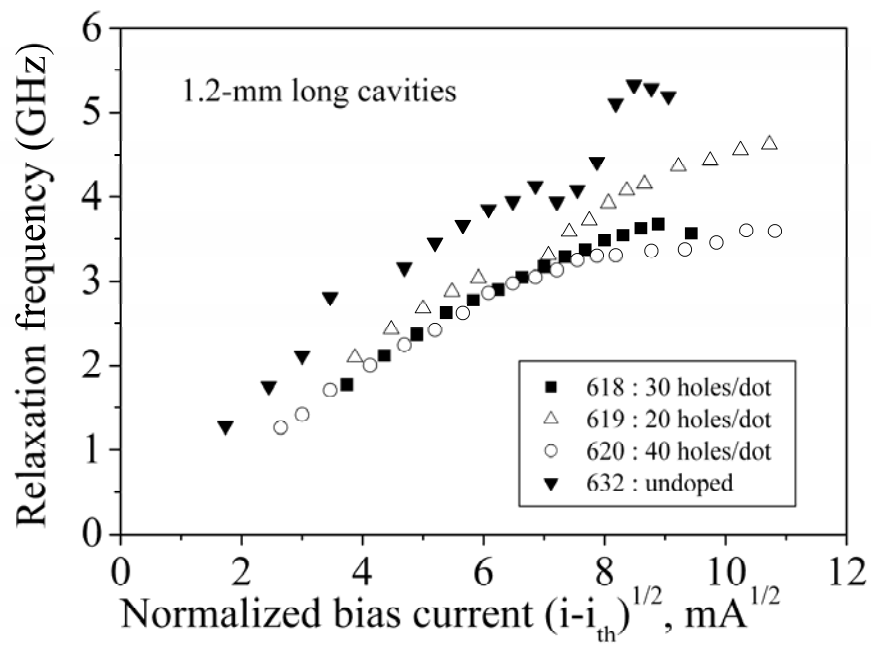
Fig. 2.5. Relaxation frequency versus the square root of the bias current above threshold of 1.2 mm-long cavity length un-doped and p-doped lasers.
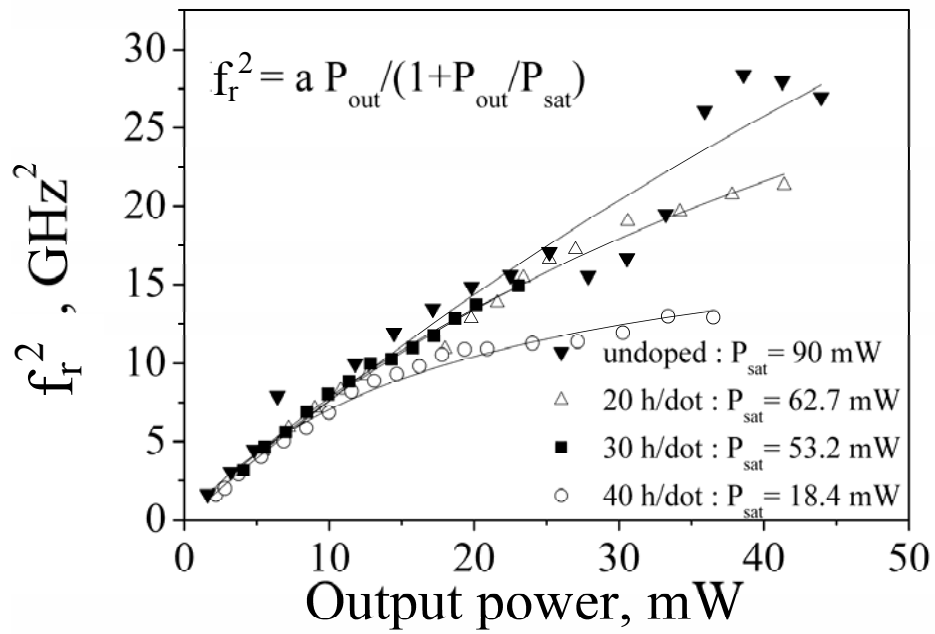
Fig. 2.6 Squared relaxation frequency versus output power for four lasers the set of QD lasers with different p-doping level.

2.6. Small signal modulation response of 0.8 mm HR coated devices.

To confirm the observed trend with p-doping, the hi-speed performance of p-doped QD lasers was further examined using 800-μm long RWG devices with a 95% high-reflection (HR) coating on one facet only. For comparison, the relation between f_r and ($I-I_{th}$)$^{1/2}$ is plotted too in Fig. 2.7 for the four different lasers. Compared to the 1.2-mm as-cleaved lasers, these HR-coated lasers show larger maximum relaxation frequencies equal to 5.0 GHz, 5.5 GHz and 4.3 GHz for the p-doped device set. Normally, HR coating results in a decreased modulation bandwidth since it increases the photon lifetime of the lasers. This bandwidth improvement in HR-coated devices is presumably due to reduced gain saturation. The lower relaxation frequency of the wafer 619 lasers compared to 618 could be attributed to a less efficient HR-coating. A comparison of the modulation efficiencies in the linear regime (up to a ($i-i_{th}$)$^{1/2} \cong 7$) led to 0.60 GHz/ mA$^{1/2}$, 0.58 GHz/ mA$^{1/2}$ and 0.44 GHz/ mA$^{1/2}$ for the three p-doped QD wafers. These results further confirm that the differential gain of p-doped QD lasers decreases with doping density in the range explored given a constant cavity length.
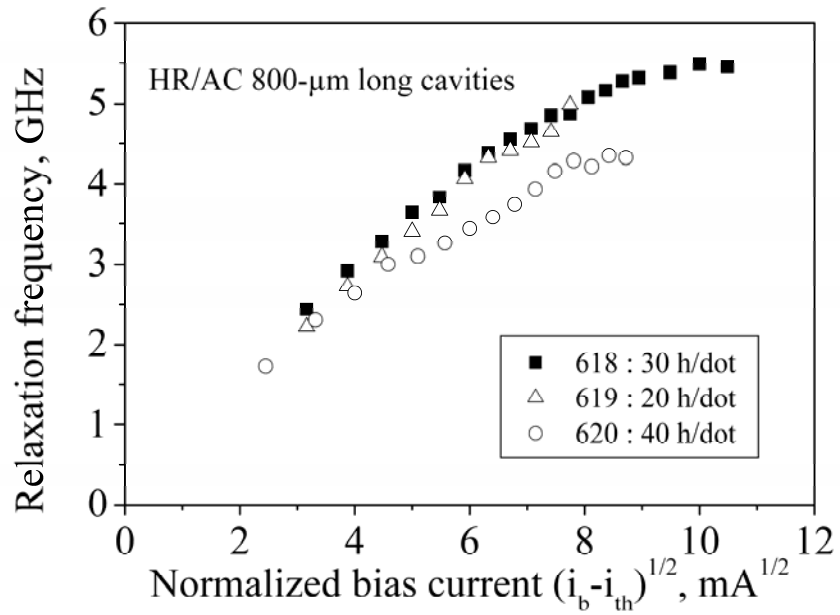
Fig 2.7 Relaxation frequency versus the square root of the normalized bias current of the

three doped lasers with one HR-coated facet and cavity length of 800 μm.

2.7. Summary

In conclusion, the static performance and modulation frequency response of un-doped and p-doped InAs/GaAs QD lasers were studied in this chapter. The internal loss increases with p-doping level from 7.5 cm^{-1} for the 20 holes/dot wafer to 10 cm^{-1} for 40 holes/dot wafer, which are much larger than the value of 2 cm^{-1} for un-doped lasers. Although the maximum ground state gain of the p-doped laser is larger than that of un-doped lasers and increases with p-doping level, the corresponding increase in internal losses induces gain saturation and gain compression and, thus, degrades the high-speed performance of p-doped QD lasers. The modulation efficiency and the highest relaxation frequency of 1.2-mm cavity length lasers decrease monotonically with the p-doping level from 0.54 GHz/mA$^{1/2}$ and 5.3 GHz (un-doped wafer) to 0.46 GHz/mA$^{1/2}$ and 3.6 GHz (40 holes/dot). The net result is that a p-type concentration in the range of 20 to 40 holes/dot decreases the differential gain for lasers with constant cavity length. Based on curve-fitting procedure, the saturation power is found to decrease with the p-type level from 90 mW (un-doped) to 18.4 mW (40 holes/dot). The degrading of modulation performance of p-doped device is attributed to higher gain saturation factor due to carrier heating effect. More promising methods to improve the modulation bandwidth in QD devices is improve the uniformity of dots, implement the gain lever effect, or employing injection-locking. The last two will be studied in the next two chapters.

References

[1]   D. Bimberg, N. Kirstaedter, N. N. Ledentsov, Z. I. Alferov, P. S. Kopev, V. M. Ustinov, "InGaAs-GaAs quantum-dot lasers", *IEEE Journal of Selected Topics in Quantum Electronics*; vol.3, no.2, pp.196-205, 1997.

[2] M. Sugawara, N. Hatori, M. Ishida, H. Ebe, Y. Arakawa, T. Akiyama, K. Otsubo, T. Yamamoto, Y. Nakata, "Recent progress in self-assembled quantum-dot optical devices for optical telecommunication: temperature-insensitive 10 Gbs(-1) directly modulated lasers and 40Gbs(-1) signal-regenerative amplifiers", *Journal of Physics D-Applied Physics*, vol.38, no.13, pp.2126-2134, 2005.

[3]   K. Kamath, J. Phillips, H. Jiang, J. Singh, P. Bhattacharya, "Small-signal modulation and differential gain of single-mode self-organized In0.4Ga0.6As/GaAs quantum dot lasers", *Applied Physics Letters*, vol.70, no.22, pp.2952-2953, 1997

[4] H. Su, L. F. Lester, "Dynamic properties of quantum dot distributed feedback lasers: high speed, linewidth and chirp", *Journal of Physics D-Applied Physics*, vol.38, no.13, pp.2112-2118, 2005

[5]   S. Krishna, J. Sabarinathan, K. Linder, P. Bhattacharya, B. Lita, R. S. Goldman, "Growth of high density self-organized (In,Ga)As quantum dots with ultranarrow photoluminescence linewidths using buried In(Ga,Al)As stressor dots", *Journal of Vacuum Science and Technology*, vol.18, no.3, pp.1502-1506, 2000

[6] K. Matsuda, K. Ikeda, T. Saiki, H. Tsuchiya, H. Saito, and K. Nishi, "Homogeneous linewidth broadening in a InGaAs/GaAs single quantum dot at room temperature investigated using a highly sensitive near-field scanning optical microscope," *Phys. Rev. B*, vol. 63, pp. 121 304–121 304-4, 2001.

[7] D. R. Matthews, H. D. Summers, P. M. Smowton, M. Hopkinson, "Experimental investigation of the effect of wetting-layer states on the gain-current characteristic of quantum-dot lasers" , *Applied Physics Letters*, vol.81, no.26, p.4904-4906, 2002

[8] O. B. Shchekin, D. G. Deppe, "The role of p-type doping and the density of states on the modulation response of quantum dot lasers", *Applied Physics Letters*, vol.80, no.15, p.2758-2760, 2002

[9] P. Bhattacharya, S. Ghosh, S. Pradhan, J. Singh, Z. K. Wu, J. Urayama, K. Kim, T. B. Norris, "Carrier dynamics and high-speed modulation properties of tunnel injection InGaAs-GaAs quantum-dot lasers", *IEEE Journal of Quantum Electronics*, vol.39, no.8, p.952-962, 2003.

[10] Y. Li, T. J. Rotter, Y. C. Xin, A. Stinz, A. Martinez, K. J. Malloy and L. F. Lester, "High Characteristic Temperature of p-doped InAs Quantum Dots-in-a-Well Lasers on InP Substrate", *Proc. Conf. Lasers Electro-Opt.*, Paper CThX6, 2006,

[11]. O. B. Shchekin, J. Ahn, D. G. Deppe, "High temperature performance of self-organised quantum dot laser with stacked p-doped active region" , *Electronics Letters*, vol.38, no.14, p.712-713, 2002.

[12]. D. G. Deppe, H. Huang, O. B. Shchekin, "Modulation characteristics of quantum-dot lasers: The influence of P-type doping and the electronic density of states on obtaining high speed ", *IEEE Journal of Quantum Electronics*, vol.38, no.12, p.1587-1593, 2002

[13]. M. Sugawara, K. Mukai, H. Shoji, "Effect of phonon bottleneck on quantum-dot laser performance", *Applied Physics Letters*, vol.71, no.19, pp.2791-2793, 1997

[14]. S. Fathpour, Z -T. Mi, P. Bhattacharya, "Small-signal modulation characteristics of p-doped 1.1- and 1.3-mu m quantum-dot lasers", *IEEE Photonics Technology Letters*, vol.17, no.11, pp.2250-2252, 2005

[15]. F. Adler, M. Geiger, A. Bauknecht, F. Scholz, H. Schweizer, M. H. Pilkuhn, B. Ohnesorge, A. Forchel, "Optical transitions and carrier relaxation in self assembled InAs/GaAs quantum dots", *Journal of Applied Physics*, vol. 80, no.7, p.4019-4026, 1996.

[16]. W. W. Chow, S. W. Koch, "Theory of semiconductor quantum-dot laser dynamics", *IEEE Journal of Quantum Electronics*, vol.41, no.4, pp.495-505, 2005

[17]. P. Bhattacharya, D. Klotzkin, O. Qasaimeh, W. D. Zhou, S. Krishna, D. H. Zhu, "High-speed modulation and switching characteristics of In(Ga)As-Al(Ga)As self-organized quantum-dot lasers", *IEEE Journal of Selected Topics in Quantum Electronics*, vol.6, no.3, pp.426-438, 2000

[18].   R. Nagarajan, M. Ishikawa, T. Fukushima, R. S. Geels, J. E. Bowers, "High-speed quantum-well lasers and carrier transport effects", *IEEE Journal of Quantum Electronics*, vol.28, no.10, pp.1990-2008, 1992

[19].   L. F. Lester, B. K. Ridley, "Hot carriers and the frequency-response of quantum-well lasers", *Journal of Applied Physics,* vol.72, no.7, pp.2579-2588, 1992

Chapter 3   Gain-lever quantum dot lasers

3.1 Introduction

As was briefly discussed in chapter 1, the modulation bandwidth of direct modulated semiconductor lasers is limited by the relaxation frequency. One of the physical origins of this limitation comes from a link between threshold gain and differential gain. To obtain high modulation bandwidth, the laser cavity is chosen as short as possible to obtain shorter photon lifetime. This will cause the laser to operate at a high threshold gain resulting in a small differential gain value, due to the non-linear relationship between gain and carrier density in semiconductor QW and QD devices. Besides the bandwidth consideration, the modulation efficiency also creates a great deal of concern in analog communication systems. A typical RF link having a loss of 20-30 dB is a big challenge to overcome for semiconductor laser applications. One of the alternative ways to improve the modulation efficiency is to use gain-lever effect that implements a two-segment contact and a common applied waveguide. The gain-lever technique was proposed by Vahala et al in 1989, to improve the efficiency of modulated light conversion by RF [1-3]. They demonstrated a 6-dB enhancement of the modulation response using an optical gain-lever QW device. A 22-dB amplitude modulation (AM) was also realized by Moore and Lau, using a 220-um QW device, with only a marginal increase in the intensity noise [4, 5]. Since then, much research work has been conducted not only on AM characteristics, but also wavelength tunability [6, 7] and frequency modulation (FM)

performance [8-10]. All of the previous work has been done on QW devices and 3-dB bandwidth enhancement has yet to be reported.

In this chapter, the modulation response of a gain-lever quantum dot laser will be discussed. The concept of the gain-lever device will be introduced, and then the new response equation for gain-lever laser will be derived. The amplitude modulation efficiency enhancement and 3-dB bandwidth enhancement is predicted theoretically and demonstrated experimentally using un-doped and p-doped QD devices.

3.2. Modulation characteristic of gain-lever QD lasers

3.2.1 Basic concept of the gain-lever effect
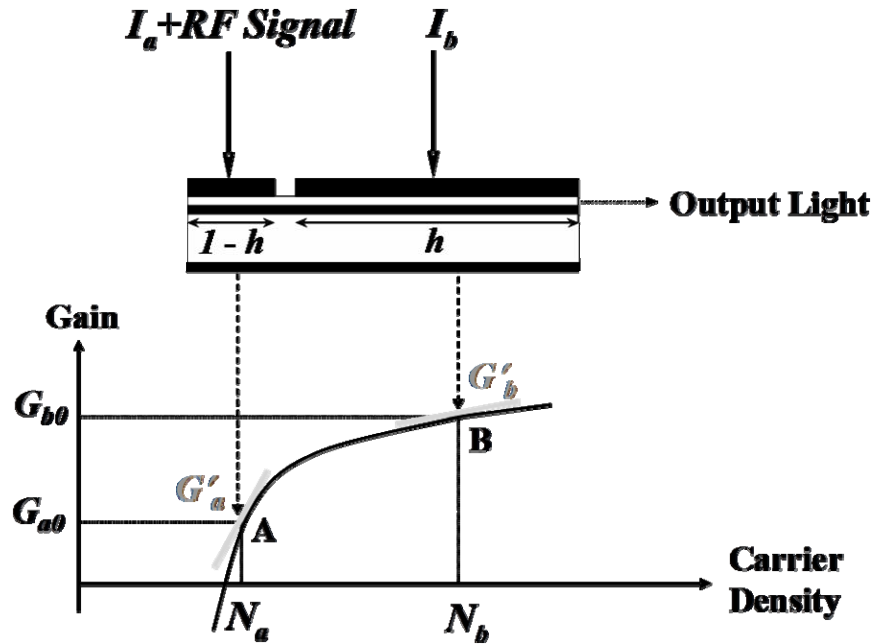
Fig 3.1 Schematic of the two-section gain-lever semiconductor laser, with the variation of modal gain versus carrier density.

The schematic of a gain-lever laser is shown in Fig. 3.1. This two-section configuration is formed by two separate contacts which are electrically isolated from each other. The two sections can be biased individually even though they always share one continuous optical cavity. The length of each section can be chosen freely. In the "normal" gain-lever configuration, the short section, which is denoted as section (a), acts as modulation section where the small RF modulation signal is applied on the top of a small DC pump level. While the longer section, denoted as section (b), is usually DC biased only. The h is

the fractional length of the section (b). To operate the gain-lever device, section (a) is biased at low gain level and section (b) is biased at a high gain level. This allows section (b) to control the above-threshold operation of the whole device.

The total gain of the two-section laser is provided by both section (a) and (b). Before threshold is reached, the total modal gain from the two sections is used to overcome the cavity loss. When the device is biased above threshold, the total modal gain is firmly clamped to the threshold gain, which is determined by the cavity loss. There is always an insignificant amount of spontaneous emission coupled into the laser mode, which can be neglected here. Above threshold, all injected carriers will be converted to an optical output and will not contribute to gain. The gain clamping effect is one of the physical foundations of the gain-lever device. The nonlinear relationship between gain and carrier density of QW and QD devices is another physical basis to understand the gain-lever device functionality. In Fig 3.1, the gain versus carrier density and the principal configuration of the gain-lever device is shown. Due to the step-function-like density of states, the ground state gain can't linearly increase with injected carrier density. Instead, it shows a saturation trend in the high carrier density region as shown in Fig. 3.1. Section (a) is usually biased at the low gain region where the differential gain is larger, and section (b) is biased at the high gain region and the differential gain is smaller. When a small modulation signal is applied to section (a), a small change on carrier density is observed.   This is a result of current fluctuation and leads to a change of optical gain in this section. Correspondingly, the gain in section (b) has to be changed in order to keep

the device clamped at the threshold value. Due to the nonlinear relationship between gain and carrier density, there has to be a larger change in carrier density in section (b) to compensate for the gain change. Consequently, the photon density is changed as well. As a result, a larger modulated output can be realized by small signal modulation. This is called the "gain-lever" effect.

3.2.2 Motivation for gain-lever QD lasers

As discussed above, the gain-lever effect requires gain clamping and a sub-linear relationship between gain and carrier density. In low dimensional media, such as a QW, this can be approximated by gain vs. injected current density. It is expected that active media with a stronger gain saturation will generate a more significant gain-lever effect. The optical gain is directly related to the density of states of the semiconductor material. In QD materials, the density of states is a delta-function-like. Compared with QW materials, which have a step-function-like density of states, QD active regions show a stronger gain saturation effect and larger differential gain. In Fig 3.2, a typical optical gain versus current density relationship for QW and QD materials is shown. The maximum optical gain is smaller for QD due to the decreased density of state [11]. The optical gain increases faster in QD and then saturates quickly. The differential gain of QD device in the un-saturated region is larger than that of the saturated region. Consequently, the devices fabricated from QD materials are promising to demonstrate the enhanced gain-lever effect.
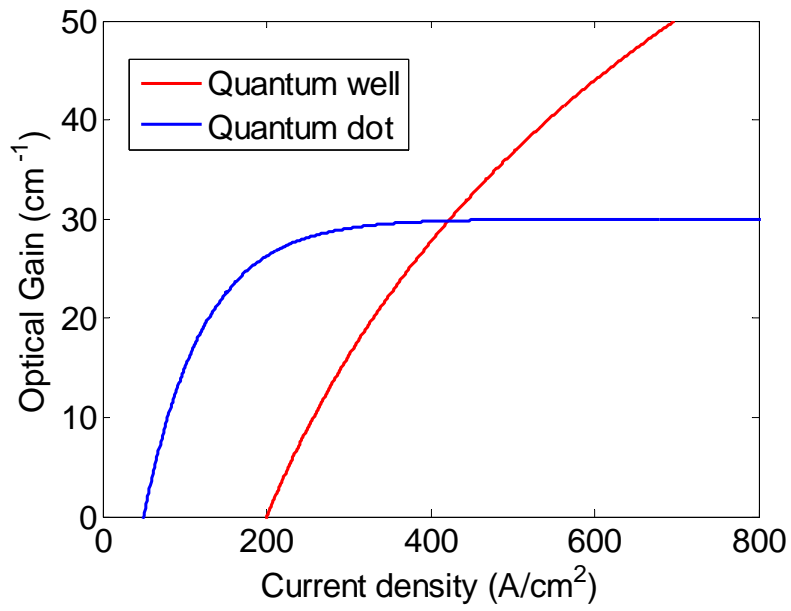
Fig 3.2 The typical optical gain versus current density relationship for QW and QD materials. QW is logarithmic and the QD demonstrates exponential saturation.

3.3. Novel response model of gain-lever lasers

3.3.1 The rate equation of gain-lever lasers

In this section, we will derive a new response model for the two section gain-lever laser. The response equation of single section semiconductor laser was introduced in the previous chapter is shown below:

$$|M(f)|^2 \propto \frac{1}{1+(2\pi f \tau_c)^2} \frac{f_r^4}{\left[(f_r^2 - f^2)+(\frac{\gamma}{2\pi})^2 f^2\right]} \qquad (3.1)$$

In Fig 3.3, the experimental data for the modulation response of a two-section gain-lever QD device is plotted along with the curve fitted data using Eqn (3.1). The response curve is taken when the current density of the two sections are different. It can be seen that the conventional single-section response function cannot describe the modulation response of the two-section laser very well. The first obvious drawback is the damping rate. For a single section laser, the laser is biased uniformly across the device, there is only one damping rate needed in a single section model, but in a two-section structure, the modulation section and gain sections are always biased at different levels, so that the differential gains of the two sections are different. Thus two damping rates are required in the new model to describe the modulation response of the two-section device. In order to derive the rate equations of the two-section laser, two separate differential equations are needed to represent the fluctuation in carrier density during intensity modulation. If we assume that the photon density is uniform in both the gain section and

modulation sections, then only one rate equation is required for the photon density fluctuations. This assumption is valid because the two sections share the same optical cavity even though they are under different carrier injection level. The electrical isolation between the two sections only introduces some minor loss in the cavity and will not effect the traveling of the optical wave. Therefore the rate equations of a two-section device can be expressed as [4]:

$$\frac{dN_a}{dt} = \frac{I_a}{eV} - \frac{N_a}{\tau_a} - G_a S \qquad (3.1)$$

$$\frac{dN_b}{dt} = \frac{I_b}{eV} - \frac{N_b}{\tau_b} - G_b S \qquad (3.2)$$

$$\frac{dS}{dt} = \Gamma[G_a(1-h) + G_b h]S - \frac{S}{\tau_p} \qquad (3.3)$$

Where S is the photon density, $I_{a,b}$, $N_{a,b}$, $\tau_{a,b}$ and $G_{a,b}$ are the injection current, carrier density, carrier lifetime and unclamped material gains (the group velocity is included implicitly) respectively, Γ is the optical confinement factor, τ_p is photon lifetime, h is the fractional length of the gain section, and d is the thickness of the active region. To simplify the problem, we do not include the non-linear gain or any carrier transport effect in the above rate equations at this time. The small signal solution of the equations is done by first making the following substitutions:

$$I_{a,b}(t) = I_{a0,b0} + i_{a,b}e^{j\omega t}$$

$$N_{a,b}(t) = N_{a0,b0} + n_{a,b}e^{j\omega t}$$

$$G_{a,b} = G_{a0,b0} + G'_{a0,b0}n_{a,b}e^{j\omega t}$$

$$S(t) = S_0 + se^{j\omega t}$$

where $G'_{a0} = \dfrac{dG_a}{dN_a}$ and $G'_{b0} = \dfrac{dG_b}{dN_b}$ are the differential gains for the two sections. The steady-state components are indicated by the subscript "0" and small AC components are indicated by lower case letters. It should be noted here that G(N) is actually a sub-linear function of the carrier density but not a linear function. However, in a steady-state operation point, it can always be linearized locally, where G_0' is the differential gain at the steady-state carrier density. For the small-signal carrier density variation n, G_0' is a constant because the steady-state carrier density is clamped to the steady state value of N_0.

By substituting the small signal quantities into rate equations (3.1) through (3.3) and setting the steady-state quantities to zero, the resulting small signal equations are:

$$j\omega n_a = \frac{i_a}{ed} - \frac{n_a}{\tau_a} - G_{a0}s - G'_{a0}n_a S_0 \qquad (3.4)$$

$$j\omega n_b = \frac{i_b}{ed} - \frac{n_b}{\tau_b} - G_{b0}s - G'_{b0}n_b S_0 \qquad (3.5)$$

$$j\omega s = \Gamma S_0 \left[G'_{a0}n_a(1-h) + G'_{b0}n_b h \right] + \Gamma s \left[G_{a0}(1-h) + G_{b0}h \right] - \frac{s}{\tau_p} \qquad (3.6)$$

Under the steady-state condition, equation (3.3) gives the relation between G_{a0}, G_{b0} and the threshold gain of the entire device (G_0)as [4]:

$$\Gamma[G_{a0}(1-h) + G_{b0}h] = \Gamma G_0 = G_{th} = \frac{1}{\tau_p} \qquad (3.7)$$

where G_{th} is the threshold modal gain. The second and third term of the RHS of Eqn. (3.6)

can be canceled by substituting Eqn. (3.7) into (3.6). Since in section "b", there is no

modulation current, the expression of n_b can be obtained as

$$n_b = \frac{-G_{b0}s}{j\omega + 1/\tau_a + G'_{a0}S_0} \tag{3.8}$$

By substituting Eqns. (3.4) and (3.8) into (3.6), the small signal response equation is

derived to be:

$$\frac{s(\omega)}{j_a(\omega)} = \frac{\Gamma G'_{a0}S_0(1-h)(j\omega+\gamma_b)/ed}{-j\omega^3 - (\gamma_a+\gamma_b)\omega^2 + iA_1\omega + A_2} \tag{3.9}$$

Where A_1, A_2 are:

$$A_1 = \Gamma S_0\left[G_{a0}G'_{a0}(1-h) + G_{b0}G'_{b0}h\right] + \gamma_a\gamma_b \tag{3.10}$$

$$A_2 = \Gamma S_0\left[G_{a0}G'_{a0}\gamma_b(1-h) + G_{b0}G'_{b0}\gamma_a h\right] \tag{3.11}$$

γ_a and γ_b are defined as the damping rates in sections (a) and (b) respectively, that are

given by:

$$\gamma_a = \frac{1}{\tau_a} + G'_{a0}P_0 \qquad (3.12),$$

$$\gamma_b = \frac{1}{\tau_b} + G'_{b0}P_0 \qquad (3.13)$$

The first term in the damping rate expression is inversely proportional to the spontaneous

lifetime and the second term represents the inverse stimulated lifetime. When $h = 0$, Eqn.

(3.9) is reduced to the modulation equation for single-section lasers.
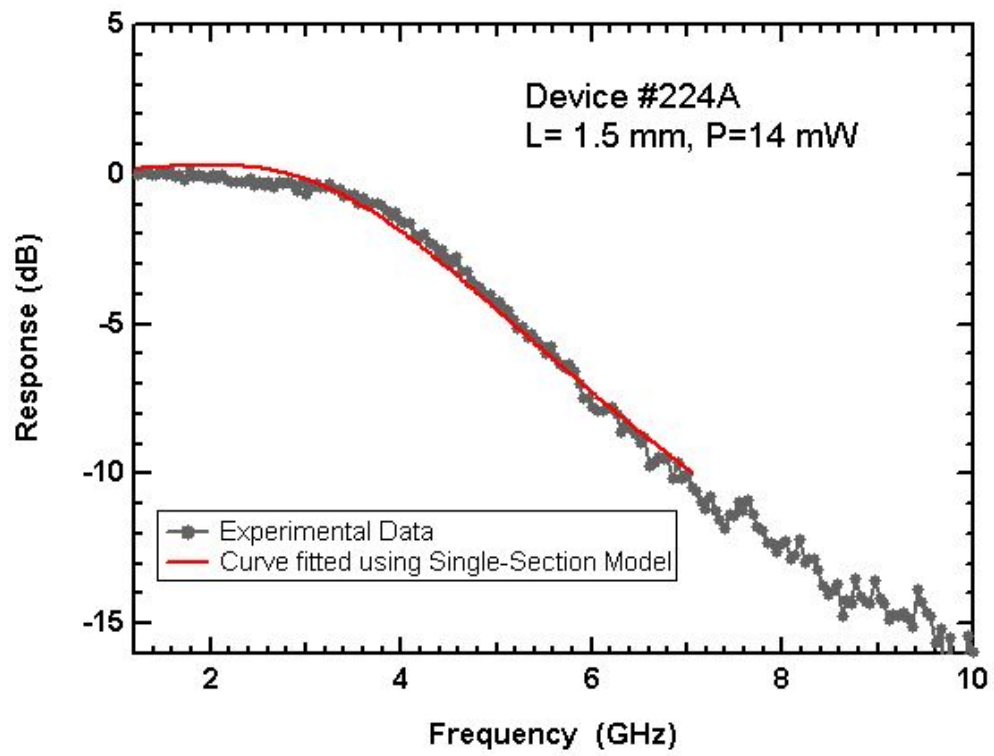
Fig 3.3. The modulation response of a two-section gain-lever QD laser, with curve-fitted data using a single section model.

3.3.2 Modulation efficiency enhancement

The gain-lever modulation efficiency or intensity modulation (IM) enhancement can be obtained by taking the ratio of the modulation response from Eqn (3.9) to that of the uniformly biased device (when $h = 0$) at the low frequency limit, which is give by [4]:

$$\eta = \frac{s/i_a}{s/i_a \big|_{h=0}} = \frac{\gamma_b}{(1-h)\gamma_b R + (h\gamma_a/g)Q} \tag{3.14}$$

where $R = G_{a0}/G_0$, $Q = G_{b0}/G_0$, and $g = G'_{a0}/G'_{b0}$.

In Fig (3.4), the evolution of the modulation efficiency enhancement versus the fractional length h is plotted for differential gain values equal to 5, 10 and 15. For these plots it is assumed that the modulation section is biased at $R = 0.2$. The modulation efficiency enhancement increases monotonically with h when the other parameters are kept unchanged. Therefore, the two-section device with a shorter modulation section is preferred to achieve a high efficiency enhancement.

In the case of a very short modulation section (h close to 1), which is the device configuration we use in this experiment, Eqn (3.14) is reduced to

$$\eta = \frac{\gamma_b G'_{a0} G_0}{\gamma_a G'_{b0} G_{b0}} \approx \frac{\gamma_b G'_{a0}}{\gamma_a G'_{b0}} \tag{3.15}$$

When the gain-lever device is biased at a low level, the photon density inside the cavity is small. As a result, the spontaneous damping term dominates the damping rate. Therefore, Eqn. (3.15) is reduced to

$$\eta \approx \frac{\tau_a G'_{a0}}{\tau_b G'_{b0}} \qquad\qquad (3.16)$$

Thus, under low power level operation, the modulation efficiency enhancement comes from two aspects: the ratio of the carrier lifetimes and the ratio of differential gains of the two sections. Consider a lower photon density situation in which $\tau_a = \tau_b$ is a valid approximation. The IM efficiency enhancement can be realized when G'_{a0} is larger than G'_{b0}. As we discussed above, the operation point of the gain-lever device is chosen where the modulation section is biased at a high differential gain level and the gain section is biased at a low differential gain level. Eqn (3.16) also indicates that even at the point where differential gain is equivalent for both sections, like bulk semiconductor optical devices, one can still obtain a substantial improvement on modulation efficiency. This can be achieved by decreasing the carrier lifetime in the gain section. For this situation, the gain section needs to be biased at a very high level in order to decrease the carrier lifetime, which is not good for device reliability. It should be mentioned that lower photon density (lower optical power) is not desired since the relaxation frequency and 3-dB bandwidth are small. The more interesting case is at high power levels. Also, it can be seen that the differential gain ratio is actually key factor for gain-lever laser due to the sublinear relationship between gain and current density.

Another extreme case of Eqn (3.15) is where the device is operated at very high power. The inverse stimulated lifetime term dominates the damping rate since the photon density is very large (the relaxation frequency is proportionally to photon density). This

reduces Eqn. (3.15) to:

$$\eta \approx \frac{G'_{b0}G'_{a0}G_0}{G'_{a0}G'_{b0}G_{b0}} = \frac{G_0}{G_{b0}} \approx 1 \qquad (3.17)$$

Clearly, there will be no modulation efficiency improvement at very high photon density and large pumping asymmetry condition. The stimulated damping rate counteracts the original low photon density IM efficiency enhancement. It is suggested that the gain-lever device should operate at a relatively high power level to take advantage of the improved modulation efficiency and maintain a useful level of output power simultaneously where $g = G'_{a0}/G'_{b0}$
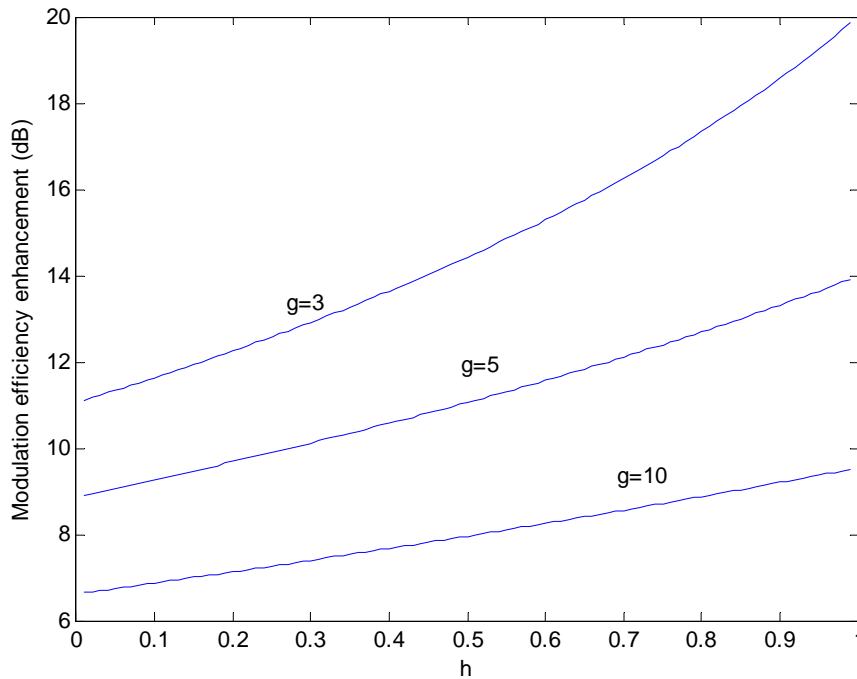

Fig 3.4 Calculated modulation efficiency enhancement vary with h for g =3, 5 and 10,

3.4 IM efficiency enhancement of p-doped gain-lever QD lasers

As we discussed in chapter 2, p-doped devices show high differential gain and possibly higher bandwidth. In this section, the small signal modulation response on p-doped gain-lever QD lasers is studied. The wafer structure and static performance of p-doped devices is presented first, followed by a new gain model for QD devices is introduced to extract the gain profile. Finally, the 8-dB modulation efficiency enhancement of the gain-lever QD laser is presented using a RF modulation experimental setup.

3.4.1 Wafer structure and device fabrication

The layer structure of the device under investigation is illustrated in Fig 3.5. It was grown by the Molecular Beam Epitaxy (MBE) growth technique on n^+ (001) GaAs substrate. The active region consisted of 10 stacks of self-assembled InAs QDs covered by 5-nm $In_{0.15}Ga_{0.85}As$ QWs in a DWELL structure. The QW layers are separated by 33-nm GaAs spacers. A δ-doped layer is added in the GaAs barrier 10 nm above each QW. The device's cladding layers are step-doped 1.5-μm thick $Al_{0.35}Ga_{0.65}As$. The entire laser structure is then capped with a 400-nm thick heavily carbon-doped GaAs. 50-μm-wide broad area (BA) lasers were fabricated and then cleaved to different cavity lengths to extract the *G-J* relationships. The two-section devices were fabricated by the standard RWG processing technique. The two (multi)-section device processing flow chart is shown in Fig. 3.6. The electrical isolation between each section was achieved by proton

implantation.   The length of each isolated section is 0.5-mm.

GaAs	C: 2e19	400nm
Al$_{.35}$Ga$_{.65}$As/GaAs	C: 3e18	20nm
Al$_{.35}$Ga$_{.65}$As	C: 1e18	1000nm
Al$_{.35}$Ga$_{.65}$As	C: 5e17	500nm
GaAs		9nm
GaAs	C: 5e17	10nm
GaAs		14nm
In$_{.15}$Ga$_{.85}$As quantum well		5nm
InAs quantum dots		
GaAs		33nm
Al$_{.35}$Ga$_{.65}$As	Si: 5e17	500nm
Al$_{.35}$Ga$_{.65}$As	Si: 1e18	1000nm
GaAs/Al$_{.35}$Ga$_{.65}$As	Si:3e18	20nm
GaAs	Si:3e18	500nm
GaAs substrate		

10X

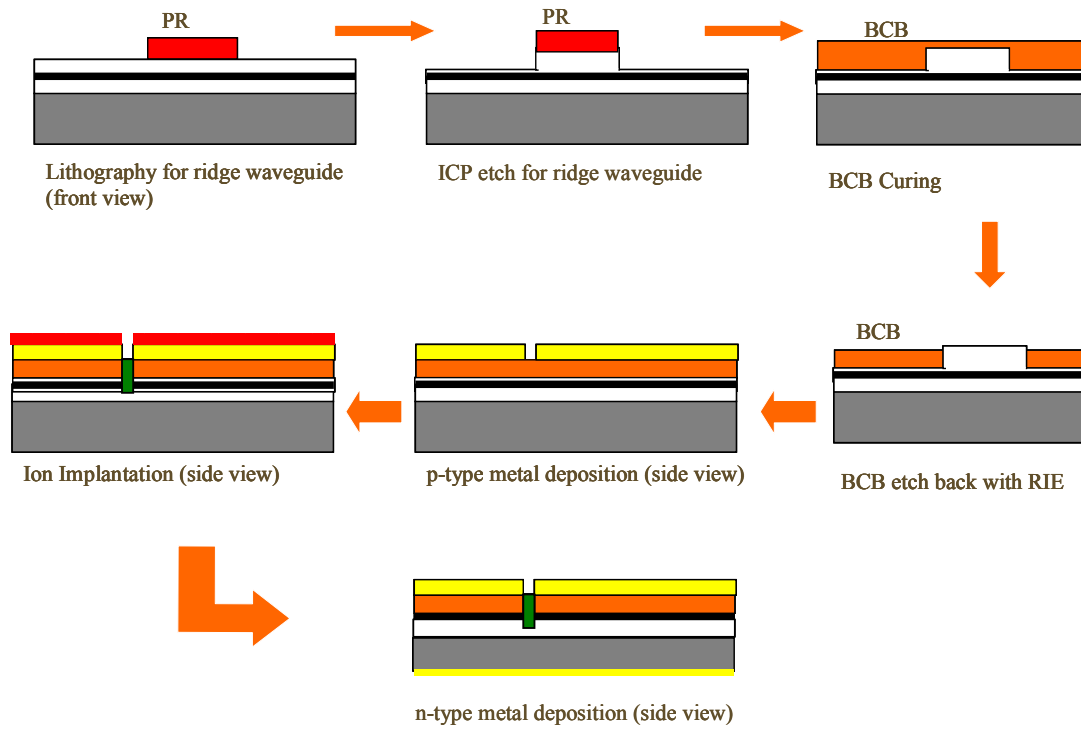Fig 3.5. The layer structure of p-doped QD lasers (wafer #224)

Fig 3.6. The flow chart of the processing procedure for a two (multi)-section device.

3.4.2 Static characterization and gain measurement

To perform the gain-lever experiment, it is important to get the whole spectrum for the relationship between gain and current density. This relationship can be extracted based on the fact that threshold modal gain is equal to the total cavity loss at threshold. Therefore, the broad area lasers were fabricated first for this purpose. The BA samples were cleaved to different cavity length ranging from 0.75-mm to 2.8-mm. The lasers with cavity length shorter than 0.75-mm cannot sustain ground state lasing. The cavity dependent output power versus current (*P-I*) characteristics were measured under pulsed condition (500-ns pulse width and 1% duty cycle). We can calculate the differential quantum efficiency η_d from this set of *P-I* curves. The trend of $1/\eta_d$ versus cavity length is shown in Fig 3.7. The internal loss, α_i, and the internal quantum efficiency, η_i, can be calculated by fitting the data to *$1/\eta_d = 1/\eta_i$ [1- $\alpha_i L/\ln(R)$]*, where *L* is the cavity length and *R* = 0.32 is the reflectivity of the laser facets. From the calculation, η_i is 48% and the internal loss α_i is 2.7 cm^{-1}.
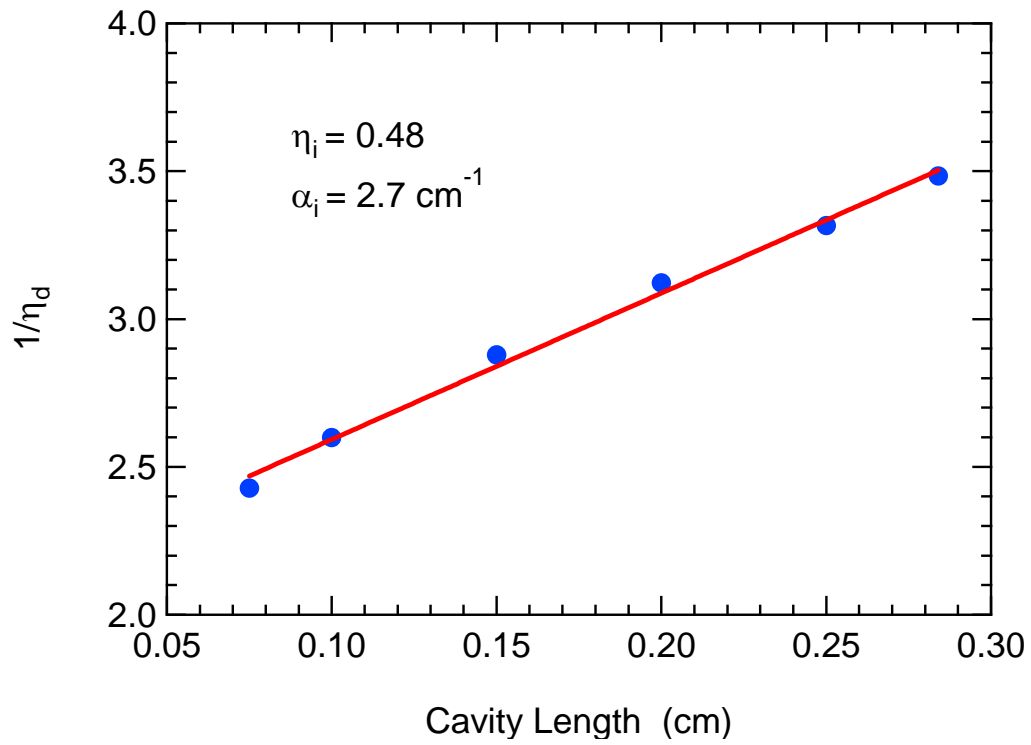
Fig 3.7. The evolution of inverse differential efficiency with cavity length for p-doped QD lasers. The internal loss and injection efficiency are calculated by curve fitting the measured data.

The threshold modal gain can be calculated using the fact that modal gain is equal to the sum of internal loss and mirror loss at the threshold, i.e.: $G_{th} = \alpha_i + \alpha_m$. The mirror loss is expressed as $\alpha_m = \frac{1}{L}\ln\left(\frac{1}{R}\right)$. The calculated G_{th} with threshold current density is plotted in Fig. 3.8 and the experimental data is expressed as blue dots.

The data in Fig 3.8 offers the isolated points for the *G-J* relationship. However, in the two-section configuration, the currents of each section could be far beyond the current range shown in this figure. Thus we need an accurate gain model to curve fit this experimental data. Equation (3.18) is an empirical gain model, which was used to describe the *G-J* behavior in QD materials [9]:

$$G = G_{max}\left(1 - \exp(-\ln 2(\frac{J_{th}}{J_{tr}} - 1))\right) \qquad (3.18)$$

where G_{max} is the maximum gain for ground state lasing in the quantum dot media, and J_{th}, J_{tr} are the threshold and transparency current densities, respectively. This model works well with un-doped QD materials. In Fig 3.8 (a), the calculated modal gain data is plotted as a function of threshold current density, and the data is curve-fitted using Eqn (3.18). It was found that the exponential threshold current density dependence in this mode did not fit very well with the experimental data. The exponential model was originally derived for un-doped QD materials, which have a stronger gain saturation effect. However, for this p-doped QD material, this model overestimates the saturated gain. In Ref [13], a more accurate model with square-root current density dependence is derived by our research group, which is given by:

$$G(J) = G_{\max} \left[\frac{2\sqrt{J}}{\sqrt{J} + \sqrt{J_{tr}}} - 1 \right] \qquad (3.19)$$

It is known that the optical gain is a function of wavelength. Eqn (3.19) is actually a function of the peak gain varied with current density. In a real device, the gain peak shifts towards shorter wavelengths (blue shift) as current density increases due to the band filling effect. Using Eqn (3.19) the calculated G_{th}-J data was curve-fitted and the maximum gain and transparency current density were calculated to be 86 cm^{-1} and 232 A/cm^2 respectively.   It can be seen that Eqn (3.19) fits better than the exponential model. As we discussed in chapter 2, the p-doped technique helps increase the ground state gain in QD media. The data in the Fig 3.8 also shows that the gain does not saturate strongly as expected in the current range we investigated.
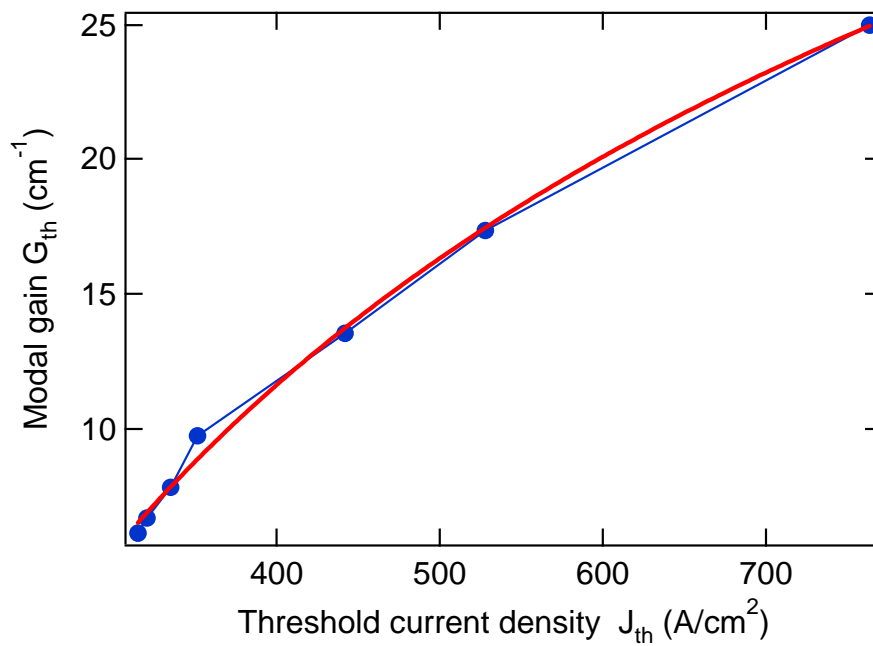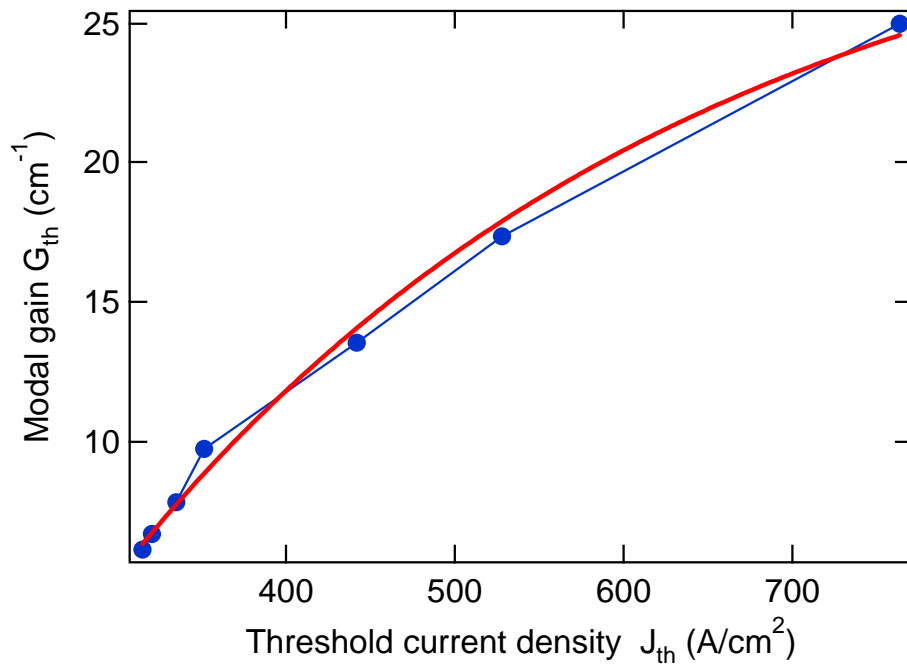
Fig. 3.8 The calculated threshold modal gain as a function of threshold current density. The data was curve-fitted using (a) the exponential gian model, (b) new square-root gain model.
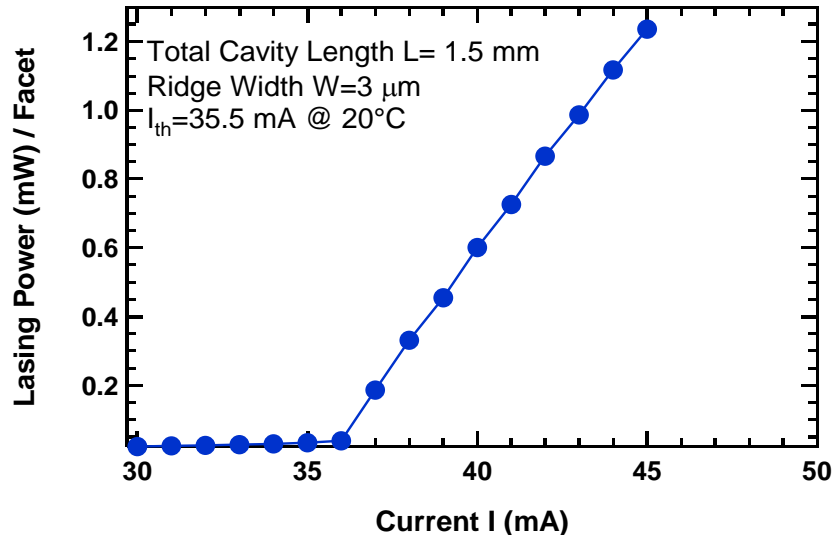
3.4.3 Experiment setup for dynamic characterization of p-doped gain-lever QD laser

The total length of the two-section laser diode for the intensity modulation experiment is 1.5-mm long. The modulation section is 0.5-mm long so that the fractional length h is 2/3. Figure 3.9 shows the P-I characteristics of the device under uniform bias. The threshold current is 35.5 mA at 20 ^{0}C. The lasing spectrum is shown in Fig 3.10. The peak wavelength is 1.29 μm.

The high-speed experimental setup is shown in Fig 3.11. It is similar to the one we described in chapter 2, except two precision current sources are used to provide the current flow into each section. A DC signal and small microwave signal are applied to section (a) from port 1 of the HP8722D vector network analyzer. The section (b) is DC biased only. The coupling efficiency to the lensed fiber was measured to be 10%.

It is necessary to clarify some terms we use to describe the gain-lever experimental results. The modulation efficiency enhancement was measured by comparing the modulation responses for uniform and asymmetric pumping cases. Uniform pumping means the two sections have equal current density. For the specific device we tested, the cavity length ratio of the two sections is 2:1, so the uniformly pumping requires the bias current ratio to be 2:1 as well. The asymmetric pumping situation corresponds to the case where the two sections have different current densities. The criteria to determine the current ratio of the two sections is to keep the output power similar to the uniformly pumping case. In our actual experiment, the current modulated section is set first, then

the current of the gain section was adjusted to maintain an output power equal to the uniformly pumped case. Equal output power is considered to be the valid experimental condition for comparisons of different pumping scenarios

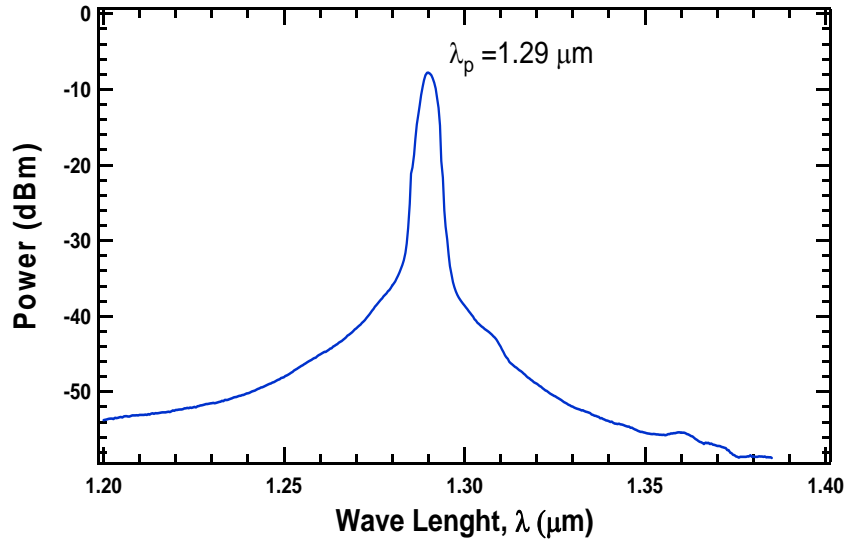. Fig 3.9 P-I curve of the gain-lever device under the uniformly biased condition

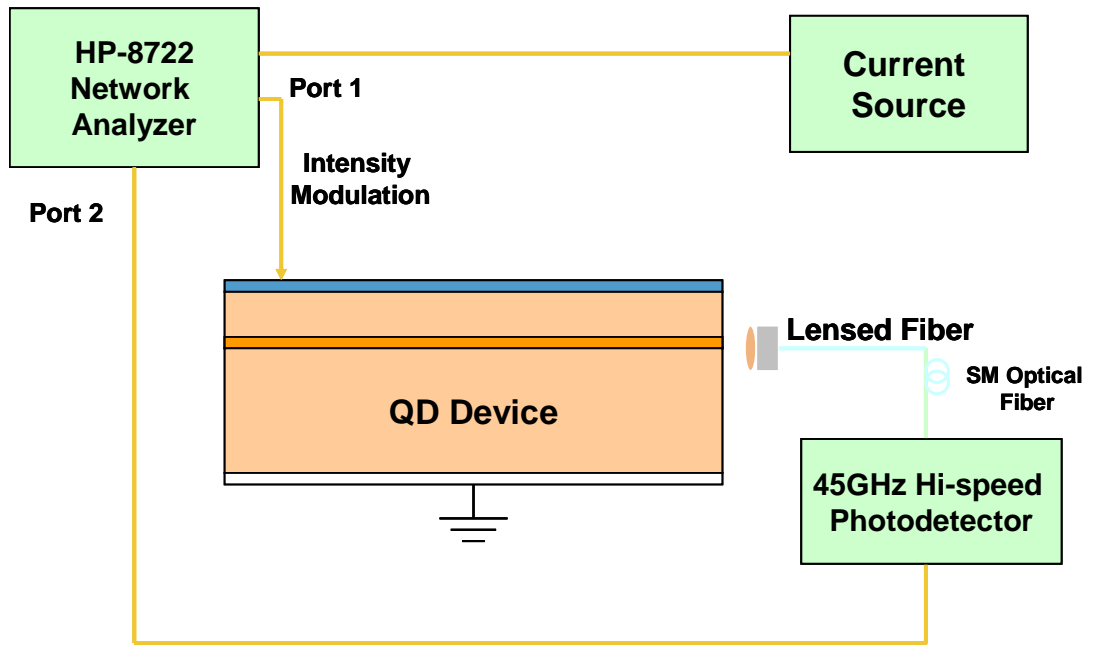Fig 3.10 The lasing spectrum of the p-doped gain-lever RWG laser.

Fig 3.11 The high-speed testing set up for dynamic characterization of the p-doped gain-lever laser.

The modulation response of the uniformly-pumped gain-lever laser was examined first to get a general idea of the effect of the spontaneous damping term compared to the total damping rate for this p-doped QD laser. Fig 3.12 gives response curves at different biases. The highest current is 120-mA which is about 4 times greater than threshold. The experimental data was curve-fitted using the single-section response equation. The maximum relaxation frequency is calculated as 5-GHz. Based on curve fitted data, the evolution of damping rate, γ_{uni}, versus the square of relaxation frequency f_r is plotted in Fig 3.12. The relationship between γ_{uni} and f_r is

$$\gamma_{uni} = \frac{1}{\tau_c} + 4\pi f_r^2 \tau_p = \frac{1}{\tau_c} + G'S . \tag{3.20}$$

Using the above equation, the experimental data in Fig 3.12 is curve-fitted and the variation of γ_{uni} as a function of f_r^2 is plotted in Fig 3.13. The linear relationship between γ_{uni} and f_r^2 indicates that the gain saturation effect is not significant in this testing range. This is consistent with our gain data in the last section. Fig 3.13 shows how the damping rate, especially the stimulated damping component, varies with the power level. Although the stimulated damping component is no more larger than about 4X greater spontaneous damping rate for the uniformly pumping case, it should be realized that the stimulated damping rate could be dominant due to high photon density or differential gain in the asymmetric pumping case. The y-axis intercept of the fitting curve is the spontaneous damping rate (8-GHz, which corresponds to 0.12-ns differential carrier lifetime). This value is relatively small compared to the typical carrier lifetime values of 1-ns for

un-doped lasers. However, since τ decreases with doping level, this value is not too surprising in our p-doped QD device.
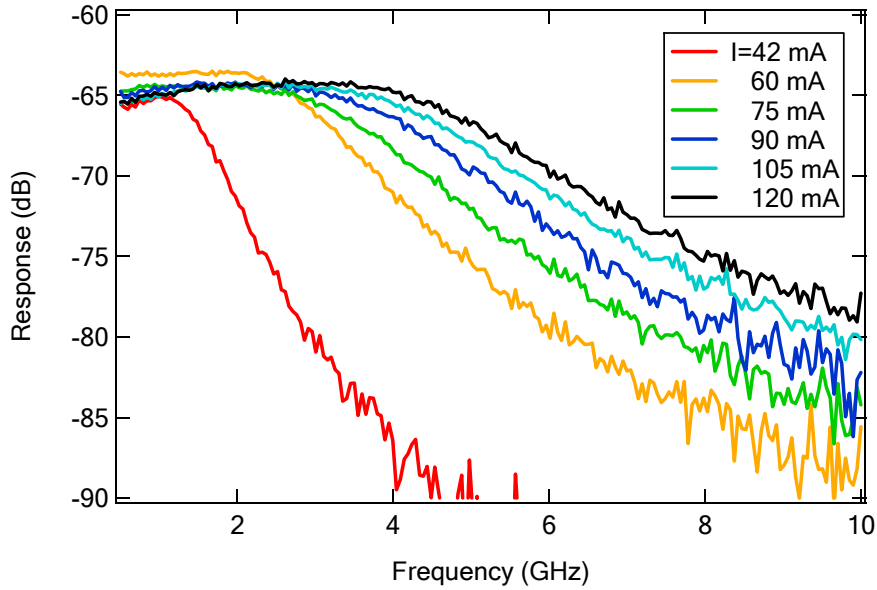

Fig 3.12 Modulation response of the gain-lever laser under different uniformly bias condition.
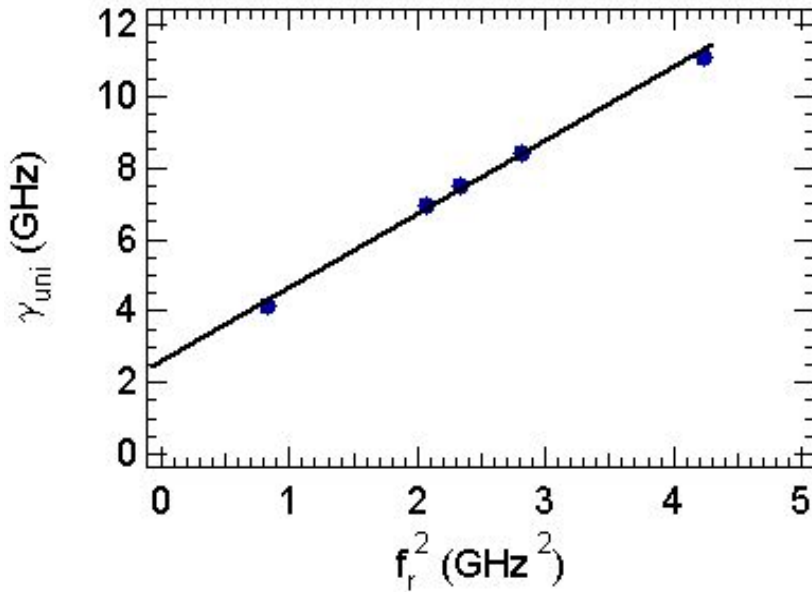

Fig 3.13. The evolution of damping rate with relaxation frequency under different uniformly bias conditions.

3.4.4 Modulation efficiency enhancement

It is known that the gain-lever device should be biased in such a way that the differential gain ratio is as large as possible to obtain the largest modulation efficiency enhancement. The differential gain ratio can be calculated according to Eqn. (3.19) after G_{a0} and G_{b0} were determined from Fig 3.8. It is clear that G_{a0} and G_{b0} are two fundamental parameters to characterize this asymmetric pumping scenario. Following Moore's and Lau's convention, we choose G_{a0}, for this work.

The G_{a0} and G_{b0} can be calculated as

$$G_{a0}(J_a) = \frac{G_a(J_a)G_{th}}{hG_b(J_b)+(1-h)G_a(J_a)} \tag{3.20}$$

$$G_{b0}(J_b) = \frac{G_b(J_b)G_{th}}{hG_b(J_b)+(1-h)G_a(J_a)} \tag{3.21}$$

where, G_{a0} and G_{b0} are the threshold gains in section (a) and sections (b) respectively, G_a and G_b are the unclamped gains in the respective sections, G_{th} is the threshold gain of the device.

In Fig. 3.14, modulation responses for the uniform and asymmetric pumping cases at a constant power level of 3 mW/facet are plotted. A modulation efficiency enhancement as high as 8-dB was observed for our two-section QD device when the shorter section was biased such that $G_{a0}/G_{th}=0.56$ (note: $G_{a0}/G_{th}=1$ corresponds to the uniform pumping case). As G_{a0} increases, G_{a0}' decreases. According to Eqn. (3.17), the modulation efficiency enhancement decreases as shown in the figure.

According to previous research on the modulation efficiency enhancement [7]:

$$\eta = \frac{\eta_{gainlever}}{\eta_{uniform}} = \frac{\tau_a}{\tau_b} \frac{G'_{a0}}{G'_{b0}}$$

(3.22)

Making the reasonable assumption that the carrier lifetimes τ_a and τ_b are very close to each other, the 8-dB improvement in η corresponds to a differential gain ratio of 2.5. This value is surprising to us since it is not as large as being expected. The reason is that in p-doped material, the gain does not saturate strongly with current density, as pointed out in the last section.
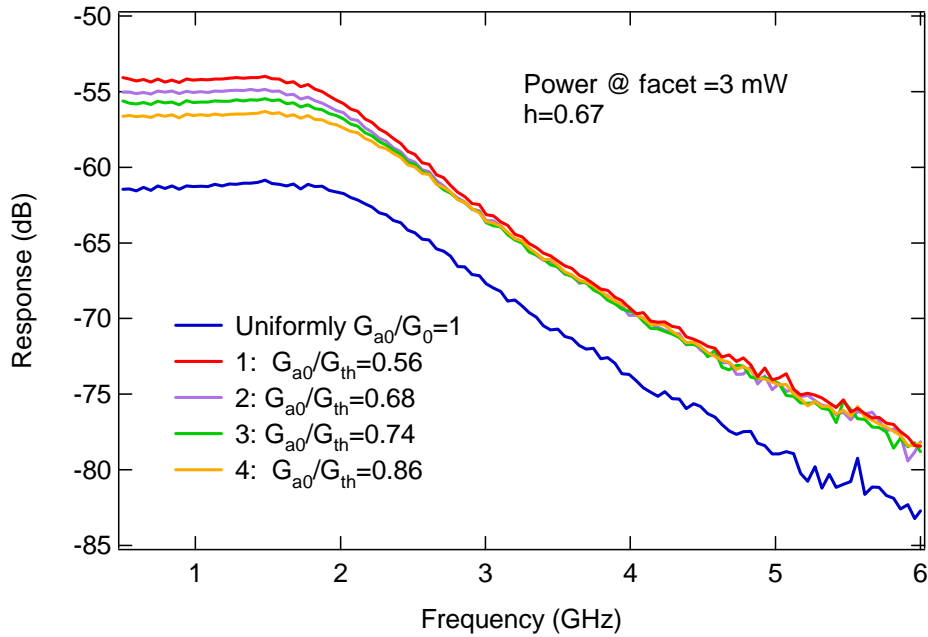
Fig 3.14 Modulation efficiency enhancement of p-doped QD gain-lever lasers

3.5 Relative modulation response equation

The relative modulation response function can be derived by taking Eqn (3.9) normalized to the response at zero frequency and is expressed as follows:

$$R(\omega) = \frac{\dfrac{s(\omega)}{i_a(\omega)}}{\dfrac{s(0)}{i_a(0)}} = \frac{A_2(i\omega + \gamma_b)}{-i\omega^3 - (\gamma_a + \gamma_b)\omega^2 + i\omega A_1 + A_2} \tag{3.23}$$

It is difficult to obtain a clear physical understanding of the above equation, without applying some approximations. Considering the low photon density case is not desired, the device in our experiment is always running at relatively high power level. Thus, a high photon density approximation can be made.

Under a high photon density approximation, the spontaneous damping term is neglected in γ_a and γ_b. The parameters A_1 and A_2 are reduced to

$$A_1 = \omega_r^2 + \gamma_a \gamma_b \tag{3.24},$$

$$A_2 = \frac{\gamma_b \gamma_a}{\tau_p} \tag{3.25}$$

where frequency ω_r is derived from Eqn (3.9) under the high frequency approximation. It is given by:

$$\omega_r = \left(\Gamma P_0 \left[G_{a0} G'_{a0}(1-h) + G_{b0} G'_{b0} h \right]\right)^{\frac{1}{2}} \tag{3.26}$$

Substituting Eqns (3.24) and (3.25) into Eqn (3.23), the new relative modulation response equation in terms of frequency is given by:

$$|R(f)|^2 = \frac{\left(\dfrac{\gamma_a \gamma_b}{8\pi^3 \tau_p}\right)^2 \left(1 + \left(\dfrac{2\pi f}{\gamma_b}\right)^2\right)}{\left[\dfrac{\gamma_a \gamma_b}{8\pi^3 \tau_p} - (\gamma_a + \gamma_b)\dfrac{f^2}{2\pi}\right]^2 + \left[\left[f_r^2 + \dfrac{\gamma_a \gamma_b}{4\pi^2}\right]f - f^3\right]^2} \qquad (3.27)$$

where the relation $\omega = 2\pi f$ is used.

In Eqn (3.27), the denominator has three poles instead of the usual two associated with a single section laser diode as shown in Eqn (3.1), which has a quadratic dependence of frequency. Also, in this equation the two different damping rates are included to describe the damping effect on the resonance frequency and modulation response. We use this equation to fit the same experiment data that is used in Fig 3.1, the result is shown in Fig 3.15. Now we can specify that this response curve is taken at $G_{a0}/G_0 = 0.5$ and the power level is 14-mW (a very high power level). Apparently, the new model fits better with two-section response than a single section model.
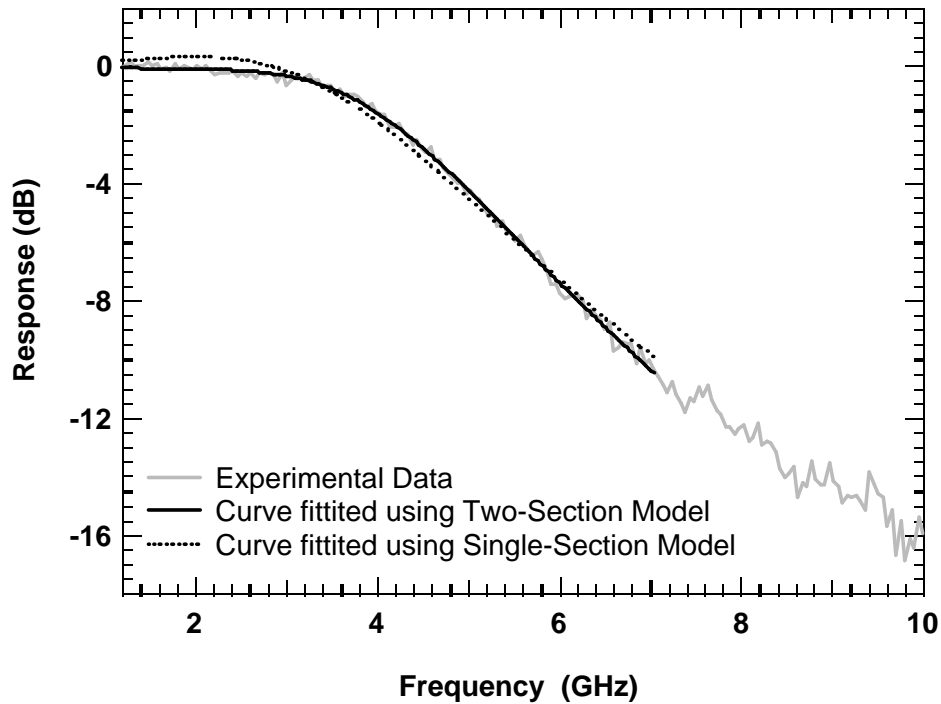
Fig 3.15. The modulation response of a two-section gain-lever QD laser, with fitted curves using single-section and new two-section model

One may argue that good curve-fitting comes from an additional damping rate fitting parameter in the two-section model, to further explore the validation of the relative two-section response equation, in Fig 3.16 and 3.17, the dependence of the normalized resonance frequency f_r/f_{r0} on the normalized gain in the modulation section is plotted. The f_r are curve-fitted by the one-section model and new two-section model, respectively. The normalized resonance frequency is obtained by the relaxation frequency of the asymmetrically pumped case over the relaxation frequency of the uniformly pumped case. Fig 3.16 shows the data that is curve fitted using the single-section model, while Fig 3.17 presents the two-section model data. The normalized gain is calculated in the same

method. Due to the parabolic shape of the p-doped QD gain characteristics, the gain-differential gain product in the two sections must staying relatively constant, i.e., $G_{a0}G'_{a0} \cong G_{b0}G'_{b0}$. According to Eqn (3.21), the resonance frequency f_r, should remain almost the same for different pumping values at a constant output power. This trend can be verified by the data in Fig 3.17. However, in Fig 3.16, the sudden increase in the resonance frequency for values below $G_{a0}/G_{th} = 0.4$ seems to be totally unphysical. We can conclude that for values below $G_{a0}/G_{th} = 0.4$, the conventional single-section model is no longer valid for the two-section configuration.
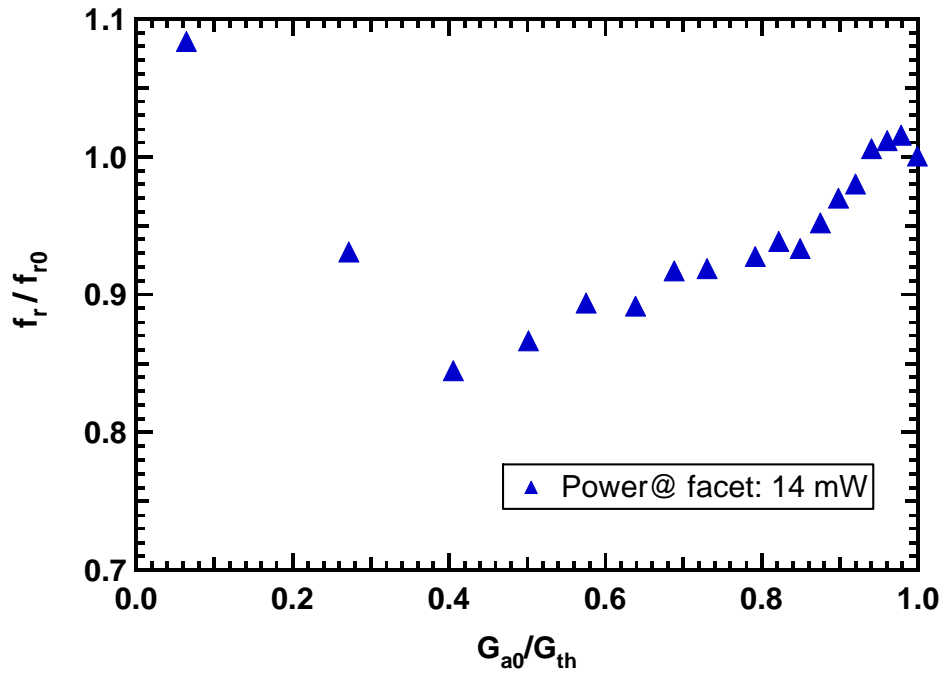
Fig 3.16 Normalized resonance frequency as a function of normalized gain in the modulation section plotted based on the one-section model.
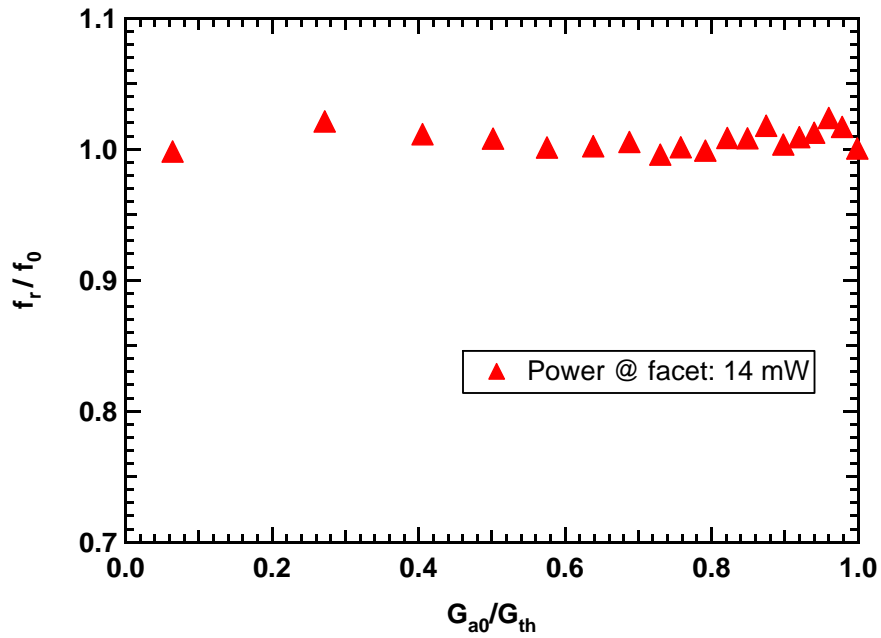
Fig 3.17 Normalized resonance frequency as a function of normalized gain in the modulation section plotted based on the new two-section model

3.6 Bandwidth enhancement in the gain-lever device

Above all, we just talked about IM modulation efficiency enhancement. The question that is put forth at the beginning of this chapter still remains: Is it possible that the gain-lever device can improve the modulation bandwidth?

We know under the high photon density approximation that the stimulated emission contribution to the damping rate is dominant. The ratio of the damping rate is equal to the ratio of the differential gain, i.e:

$$g = \frac{G'_{a0}}{G'_{b0}} = \frac{\gamma_a}{\gamma_b} \qquad (3.28)$$

Consider an extreme asymmetrically pumped case, in which $G_{a0} = 0$ and h $\approx$1. Under this circumstance, the gain section occupies most of the device. The damping rate of the gain section, γ_b, is approximated as the damping rate of the uniformly pumped device, then we have

$$\gamma_b \approx \gamma_{uni} = Kf_r^2 \qquad (3.29)$$

where K is the damping rate over the square of the relaxation frequency for a single section device. Eqn.(3.27) can be modified to be

$$|R(f)|^2 = \frac{\left(\frac{gKf_r^4}{2\pi}\right)^2 \left(1 + \left(\frac{2\pi f}{Kf_r^2}\right)^2\right)}{\left[\frac{gKf_r^4}{2\pi} - \frac{(g+1)}{2\pi}Kf_r^2 f^2\right]^2 + \left[\left[f_r^2 + \frac{gK^2 f_r^4}{4\pi^2}\right]f - f^3\right]^2} \qquad (3.30)$$

where g is the ratio of the differential gain. In Fig 3.18, the calculated response curve is

plotted based on the above equation for g =1, 3, 5 and 7. g =1 corresponds to the uniformly pumping case. As g increases, the 3-dB bandwidth increases as well. The relaxation frequency is set at 4-GHz, which is a typical value for our p-doped device. The similar bandwidth enhancement was also demonstrated by two-section DFB lasers [14].

Although p-doped devices can provide a larger ground state gain and differential gain, it is not favorable for gain-lever applications, which needs strong gain saturation to produce a larger differential gain ratio instead of the absolute value of differential gain. Therefore, larger IM efficiency and 3-dB bandwidth enhancement are hard to achieve. In the next section, we will continue to study the gain-lever device using an un-doped QD laser, a higher improvement is expected.
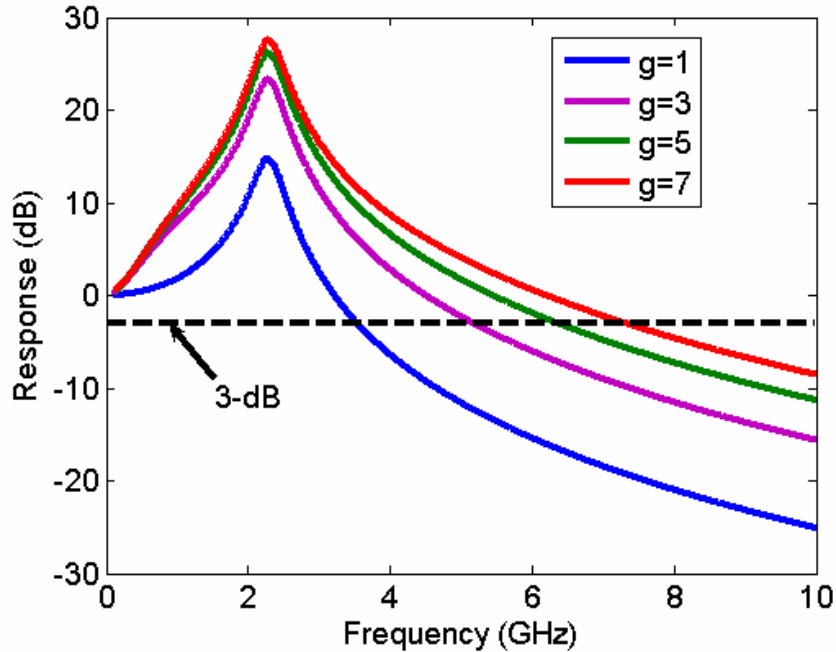

Fig 3.18 The simulation of the modulation responses of a gain-lever QD laser which is under extreme asymmetrically pumping.

3.7 Un-doped gain-lever QD device

3.7.1 Gain measurement using the segmented-contact method.

In previous sections, we introduced an accurate gain versus current density relationship which is critical to perform the gain-lever experiment. There are several methods to measure the *G-J* relation in semiconductor lasers. Hakki and Paoli first determined the gain from the depth of modulation, i.e., the peak-to-valley ratio, in the amplified spontaneous emission (ASE) caused by the Fabry–Perot resonances of the laser cavity. For an appropriate evaluation of the gain, the Hakki-Paoli method requires a high wavelength resolution for the measurement system, and it is only accurate below the laser threshold. In previous sections for p-doped devices, due to the issue of device availability, the *G-J* relationship was obtained by measuring the threshold gain of the lasers with different cavity lengths. However, since this involves cleaving and preparing many devices, it is not easy to get an arbitrary point on the *G-J* curve, and we lack the information about the variation of gain with wavelength. In this section, for un-doped QD devices, we use an improved segmented contact method to measure the gain spectra.[15]. This technique does not require high spectral resolution, is compatible with optical fiber butt coupling, and can extract the gain over a wide range of conditions. The added benefit of the multi-section layout is that one can vary the ratio of the modulation and gain section lengths without switching to another device

The principal of segmented contact method is illustrated in Fig. 3.19. The

multi-section device consists of three forward biased sections and an absorber section for eliminating all the back-reflected light. The amplified spontaneous emission (ASE) is measured when the first section, both the first and second section, and all three sections are biased at the same current density. Mathematically, it is expressed as:

$$P_L = \frac{S}{G}\left(\exp(G \cdot L) - 1\right) + I_{leak-1}$$
$$P_{2L} = \frac{S}{G}\left(\exp(G \cdot 2L) - 1\right) + I_{leak-2} \qquad (3.31)$$
$$P_{3L} = \frac{S}{G}\left(\exp(G \cdot 3L) - 1\right) + I_{leak-3}$$

Where G is the net modal gain, S is the pure or un-amplified spontaneous emission intensity, P is the amplified spontaneous emission and L is the length of each section. I_{leak} is the unguided spontaneous emission intensity. Under the assumption that I_{leak} is the same for the different pumping configurations as described above, a simple expression for G is obtained as:

$$G = \frac{1}{L}\ln\left(\frac{I_{3L} - I_L}{I_{2L} - I_L} - 1\right) \qquad (3.32)$$

3.7.2 Wafer structure and device configuration

The un-doped QD devices used in the following set of measurements contain a 10-stack InAs/InGaAs DWELL active region that emits around 1.23-μm. The laser structure was grown by molecular beam epitaxy (MBE) on a (001) GaAs substrate. The multi-section device was fabricated following the same procedure that is described in section 3.3. The length of each section is 0.5-mm and the total length of the device is 7 mm. Fig 3.20

illustrates the schematic of the segmented-contact device layout. The long absorber was achieved by wire-bonding multiple sections together and is used to minimize the back-reflected light.
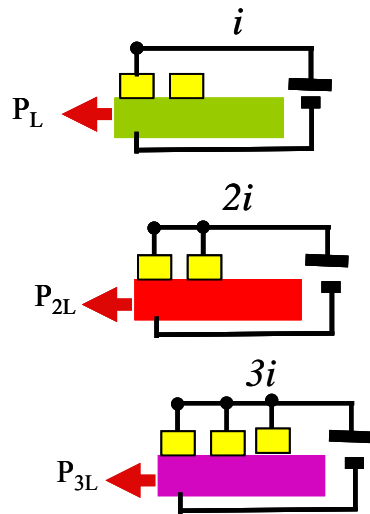
Fig. 3.19 An illustration of the basic operation procedure for the segmented-contact device
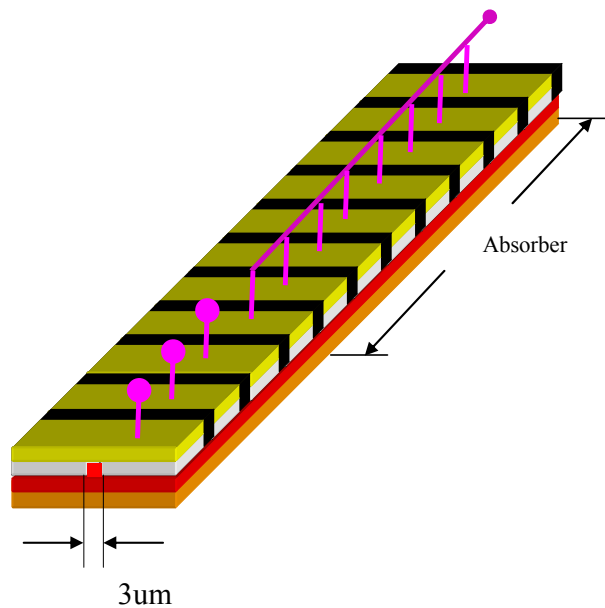
Fig 3.20. Schematic of the segmented contact device. The long absorber is achieved by wire-bonding multiple section together and used to minimize back reflection.

.   Figure 3.21 and 3.22 show the net modal gain data for a 10-stack undoped QD laser media which is used for the gain lever device. It can be seen from Fig. 3.23 that this material shows a unique camel-back gain characteristic under saturation at current densities higher than 18 mA/section (equivalent to 1200 A/cm^2). In other words, the difference in the maximum gain between the ground state and excited states is very small. Figure 3.24 show the *G(J)* curves of the ground and excited states by tracking the gain at a lasing wavelength of 1236-nm and 1172-nm, respectively. Both curves saturate at approximately 10.5-cm^{-1}. Compared with p-doped samples, this un-doped sample has smaller ground state gain, but a much stronger gain saturation effect before the peak gain moves to the excited state. Larger modulation efficiency and bandwidth enhancement are expected.
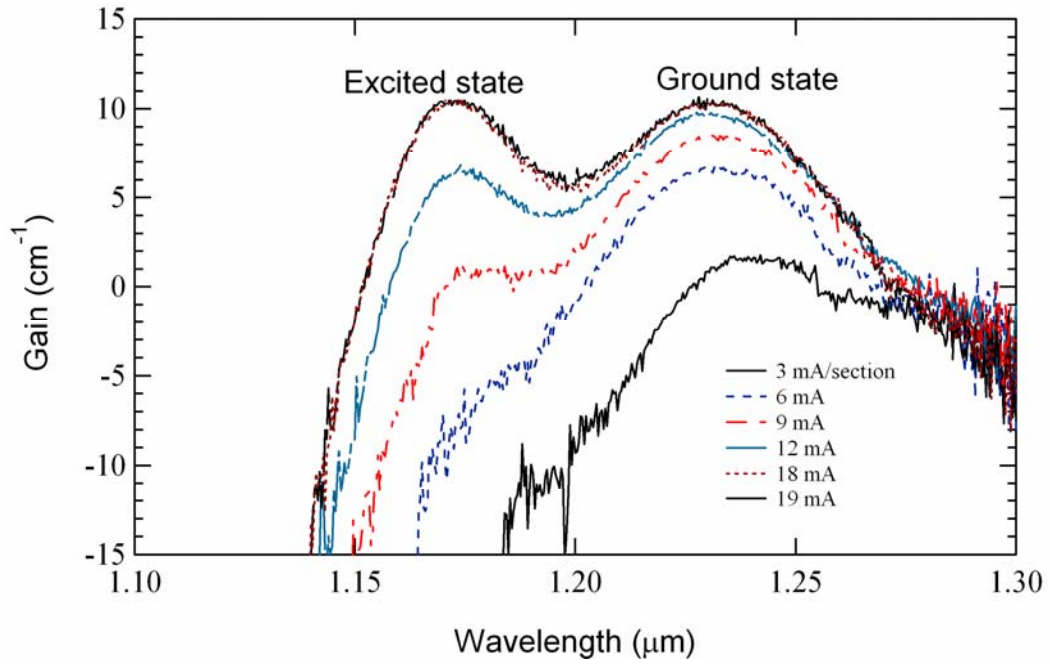
Fig. 3.21. Net modal gain spectra of a 10-stack undoped QD device
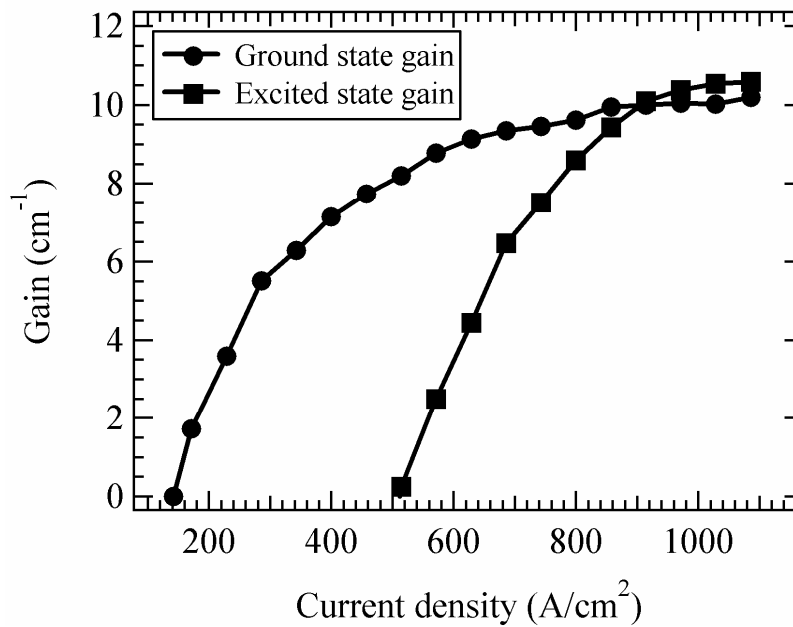
Fig. 3.22 Dependence of the net modal gain on injected current density in the QD device.

3.7.3 AM modulation for the un-doped QD gain-lever laser.

The two devices used for high-speed characterization are 1.25-mm (device #1) and 1.5-mm (device #2) long, and included 5 and 6 electrically-isolated sections, respectively. The *P-I* relations of the uniformly pumped two devices are plotted in Fig 3.23. The benefit of the multi-section layout is that one can vary the ratio of the modulation and gain section lengths without switching to another device. For example, we can use one device to perform the modulation measurement as if we had access to three devices with *h* = 0.83, 0.67, 0.5, respectively (corresponding to modulation section lengths of 0.25-mm, 0.5-mm and 0.75-mm for the 1.5-mm cavity device). The AM modulation experiment is
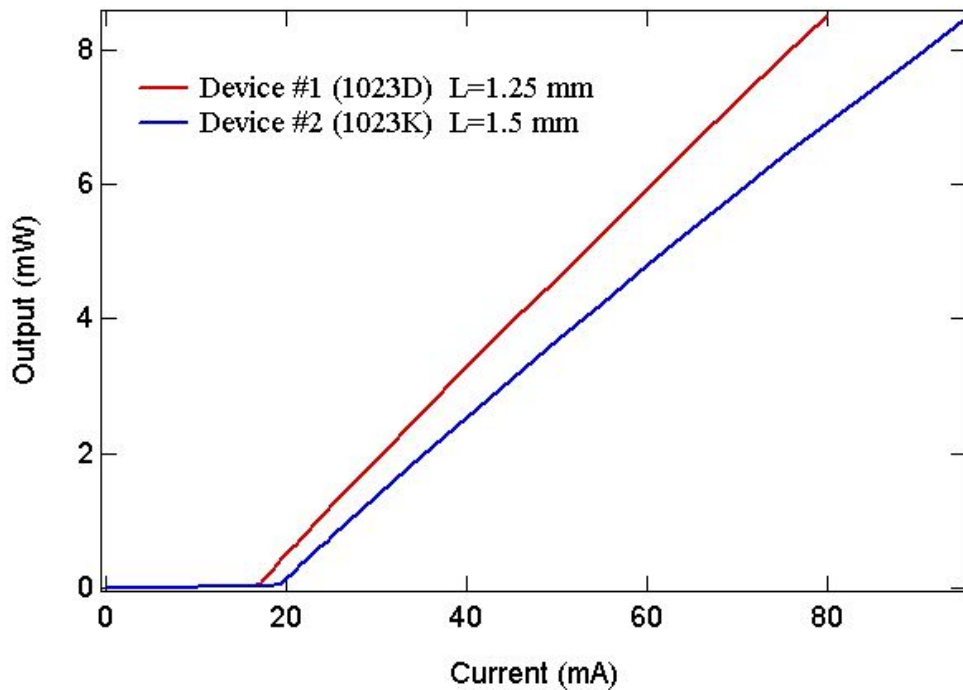
Fig 3.23. L-I characteristics of two uniformly biased un-doped QD devices.

performed on #1 device first when h is chosen as 0.8. In Fig 3.24, modulation responses for the uniform and asymmetric cases at a constant power level of 4.5 mW/facet are plotted. From the solid curve in the figure, a 20-dB modulation efficiency enhancement is obtained for device #1 when the shorter section is biased just below transparency. It is shown that the injected current when the shorter section decreases, the modulation efficiency enhancement rises due to the increasing gain-lever.

Figure 3.25 shows the modulation efficiency enhancement as a function of the normalized gain, G_{a0}/G_0, in the modulation section for different fractional lengths h in device #2. The DC bias current must be changed as the modulation section gets longer in order to keep the same current density applied on the section. As h decreases, it can be seen that the modulation efficiency enhancement increases for a given normalized gain in the modulation section.   The reason for this behavior is that the shrinking gain section must compensate for the larger gain deficit, which in turn enhances the asymmetry between the 2-sections. Since the current density in the modulation section stays roughly constant at a given normalized gain, the gain section must be biased at a higher current density to maintain the same output power. From the G-J curve obtained in Fig. 3.20, the differential gain of section "b" ($G_{b0}^{'}$) is smaller when the current density is high. Therefore, the modulation efficiency enhancement gets larger according Eqn. (3.15). Similarly, for a fixed h value, when the pump level in section "a" is increased (higher normalized gain), the differential gain becomes smaller, so the modulation efficiency enhancement decreases as the normalized gain increases. We should notice here that the

current density of the modulation section cannot be reduced too much. Otherwise, the

bias current of the gain section must be very high to keep the same output power, which

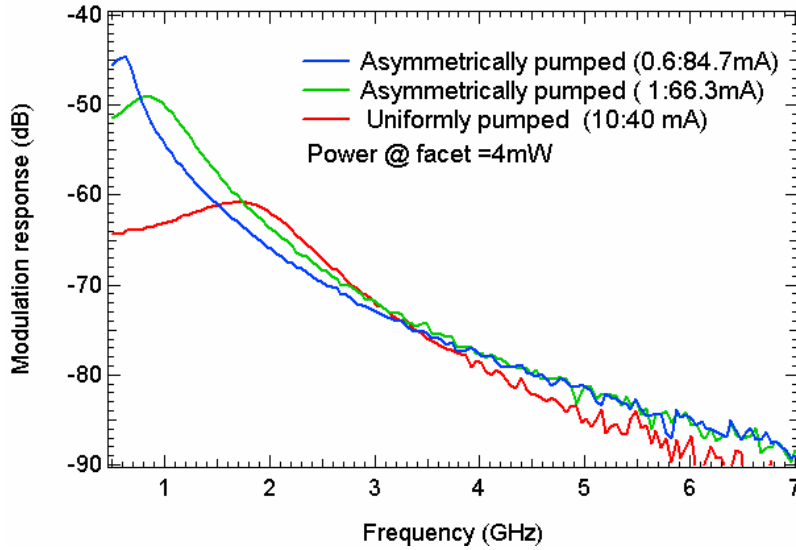may cause an undesirable mode hop to the excited state transition of the quantum dot.

Fig 3.24. The modulation responses for the uniform and asymmetrically pumped cases in the un-doped QD laser.
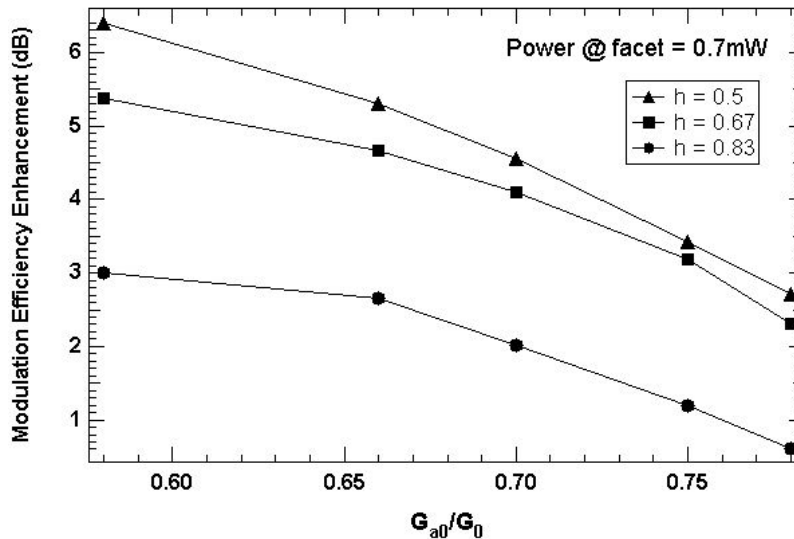
Fig 3.25 The modulation efficiency enhancement depends on normalized gain G_{a0}/G_0 for different h value.

3.7.4 Bandwidth enhancement in the un-doped device

In section 3.6, we derived that for a very asymmetrically pumped condition, the gain-lever device will show a 3-dB bandwidth enhancement. For the p-doped material, since gain does not saturate strongly, the bandwidth enhancement could not be demonstrated. However, from Fig 3.19, we know that this un-doped device will have a very strong gain saturation effect with current density; it is possible to demonstrate a 3-dB bandwidth enhancement based on this material. In Fig 3.26, and Fig 3.27, the modulation response of device #1 is plotted for the uniform and asymmetric cases at a constant power level of 6.5-mW/facet and 7.9-mW/facet, respectively. The damping rates γ_a and γ_b can be obtained by curve-fitting the experimental data using Eqn. (3.20). In Fig 3.26, the ratio of the 3-dB bandwidth of asymmetric pumping to uniform pumping case is 1.3. This is consistent with the theoretical curve of $g = 3$ (shown in Fig.3.18). In Fig 3.27, the damping rate ratio is calculated as 6.75, the 3-dB bandwidth ratio is 1.7. From Fig 3.18, it can be found that when $g = 7$, $f_{3dB}/f_{3dB\_uni} = 2$. Therefore, the gain-lever device can demonstrate bandwidth enhancement for certain conditions. In Fig 2.7, the 3-dB bandwidth of the asymmetrically biased case is about 5-GHz, which is about 3X higher than the relaxation frequency. This is the first time such an enhancement has been reported. However, it should be noticed that the operational requirement is very strict. This will limit the practical application of the device, alternative ways to improve the bandwidth need to be explored.
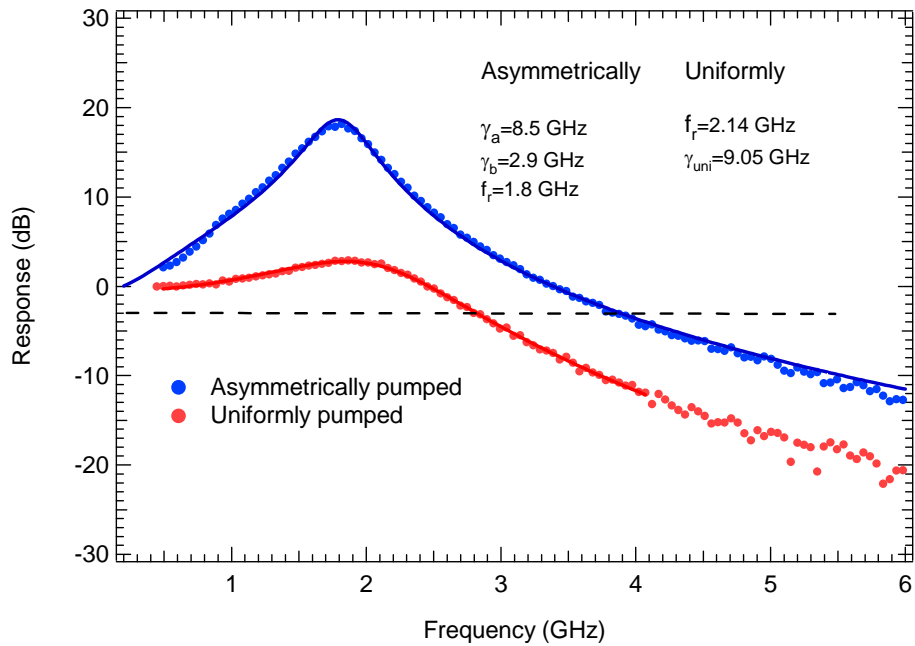
Fig 3.26 The modulation responses for device #1 biased asymmetrically and uniformly. The power lever is 6.5 mW/facet. The ratio of 3-dB bandwidth of the asymmetrically to uniformly pumping case is 1.3.
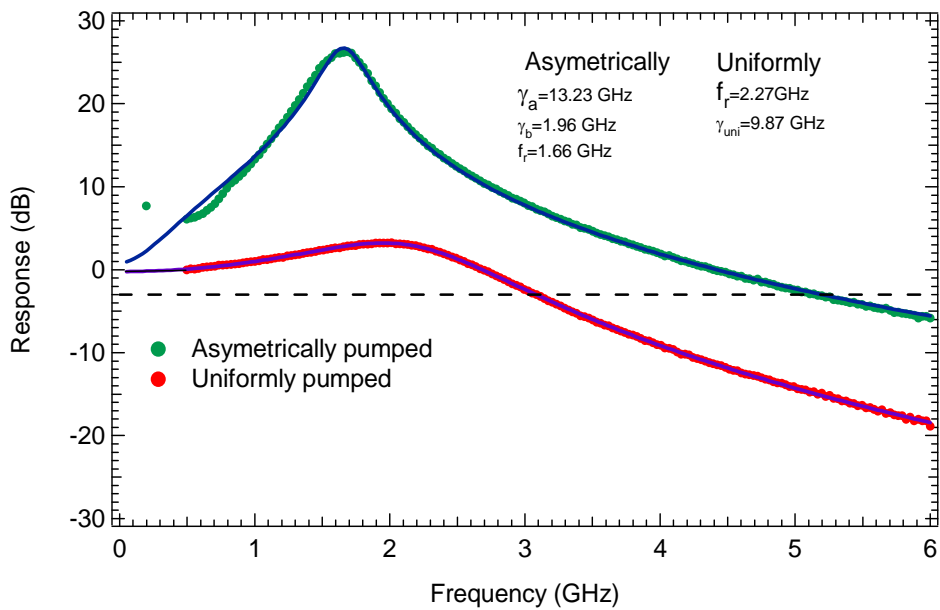
Fig 3.27 The modulation responses for device #1 biased asymmetrically and uniformly. The power level is 7.9 mW/facet. The ratio of 3-dB bandwidth of   the asymmetrically to uniformly pumping case is 1.7.

3.8 Summary

The gain-lever laser is suggested as a promising tool to increase the modulation efficiency of semiconductor lasers in analog optic links. In this chapter, the modulation response characteristics of the gain-lever quantum dot lasers were studied. The 8 dB modulation efficiency enhancement is achieved using p-doping   Due to the stronger gain saturation, the un-doped device shows a higher gain-lever effect over the p-doped device. A 20 dB enhancement of the modulation efficiency is demonstrated by the un-doped QD laser. Under the high photon density approximation, a new relative response equation which includes two damping rates was developed for the two-section gain-lever laser. The new model has three poles in the denominator instead of two like the classical single-section equation.   This allows a better fit with the experimental response curves for the gain-lever lasers. A 1.7X 3-dB bandwidth improvement is theoretically predicted by the new model and realized in the un-doped QD gain-lever laser under an extreme asymmetrically biased condition.   It is also demonstrated for the first time that in a gain-lever laser, the 3-dB bandwidth can be 3X higher than relaxation frequency instead of 1.55X in a typical single section laser.

References:

[1]. K. J. Vahala, M. A. Newkirk, T. R. Chen, "The optical gain lever - a novel gain mechanism in the direct modulation of quantum well semiconductor-lasers"**,** *Applied Physics Letters*; vol. 54, no.25, pp.2506-2508, 1989

[2]. C. P. Seltzer, L. D. Westbrook, H. J. Wicks, "The Gain-Lever effect in InGaAsP/InP Multiple-Quantum Well Lasers",   *Journal of Lightwave Technology*, vol.13, no.2, pp. 283-289, 1995.

[3]. K. Y. Lau, "Passive microwave fiberoptic links with gain and a very low-noise figure, *IEEE Photonics Technology Letters*; vol.3, no.6, p.557-559, 1991

[4]. N. Moore, K. Y. Lau, Ultrahigh efficiency Microwave signal transmission using tandem-contact single quantum well GaAlAs lasers, *Applied Physics Letters*, vol. 55, no.10, p.936-938, 1989

[5]. D. Gajic, K. Y. Lau, "Intensity noise in the ultrahigh efficiency tandem-contact quantum-well lasers", *Applied Physics Letters*; OCT 29 1990; v.57, no.18, p.1837-1839.

[6]. K. Y. Lau, "Broad wavelength tunability in gain-levered quantum-well semiconductor-lasers"**,** *Applied Physics Letters*, vol. 57, no.25, pp.2632-2634, 1990.

[7]. G. Griffel, R. J. Lang, A. Yariv, "Two-section gain-levered tunable distributed-feedback laser with active tuning section" **,** *IEEE Journal of Quantum Electronics*; vol. 30, no.1, pp.15-18, 1994

[8]. K. Y. Lau, "The inverted gain-levered semiconductor-laser direct modulation with

enhanced frequency-modulation and suppressed intensity modulation", *IEEE Photonics Technology Letters*; vol. 3, no.8, pp.703-705, 1991

[9]. K. Y. Lau, "Frequency-modulation and linewidth of gain-levered 2-section single Quantum-well lasers", *Applied Physics Letters*; vol. 57, no.20, pp.2068-2070, 1990

[10]. H. Olesen, J. I. Shim, M. Yamaguchi, M. Kitamura, "Proposal of novel gain-levered mqw dfb lasers with high and red-shifted fm response", *IEEE Photonics Technology Letters*; vol. 5, no.6, pp.599-602, 1993

[11]. L. F. Lester, A. Stintz, H. Li; T. C. Newell, E. A. Pease, B. A. Fuchs, K. J. Malloy, "Optical characteristics of 1.24-mu m InAs quantum-dot laser diodes", *IEEE Photonics Technology Letters*, vol. 11, no.8, pp.931-933, 1998

[12]. Y.–C. Xin, "Long wavelength Quantum Dot Lasers on GaAs: New materials and modal gain analysis", Master Thesis, University of New Mexico, 2002.

[13]. B.W. Hakki and T. L. Paoli, "Gain spectra in GaAs double-Heterostructure injection lasers," *J. Appl. Phys.*, vol. 46, pp. 1299–1305, 1975.

[14]. E. Goutain, J. C. Renaud, M. Krakowski, D. Rondi, R. Blondeau and D. Decoster, "30 GHz bandwidth, 1.55μm MQW-DFB laser diode based on a new modulation scheme", *Electron. Lett.* vol. 32, pp. 896-897, 1996.

[15] Y.-C. Xin, H. Su and L. F. Lester, "Determination of optical gain and absorption of quantum dots with an improved segmented contact method", *SPIE Photonics West Annual. Mtg,*. San Jose, CA, 2005

Chapter 4. Modulation Characteristics of Injection-locked Quantum Dash Lasers

4.1 Introduction

In the previous chapter, we already demonstrated that the gain-lever device can offer bandwidth enhancement under some certain bias conditions. Generally speaking, the gain-lever device is a constraint coupled oscillator system with particular constraints. Two electrically isolated sections share a common optical cavity, thus the phase of two sections are automatically matched, while the photon density related component of the damping rate of the two sections can not vary randomly, especially for the damping rate of the gain section. In order to enhance the bandwidth, the gain-lever device needs to be extremely asymmetrically pumped and operated at very high power level, which is not healthy for device reliability. An injection locking laser, which is another coupled oscillator system, is expected to demonstrate bandwidth enhancement in semiconductor lasers [1-3]. In this chapter, injection locked lasers are studied theoretically and experimentally. The 3-dB bandwidth enhancement is demonstrated using 5-layer quantum dash (QDash) Fabry-Perot (F-P) laser under different injection power ratio and frequency detuning. As much as 4 times bandwidth enhancement was demonstrated. The modulation responses were examined when different lasing modes were injection-locked. It was found that the injection-locking laser can share the same modulation response

function as the with gain lever laser in a particular injection strength range. The relaxation frequency was derived from this equation and the maximum achievable 3-dB bandwidth in the period 1, non-linear regime.

4.2 Basic concept of injection-locking

4.2.1 Injection locking concept and history

The injection locked system can be very complicated but the basic concept is simple. An injection locked system consists of two coupled lasers which are assigned as a master and a slave laser. The schematic of the injection locked laser is shown in Fig 4.1. The light emitted from the master laser is fed into the slave laser. When the frequency of the master laser is very close to the lasing mode of the slave laser, the slave laser can oscillate at the frequency of the master laser and keep a constant phase shift. In strong injection locking system, the master laser is usually a narrow linewidth, tunable high power laser, thus either tunable DFB lasers or an external cavity laser are good candidates.
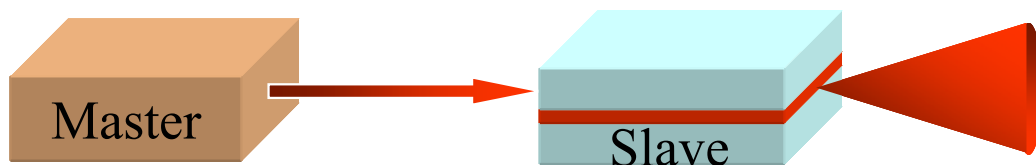
Fig 4.1 The schematic of optical injection locking system.

Figure 4.2 shows typical optical spectra of a free-running (a) and an injection-locked F-P laser (b).   The F-P laser has a multi-mode output under free-running condition with the linewidth of each mode being about 0.1 nm. When the wavelength of the master laser is tuned sufficiently close to one of the lasing modes of free running slave lasers and the injection power is strong enough to create the needed injection ratio, injection-locking can happen. In an injection-locked F-P laser, only the mode closest to the wavelength of the master locks and all other modes are suppressed. The side mode suppression ratio is improved from 5 dB to nearly 40 dB. Also, the linewidth of the injection locked slave laser is reduced to 100 KHz, which is similar to the linewidth of the DFB master laser.

The injection locking between two lasers was reported by Stover and Steier in 1966. It wasn't until 1980 that single-mode injection-locked semiconductor lasers was realized on AlGaAs F-P lasers by Kobayashi and Kimura [4]. Lately, optical phase modulation by direct modulation of the slave laser current has been demonstrated. C. Henry explored the locking range of an InGaAsP laser diode [5]. Many advantages in injection-locked lasers have been achieved including modulation bandwidth enhancement, reduction in non-linearities, reduction in chirp and reduction in relative intensity noise (RIN) [6-8].

4.2.2 Advantages of optical injection locking

The nonlinear coupling between carriers and photons induces the nonlinear distortion in directly-modulated lasers. The distortions are enhanced when the laser is modulated by

signals with frequency components close to the relaxation oscillation frequency. It is also known that the RIN spectrum peak coincides with the laser's relaxation oscillation. The injection locking can increase the relaxation frequency of the slave laser, therefore the nonlinear distortion and RIN in few gigahertz range can be reduced and the spur free dynamic range (SFDR) is increased as well [1, 7]. The frequency chirp is suppressed in injection-locked lasers by preventing the laser wavelength drifting from its CW value [6]. One of the most interesting consequences of injection locking is the improved bandwidth of the laser. The presence of the external light helps reduce the threshold of the locked laser compared to its free running case. Based on the sublinear relationship between gain and carrier density, the differential gain is larger if the threshold carrier density is lower. The single mode operation and reduced linewidth increases the photon density of the locked mode, thus stimulated emission is enhanced and the spontaneous emission is suppressed. All these factors help to increase the bandwidth of injection-locked lasers. An intrinsic modulation bandwidth of 35 GHz was achieved in injection –locked 1.3μm DFB lasers [8], and under ultra strong optical injection condition, the resonance frequency of a 1.55μm VCSEL was enhanced from a free-running frequency of 6 GHz to up to 50 GHz [9]. Jin *et. al* demonstrated a bandwidth of an injection-locked F-P of 10.5 GHz, which was around twice of the free-running laser [10]. The bandwidth enhancement in QDash F-P lasers will be studied experimentally and theoretically in this chapter.
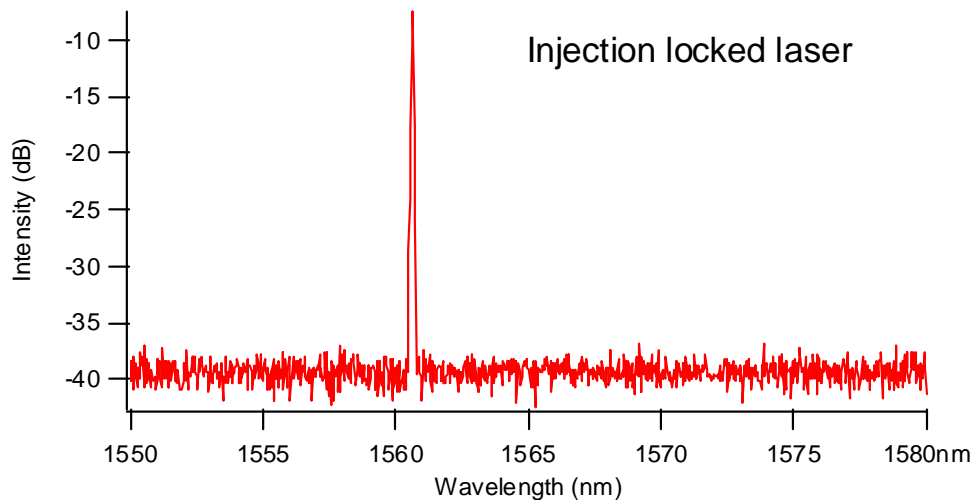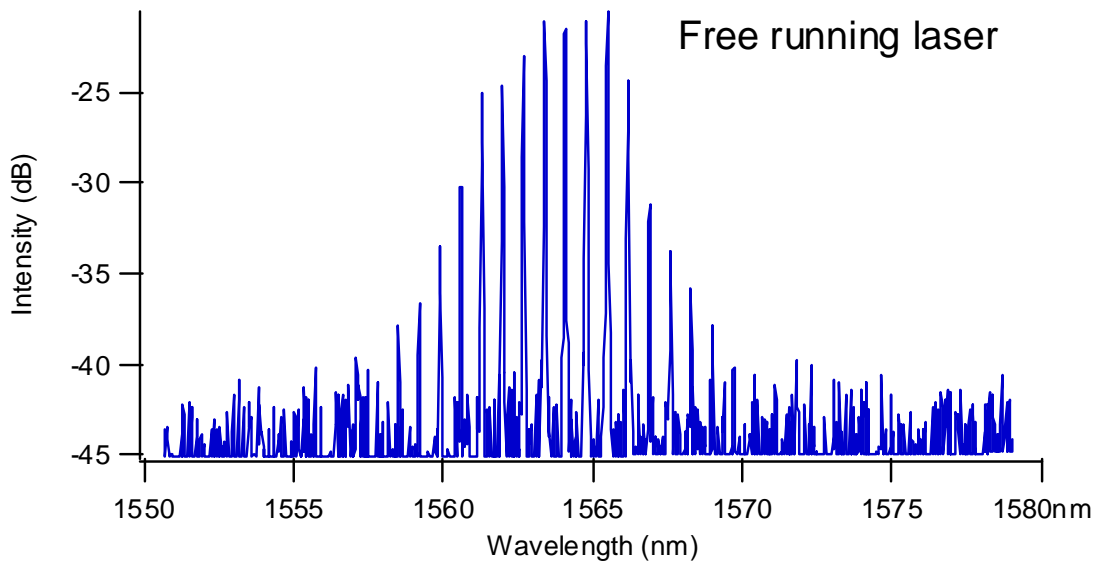
Fig 4.2 The spectra of the free running and the injection locked F-P laser

4.3 Device description and experimental set up

4.3.1 Wafer structure and device fabrication

A quantum dash is similar to a quantum dot but elongated in one direction. QDash lasers have similar optical characteristics with typical QD lasers [11]. The multi-mode F-P QDash lasers used in this work were grown on an n^+-InP substrate. The layer structure is shown in Fig 4.3 and the AFM image of the QDash is shown in Fig. 4.4. The DWELL active region consists of 5 layers of InAs quantum dashes embedded in compressively-strained $Al_{0.20}Ga_{0.16}In_{0.64}As$ quantum wells separated by 30-nm un-doped tensile-strained $Al_{0.28}Ga_{0.22}In_{0.50}As$ spacers. Lattice-matched $Al_{0.30}Ga_{0.18}In_{0.52}As$ waveguide layers of 105 nm are added on each side of the active region. The p-cladding layer is step-doped AlInAs with a thickness of 1.5 μm to reduce free carrier loss. The n-cladding layer is 500-nm thick AlInAs [11]. The laser structure is capped with a 100-nm heavily p-type doped InGaAs layer. Four-micron wide ridge waveguide lasers (RWG) were fabricated with 500 μm cleaved cavity lengths. The threshold current is about 45 mA, with a slope efficiency of 0.2 W/A, and a nominal emission wavelength in the C-band.

| p InGaAs (100 nm) |
| p AlInAs (1.5 µm) |
| $Al_{0.30}Ga_{0.18}In_{0.52}As$ (105 nm) |
| $Al_{0.28}Ga_{0.22}In_{0.50}As$ (15 nm) |
| $Al_{0.20}Ga_{0.16}In_{0.64}As$ (6.3 nm) |
| InAs Dashes |
| $Al_{0.20}Ga_{0.16}In_{0.64}As$ (1.3 nm) |
| $Al_{0.28}Ga_{0.22}In_{0.50}As$ (15 nm) |
| $Al_{0.30}Ga_{0.18}In_{0.52}As$ (105 nm) |
| n^+ AlInAs (500 nm) |
| n InP substrate |

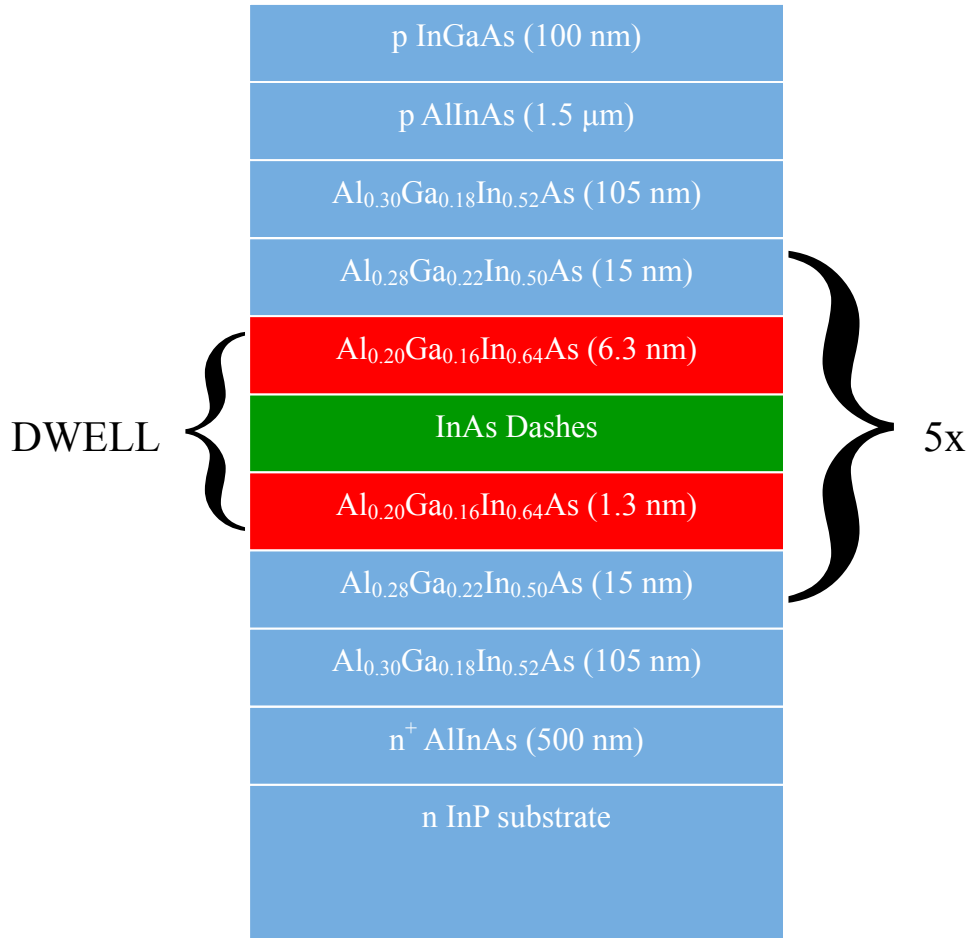DWELL { (Al, InAs Dashes, Al layers) } 5x

Fig 4.3 The layer structure of the 5-stack InAs QDash laser designed for 1550 nm operation.
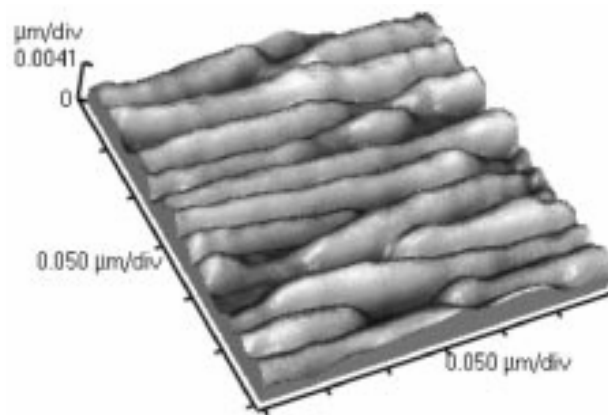
Fig 4.4 AFM image of the QDash layer

4.3.2 Experimental setup

Figure 4.5 is a schematic of the experimental setup used to measure the modulation properties of the injection-locked QDash lasers. The master laser is an HP 8168C tunable laser. The light is amplified by an erbium doped fiber amplifier (EDFA) and then injected into the slave laser. The isolators block undesired light from coupling into the master and slave. The power meter connected to the 1/99 coupler is used to monitor the output power of the master laser. The majority of the master laser's output is injected into the QDash slave laser through one of two branches of 50/50 fiber coupler. Another branch is connected to the test arm. The optical and RF spectra of the slave laser are obtained by an optical spectrum analyzer (OSA) and an HP 8722D network analyzer, respectively. The DC and microwave signal is applied to the slave laser from port 1 of network analyzer. It should be mention here that the polarization status of the traveling light was not fully optimized in this setup even though the a polarization controller was used to provide the highest coupling between master and slave lasers, the optical isolator is not polarization maintaining.

Fig 4.5 Schematic of the injection locking experimental setup

4.4 Bandwidth enhancement of injection locking QDash laser

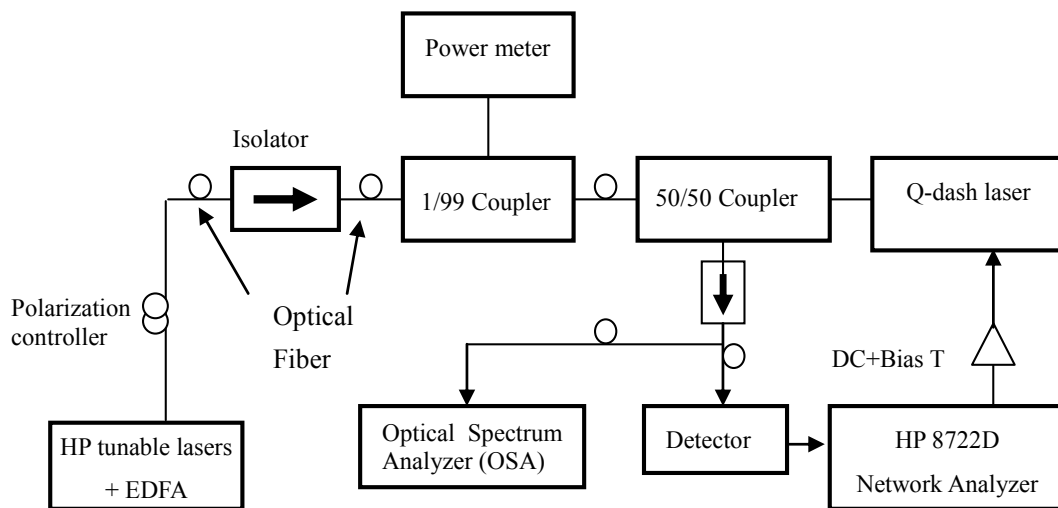The bandwidth enhancement of an injection-locked laser can be achieved by varying the power injection ratio and detuning frequency of the master laser. The power injection ratio is defined as the ratio of the optical power from the master injected into the slave cavity over the total power of the slave laser: $\eta = \dfrac{P_{master}}{P_{slave}}$. The detuning is defined as the difference in wavelength of the master and the slave laser: $\Delta\lambda = \lambda_{master} - \lambda_{slave}$ (correspondingly, the frequency detuning is defined as $\Delta f = f_{slave} - f_{master}$). The variation of the modulation response with different power injection ratio is shown in Fig. 4.6. The slave laser was biased at 60mA, which corresponds to a free-running output power of about 6.5 dBm. The lasing mode was locked at 1563.70 nm. All responses were taken at the zero detuning condition. The 3-dB bandwidth of free-running laser is 3.4 GHz. As the injection power increases, the 3-dB bandwidth increases to a maximum of 8.7 GHz at an injection ratio of -18.2 dB, which is about 2.6 times bigger than the free-running laser.

The F-P laser has a multimode output and each mode has different intensity. It is interesting to examine how the modulation response changes when different lasing modes are locked because of the differential gain varies at different frequencies, then the bandwidth should change. In Fig 4.7, the spectra of 8 locked modes and the corresponding modulation responses are plotted. The mode #1 is the dominant mode in

the free-running condition and from mode 2 to 7, the wavelength of the mode increases.

The responses were taken at zero detuning and a constant overall power injection ratio of

-11.9dB condition. The 3-dB bandwidth of the injection-locked laser is increased to about

11.2 GHz. The bandwidth variation among the side modes is relatively small. Clearly, the

side mode locking variation has no significant impact on modulation response. The power

injection ratio should refer to the total slave power, not the individual mode. The results

also indicate that the differential gain does not vary significantly across the 17 nm
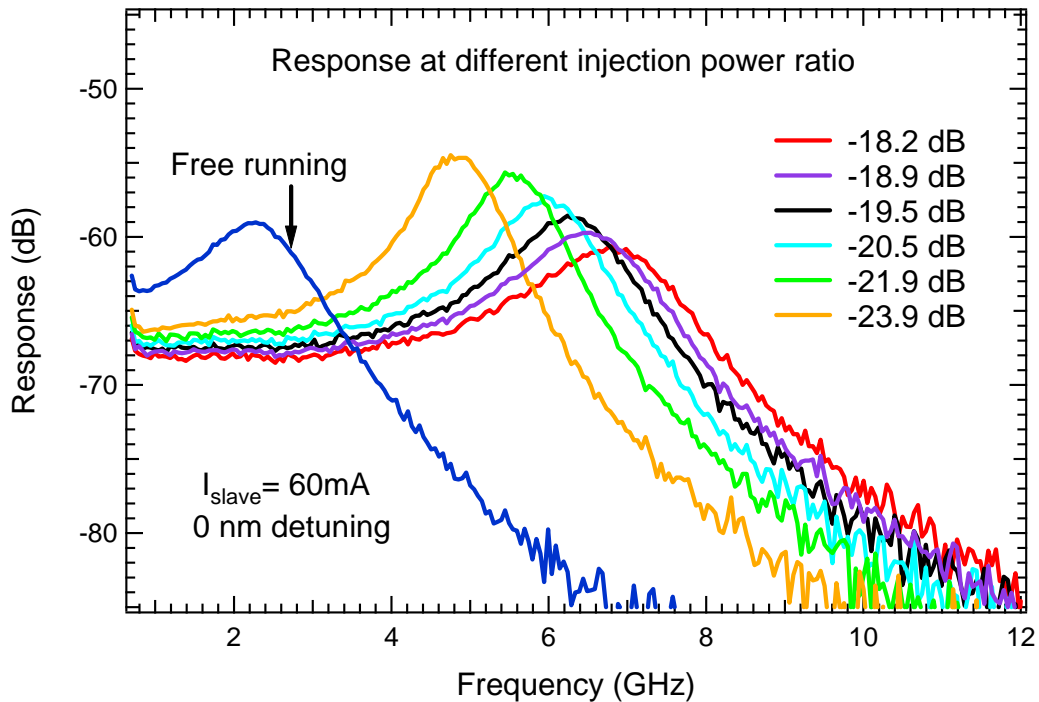
spectral range.

Fig. 4.6. The modulation responses of the injection-locked laser at different injection
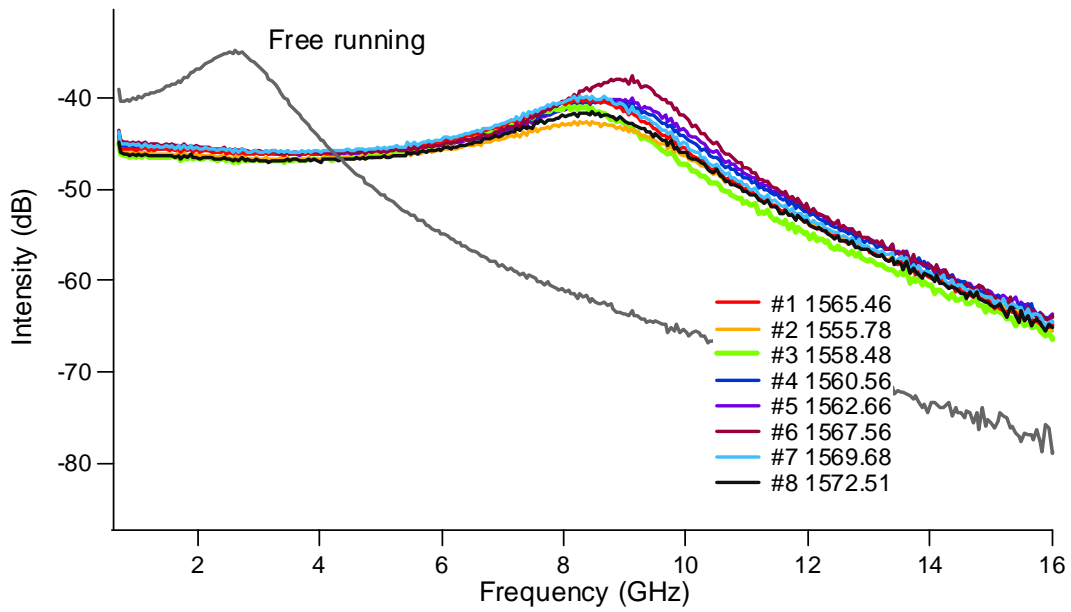power levels.
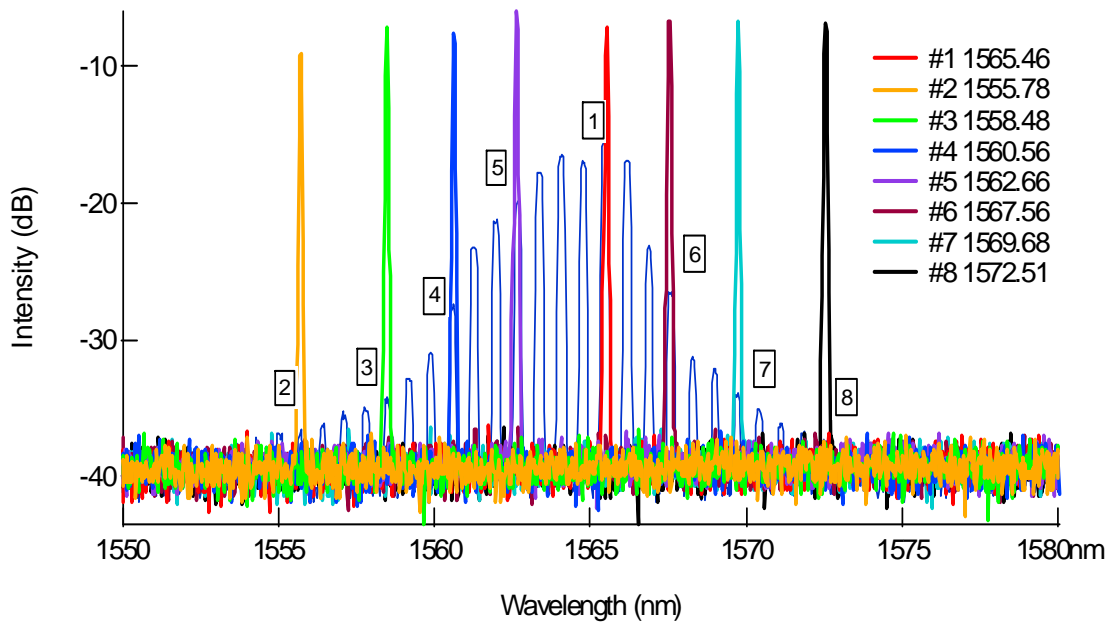
Fig. 4.7. The spectra of the free-running QDash Fabry-Perot and injection-locked laser (upper), with the corresponding modulation responses of the injection-locked laser locked at different side modes (lower).

The modulation enhancement can be achieved by wavelength (or frequency) detuning. The variation of the modulation responses with different detuning are shown in Fig. 4.8 with a fixed injected power ratio of -19.5 dB. The 3-dB bandwidth of the free running laser is 3.4 GHz. The maximum bandwidth at -0.02 nm detuning is 8.5 GHz, which is 2.7X larger than the 3-dB bandwidth of the free-running laser. One can see that a larger bandwidth enhancement occurs in the negative detuning regime (The master laser has a shorter wavelength) and the modulation response is more damped on the positive detuning side although there is still a bandwidth increase. The same trend was reported in Ref. [2]. In that paper, the modulation enhancement for the negative detuning case is simulated numerically by a derived response function, however it is hard to get a clear physical understanding out of this numerical simulation. In the next section, the response of injection locking laser will be re-investigated using the response function of gain-lever lasers and a more physical explanation will be given. It should be noticed that in separate experiments done on same device [13], the injection locking map was drawn in terms of power injection ration and detuning. The device shown in Fig 4.8 was operated at period 1, non-linear regime based on the power injection ratio and detuning condition.
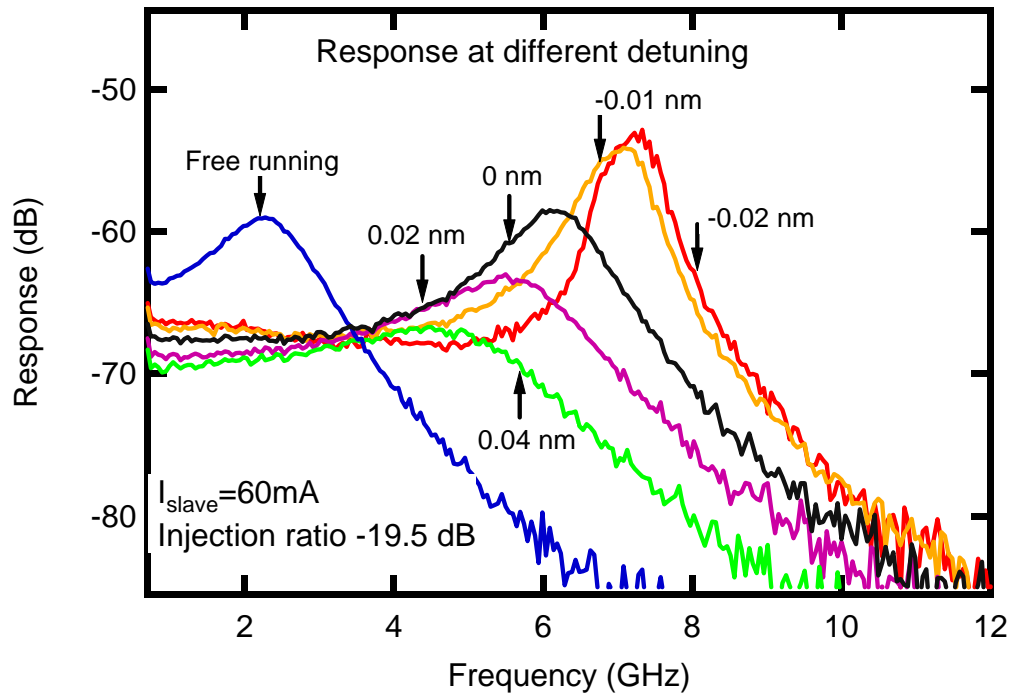
Fig. 4.8 Modulation responses of the free-running FP laser and the injection-locked laser under different detuning conditions

4.5 Injection-locking and the gain-lever

C.-H. Chang *et. al.* introduced a general notation for the relative modulation response function of an injection-locked laser [2]:

$$|H(\omega)|^2 = |A|^2 \frac{\left(\omega^2 + p_0^2\right)}{\left(q_0 - q_2\omega^2\right)^2 + \left(q_1\omega - \omega^3\right)^2} \qquad (4.1)$$

The coefficients are given as:

$$p_0 = k_c \sqrt{\frac{S_{inj}}{S_0}} \left(\cos\phi - \alpha\sin\phi\right) \qquad (4.2a)$$

$$q_2 = a_N S_0 + \frac{1}{\tau_n} - \left(g - \frac{1}{\tau_p} - a_S S_0\right) \qquad (4.2b)$$

$$q_1 = a_N S_0 (a_S S_0 - g) - k_c^2 \frac{S_{inj}}{S_0} - \left(g - \frac{1}{\tau_p} - a_S S_0\right)\left(a_N S_0 + \frac{1}{\tau_n} + k_c\sqrt{\frac{S_{inj}}{S_0}}\cos\phi\right) \quad (4.2c)$$

$$q_0 = -k_c a_N \sqrt{S_{inj} S_0} (a_S S_0 - g)(-\alpha\sin\phi + \cos\phi)$$
$$-\left[\left(g - \frac{1}{\tau_p} - a_S S_0\right)k_c\sqrt{\frac{S_{inj}}{S_0}}\cos\phi + k_c^2 \frac{S_{inj}}{S_0}\right]\left(a_N S_0 + \frac{1}{\tau_n}\right) \qquad (4.2d)$$

Where S_{inj} and S_0 are the photon density of the injected light and free-running laser respectively, τ_p is the photon lifetime, τ_n is the carrier lifetime, g is the optical gain of the locked laser, a_N is the differential gain, a_s accounts for gain compression effects and α is the linewidth enhancement factor. $k_c = \frac{c}{2n_g L}$ is the coupling coefficient and, where c

is the speed of light in vacuum, n_g is the group index and L is the cavity length of the slave laser. ϕ is the phase offset between the master and slave and can be related to frequency detuning, $\Delta\omega$, as:

$$\phi = -\sin^{-1}\left(\frac{\Delta\omega}{k_c\sqrt{1+\alpha^2}\sqrt{S_{inj}/S_0}}\right) - \tan^{-1}\alpha \qquad (4.3)$$

The expressions in Eqn (4.2) are very complicated and it is not easy to get the clear relationship between the various parameters. Some simplification should be done before further investigation. The damping rate of the slave laser is

$$\gamma_{fr} = \frac{1}{\tau_n} + a_N S_0 = \frac{1}{\tau_n} + \omega_r^2\tau_p \qquad (4.4a)$$

Where ω_r is angular relaxation frequency of the slave laser and $\omega_r = 2\pi f_r$. Under the high photon density approximation, the stimulated damping term is dominant as discussed in chapter 3, and the γ_{fr} can be expressed as:

$$\gamma_{fr} \approx a_N S_0 = \omega_r^2\tau_p \qquad (4.4b)$$

From the rate equation in Ref [2], the following relationship can be derived assuming the gain compression effect is negligible:

$$\gamma_{th} = -\left(g - \frac{1}{\tau_p}\right) = 2k_c\sqrt{\frac{S_{inj}}{S_0}}\cos\phi = 2\eta\cos\phi \qquad (4.5)$$

If we define γ_{inj} as a injection rate and let it equal p_0, then substitute Eqn (4.4)-(4.5) into Eqn (4.2), we obtain:

$$p_0 = \gamma_{inj} \qquad (4.6a)$$

$$q_2 = \gamma_{fr} + \gamma_{th} \qquad\qquad (4.6b)$$

$$q_1 = \omega_r^2 + \gamma_{fr}\gamma_{th} + \left(\frac{\gamma_{th}^2}{2} - \eta^2 \right) \qquad\qquad (4.6c)$$

$$q_0 = \frac{\gamma_{fr}\gamma_{inj}}{\tau_p} + \gamma_{fr}\left(\frac{\gamma_{th}^2}{2} - \eta^2 \right) \qquad\qquad (4.6d)$$

The γ_{inj} and γ_{th} are purely functions of power injection ratio and detuning, which depend on the master laser only. The f_r, τ_p and γ_{fr} are the characteristic parameters of the slave laser only, their values can be extracted from the response of the slave laser under the free-running condition or calculated using the single section response function Eqn (3.1) in chapter 3, f_r = 2.5 GHz , τ_p = 5 ps and γ_{fr} = 8 GHz can be obtained by curve fitting. Now we can use Eqn (4.1) to curve-fit the experimental data in Fig. (4.8) according to the coefficients in Eqn (4.6). The f_r, τ_p and γ_{fr} should be fixed during curve fitting since they are free-running parameters of the slave lasers and not affected by external injection. The critical parameters obtained by curve fitting are listed in Table 4.1

Substituting the data in Table 4.1 into Eqn (4.6c) and (4.6d), it was found that the last term parenthesis are much smaller than the rest of the terms in the equations. The ratios of the last term to the other terms in both Eqn (4.6c) and Eqn (4.6d) are listed in Table 4.1 too. It is clear that the last term can be neglected in two equations and q_1, q_0 can be simplified to :

$$q_1 = \omega_r^2 + \gamma_{fr}\gamma_{th} \qquad\qquad (4.7a)$$

$$q_0 = \frac{\gamma_{fr}\gamma_{inj}}{\tau_p} \qquad\qquad (4.7b)$$

Table 4.1 The curve fitting results for response curves at different detuning using Eqn (4.6) and Eqn (4.1).

Detuning （nm）	γ_{inj} (GHz)	γ_{th} (GHz)	η (GHz)	Ratio in q_1	Ratio in q_0
-0.02	57.84	41.28	29.22	0.0031	0.00014
-0.01	50.30	39.8	28.1	0.0043	0.002
0	40.53	38.1	24.98	0.006	0.0003
0.01	26.39	35.66	25.03	0.017	0.0015
0.02	19.48	33.81	24.68	0.020	0.0024
0.03	14.63	32.42	22.73	0.017	0.0027
0.04	12.15	31.12	21.84	0.014	0.0032

Using simplified coefficients in Eqn (4.6) and Eqn (4.7), the response equation Eqn (4.1) can be re-written as:

$$|H(\omega)|^2 = \frac{\left(\dfrac{\gamma_{fr}}{\tau_p}\right)^2 \left[\omega^2 + \gamma_{inj}^2\right]}{\left[\dfrac{\gamma_{fr}\gamma_{inj}}{\tau_p} - (\gamma_a + \gamma_{th})\omega^2\right]^2 + \left[\left\{\omega_r^2 + \gamma_a\gamma_{th}\right\}\omega - \omega^3\right]^2} \qquad (4.8)$$

In chapter 3, the response function of the gain-level laser was derived under high photon density approximation [12], which is:

$$|R(\omega)|^2 = \frac{\left(\dfrac{\gamma_a}{\tau_p}\right)^2 \left[\omega^2 + \gamma_b^2\right]}{\left[\dfrac{\gamma_a\gamma_b}{\tau_p} - (\gamma_a + \gamma_b)\omega^2\right]^2 + \left[\left\{\omega_r^2 + \gamma_a\gamma_b\right\}\omega - \omega^3\right]^2} \qquad (4.9)$$

It can be seen that Eqn (4.8) and (4.9) have similar forms because both of them are used to describe the coupled oscillator system. The injection locking system can be described by gain-lever equation under the approximation that $\gamma_b \approx \gamma_{th}$. Finally, the coefficients correspondence between Eqn (4.1) and (4.9) are listed below.

$$
\begin{aligned}
p_0 &\Leftrightarrow \gamma_b \\[4pt]
q_0 &\Leftrightarrow \frac{\gamma_a\gamma_b}{\tau_p} \\[4pt]
q_1 &\Leftrightarrow \omega_r^2 + \gamma_a\gamma_b \\[4pt]
q_2 &\Leftrightarrow \gamma_a + \gamma_b \\[4pt]
|A| &\Leftrightarrow \frac{q_0}{p_0} = \frac{\gamma_a}{\tau_p}
\end{aligned}
\qquad (4.10)
$$

The first important correspondence is $p_0 \Leftrightarrow \gamma_b$, it is understandable because p_0 is purely induced by the master or control laser and γ_b is the parameter that describes the control section in the gain-lever, especially under strongly asymmetric pumping. P_0 can be thought of as the damping rate of the master laser.

4.4.2 Bandwidth enhancement explanation using gain-lever equation

We replace notation γ_b and γ_a in Eqn. (4.9) with γ_{inj} and γ_{fr} to indicate that they are effectively applied to the injection-locking scheme. Eqn (4.9) can then be re-written in terms of the frequency as following:

$$|R(f)|^2 = \frac{\left(\frac{\gamma_{fr}\gamma_{inj}}{8\pi^3\tau_p}\right)^2\left(1+\left(\frac{2\pi f}{\gamma_{inj}}\right)^2\right)}{\left[\frac{\gamma_{fr}\gamma_{inj}}{8\pi^3\tau_p} - \frac{(\gamma_{fr}+\gamma_{inj})}{2\pi}f^2\right]^2 + \left[\left(f_r^2 + \frac{\gamma_{fr}\gamma_{inj}}{4\pi^2}\right)f - f^3\right]^2} \qquad (4.11)$$

The new relaxation frequency of the injection-locked laser is approximately:

$$f_r = \frac{1}{2\pi}\sqrt{\frac{1}{\tau_p}\frac{\gamma_{fr}\gamma_{inj}}{(\gamma_{fr}+\gamma_{inj})}} \qquad (4.12)$$

Consequently, the relaxation frequency of the injection-locked laser is the geometric mean of the photon lifetime and the parallel sum of the master and slave damping rates. Since f_r does not change at a fixed slave bias, any enhancement in the relaxation frequency is dominated by γ_{inj}. At a certain power injection ratio, the variation of γ_{inj} can only be from detuning. The simulated modulation responses are plotted in Fig 4.9. The γ_{inj} increases from 20 GHz to 120 GHz, and the other coefficient are determined from experimental and curve fitting data. It can be seen that the simulated response curves are similar with experimental data with different wavelength detuning. The relaxation peak as well as the 3-dB bandwidth increase with γ_{inj}.

Using Eqn. (4.9), the actual value of the γ_{inj} can be extracted from the experimental data in Fig 4.8 and plotted in Fig. 4.10 as function of the detuning. As the detuning varies from 40 pm to -20 pm, γ_{inj} increases from 20 GHz to 160 GHz as expected.

From Eqn (4.12), the validation of gain-lever model Eqn (4.9) to simulate period 1, non-linear regime can be examined. As above mentioned, Eqn (4.9) is derived under the

high photon density approximation. At low photon density case, the two damping rate are dominated by carrier lifetime and relatively equal to each other according to Eqn (3.12), f_r is close to a constant in Eqn (4.12) and there will no bandwidth variation. The gain-lever model can not be applied. To enhance to bandwidth, first, the damping rate should be dominated by the stimulated lifetime, which can be achieved in the high photon density operation situation; second, γ_{inj} should be significantly different from γ_{fr}, i.e. $\gamma_{inj} \gg \gamma_{fr}$. (In gain-lever device, this condition requires the gain-section has higher differential gain, which is contrary to the normal gain-lever configuration, so it is called the inverted gain-lever.).

An interesting question is what is the maximum relaxation frequency and bandwidth that can be achieved at a fixed injection power level? From Eqn (4.8), the maximum relaxation frequency can be expressed under the assumption that γ_{inj} is much larger than γ_{fr}:

$$f_{fr\_max} = \frac{1}{2\pi}\sqrt{\frac{\gamma_{fr}}{\tau_p}}$$
(4.9)

Also, Eqn (4.1) can be solved to find the expression for the 3-dB bandwidth, and then assuming that $\gamma_{inj} \gg \gamma_{fr}$, the maximum achievable 3-dB bandwidth is approximately:

$$f_{3dB\_max} = \frac{1}{2\pi}\sqrt{\left(1+\sqrt{2}\right)\frac{\gamma_{fr}}{\tau_p}}$$
(4.10)

And we find the classic relationship between relaxation frequency and 3-dB bandwidth here: $f_{3dB\_max} = 1.55 f_{fr\_max}$.

The γ_{fr} and τ_p are measured and calculated as 8 GHz and 5 ps respectively from the

experimental data shown in Fig 4.8. These values lead to a predicted f_{3dBmax} of 10 GHz, which compares favorably to the measured value of 8.5 GHz at -20 pm detuning at which γ_{inj} is much larger than γ_{fr} To the best of our knowledge, this is the first time the maximum bandwidth has been predicted for injection-locked semiconductor lasers.
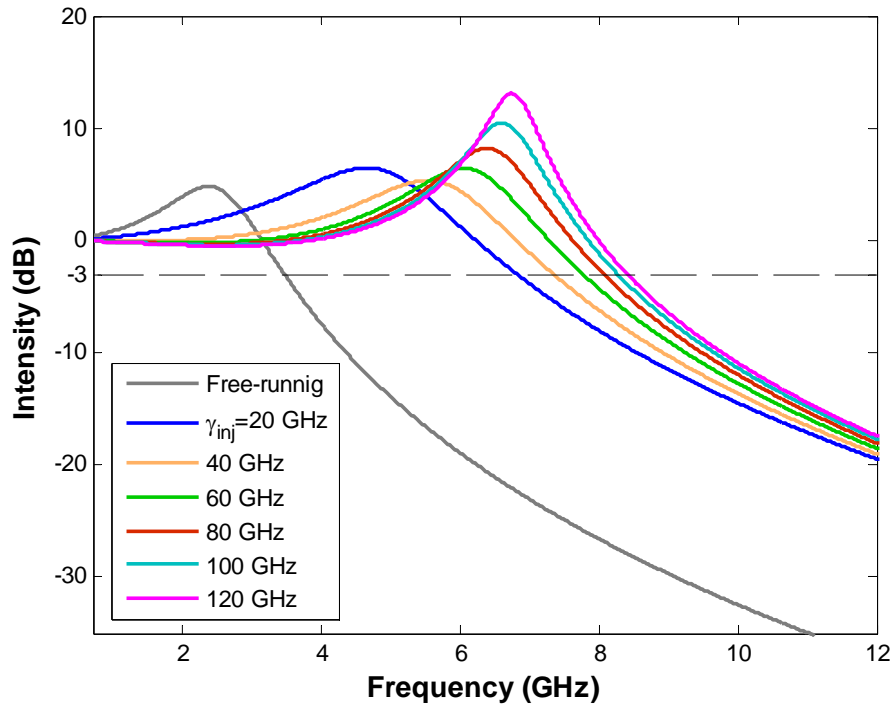

Fig 4.9 Simulated modulation responses of injection-locked lasers using Eqn (4.1), the bandwidth incrased with γ_{inj}
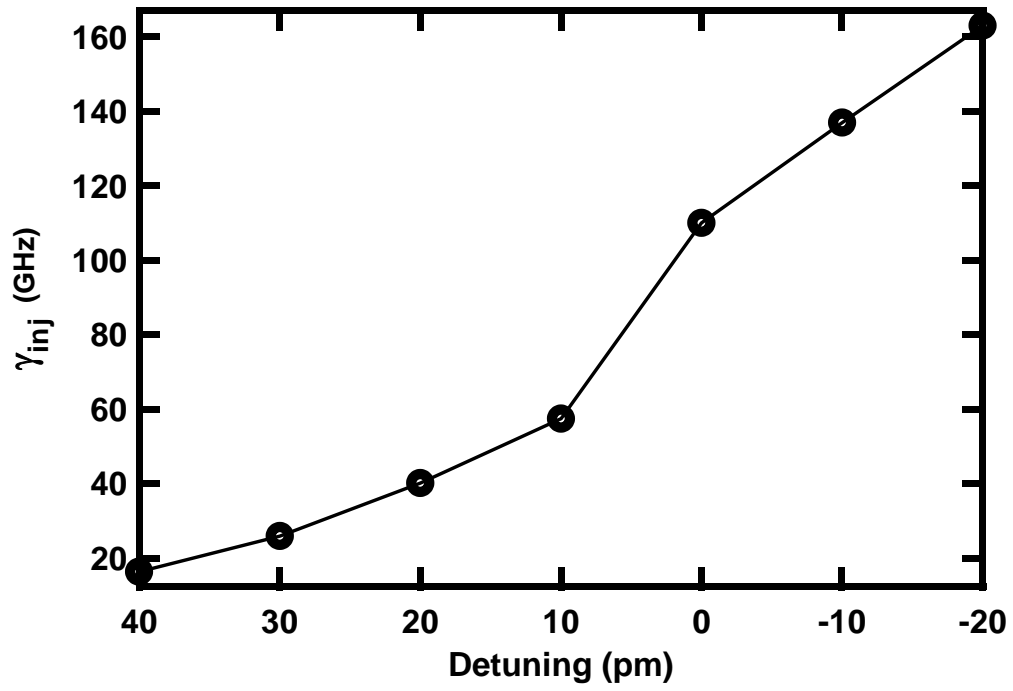
Fig. 4.10 Variation of γ_{inj} as function of detuning

4.6 Summary

The modulation characteristics of injection-locked QDash F-P laser was studied theoretically and experimentally. The 3-dB bandwidth enhancement was demonstrated under different injection power ratio and frequency detuning. A maximum 3-dB (f_{3dB_max}) bandwidth of 8.7 GHz was achieved at an injection ratio of -18.2 dB, and $f_{3dB\_max} = 11.2$ GHz was demonstrated at a higher power injection ratio of -11.9 dB, which is 4 times of the bandwidth of the free-running laser. By comparing the modulation responses of the injection-locked side mode of the F-P laser, it is found that the side mode locking variation has no significant impact on modulation response. A new equation to describe the modulation response of injection-locked laser is established, which is inspired from the gain lever model. An analytical expression of relaxation frequency is derived, and the maximum achievable 3-dB bandwidth at a fixed power level is predicted for the first time.

References

[1]. T. B. Simpson, J. M. Liu, and A. Gavrielides, "Bandwidth enhancement and broadband noise reduction in injection-locked semiconductor lasers," *IEEE Photon. Technol. Lett.*, vol. 7, no. 7, pp. 709-711, 1995.

[2]. C.-H. Chang, L. Chrostowski, and C. J. Chang-Hasnain, "Injection locking of VCSELs," *IEEE J. Sel. Topics Quantum Electron.*, vol. 9, no. 5, pp. 1386-93, 2003.

[3]. X.-M. Jin, S.-L. Chuang, "Bandwidth enhancement of Fabry-Perot quantum-well lasers by injection-locking", *Solid-State Electronics*, vol. 50 pp. 1141–1149, 2006

[4]. S. Kobayashi, S. Kimura, "Injection locking characteristics of an algaas semiconductor-laser", *IEEE Journal of Quantum Electronics*, vol. 16, no. 9, pp. 915-917, 1980

[5]. C. H. Henry, N. A. Olsson, and N. K. Dutta, "Locking Range and Stability of Injection Locked 1.54 um InGaAsP Semiconductor Lasers," *IEEE Journal of Quantum Electronics*, vol. QE-21, pp. 1152-1156, 1985.

[6]. C. Lin, J. K. Andersen, and F. Mengel, "Frequency chirp reduction in a 2.2 Gbit/s directly modulated InGaAsP semiconductor laser by CW injection," *Electron. Lett.*, vol. 21, no. 2, pp. 80-81, 1985.

[7]. X. J. Meng, T. Chau, and M. C. Wu, "Improved intrinsic dynamic distortions in directly modulated semiconductor lasers by optical injection locking," *IEEE Trans. Microw. Theory Tech.*, vol. 47, no. 7, pp. 1172-1176, 1999..

[8]. Hwang SK, Liu JM, White JK. "35-GHz intrinsic bandwidth for direct modulation in 1.3-mu m semiconductor lasers subject to strong injection locking", *IEEE Photon. Technol. Lett.*, vol. 16, no. 4, pp. 972-974, 2004

[9]. L. Chrostowski, X. Zhao, C. J. Chang-Hasnain, R. Shau, M. Ortsiefer, and M.-C. Amann, "50-GHz Optically Injection-Locked 1.55-_m VCSELs", *IEEE Photon. Technol. Lett.*, vol. 18, no. 2, pp. 367-369, 2006

[10]. X.-M. Jin, S.-L. Chuang, "Bandwidth enhancement of Fabry-Perot quantum-well lasers by injection-locking", *Solid-State Electronics*, vol. 50 pp. 1141–1149, 2006

[11]. R.-H Wang, A. Stintz, P. M. Varangis, T. C. Newell, H. Li, K. J. Malloy, L. F. Lester, "Room-temperature operation of InAs quantum-dash lasers on InP (001)", *IEEE Photon. Technol. Lett.* vol. 13, no. 8, pp. 767-769, 2001.

[12]. N. Moore, K. Y. Lau, Ultrahigh efficiency Microwave signal transmission using tandem-contact single quantum well GaAlAs lasers, *Applied Physics Letters*, vol.55, no.10, p.936-938, 1989.

[13]. A. Moscho, "Injection Locking Characteristics of Indium Arsenide Quantum Dash Lasers", Master Thesis, p 50, University of New Mexico, 2007.

Chapter 5   Conclusion and future work

5.1 Summary

In this work, the techniques for improving the high frequency modulation characteristics of quantum dot lasers were studied, including the p-doping technique in single-section QD lasers, the gain-lever effect in two-section lasers and the injection-locking method.

Firstly, the static performance and modulation frequency response of un-doped and p-doped InAs/GaAs QD lasers was studied. Contrary to the theoretical predictions, the modulation efficiency and the highest relaxation frequency of 1.2-mm cavity length lasers decrease monotonically with the p-doping level from 0.54 GHz/mA$^{1/2}$ and 5.3 GHz (un-doped wafer), 0.46 GHz/mA$^{1/2}$ and 3.6 GHz (40 holes/dot). The degradation of the modulation performance of the p-doped device is attributed to the higher gain saturation factor due to carrier heating effect. The internal loss increases with p-doping concentration from 7.5 cm^{-1} for the 20 holes/dot wafer to 10 cm^{-1} for 40 holes/dot wafer, which are much larger than the value of 2 cm^{-1} for un-doped lasers. Based on the curve-fitting procedure, the saturation power is found to decrease with the p-type level from 90 mW (un-doped) to 18.4 mW (40 holes/dot). Although the maximum ground state gain of p-doped laser is larger than that of un-doped lasers and increases with p-doping level, the undesired increased in internal losses induces gain saturation with carrier

density and gain compression. thus degrading the high-speed performance of p-doped QD lasers.

Secondly, the gain-lever effect was studied in two-section QD lasers to increase the modulation efficiency and bandwidth. An 8 dB modulation efficiency enhancement was achieved using the p-doped QD laser. Due to the stronger gain saturation with carrier density, the un-doped device shows a larger gain-lever effect over the p-doped devices. A 20 dB enhancement in the modulation efficiency is demonstrated by the un-doped QD laser. A new relative response equation is derived under the high photon density approximation. A 1.7X 3-dB bandwidth improvement is theoretically predicted by the new model and realized in the un-doped QD gain-lever laser under extreme asymmetrically biased condition. It is also demonstrated for the first time that in the gain-lever laser, the 3-dB bandwidth can be 3X higher than relaxation frequency instead of 1.55X in typical single-section lasers.

Finally, the injection-locked laser was realized in QDash lasers for the first time. By varying the power injection ratio and detuning, the modulation bandwidth of the slave laser was increased. The 4X bandwidth improvement was demonstrated in a injection-locked 0.5-mm long QDash F-P laser. By analyzing the curve fitted data, it was found that gain-lever equation can be used to describe the injection-locking system in the period 1, non-linear regime. Not only the complexity of response equation of the injection-locked laser is reduced, but also the physical meaning of coefficients in the equation is given clearly. Based on the gain-lever model, an analytical expression of the

relaxation frequency of a injection-locked laser is derived, and the maximum achievable 3-dB bandwidth at a certain power level is predicted for the first time.

5.2 Suggestions for future work

The p-doping technique is predicted as a promising way to enhance the bandwidth of high-speed QD lasers. But the theoretical model did not account the side effect of adding extra dopant, which will introduce the carrier heating effect due to increased internal loss. The results obtained in this work shows the carrier heating effect can severly degrade the modulation performance of QD laser because the QDs have smaller saturation power. More complete theoretical work needs to be developed to include the carrier heating effect. Since in this work, p-doped QDs with a doping level varies from 20-40 holes/dot were examined. These doping level are relative high. To balance the effect of high internal loss, from the experiment side, it is suggested that studying the QD materials with doping level from 5-20 holes/dot would be approprite.

The gain-lever laser provides a useful tools to enhance the modulation efficiency and bandwidth. In this work, we neglect the effect form non-linear gain compression. The full expression for damping rate should be:

$$\gamma = \frac{1}{\tau_c} + \left(G_0' + \frac{\varepsilon}{\tau_p} \right) P_0 \qquad (5.1)$$

Under extreme asymmetrically bias condition, the gain compression terms in the gain

section could have a significant impact on the damping rate of two sections. The gain-lever effect may disappear due to large non-linear gain compression. We already observed that the gain-lever effect becomes weaker at very high power level. We are trying to develop the new response model which includes the non-linear gain term. Also, the studies on the FM modulation response of inverted gain lever QD laser can be launched in the future and higher FM modulation efficiency enhancement is expected.

In Fig 5.1, an improved version of the setup for injection-locking QD laser is shown. Compared to the one used in this work, the isolators are replaced by polarization maintained (PM) circulator. The PM fiber is used in the optical path between the master and slave laser. Therefore, the polarization status can be well-controlled in this setup and the insertion loss is reduced too. We have already obtained much higher power injection ratio based on this setup. The single-mode DFB laser is expected to be used as the slave laser in the next experimental step. Not only does the lager bandwidth of DFB lasers help to push the bandwidth of injection-locked laser even further, but also the better correlation between injection-locked lasers and gain-lever lasers is expected since our gain-lever model is actually derived based on single-mode operation condition. The improved simulation model are on their way to be developed.
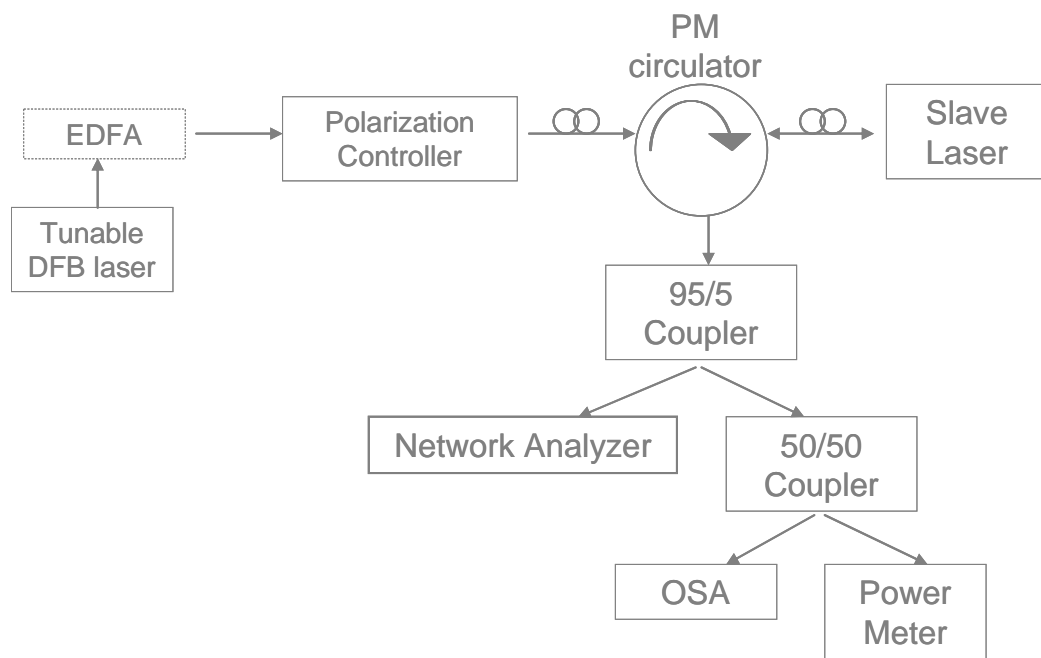
Fig 5.1 The experimental setup for injection-locked QD lasers. The polarization status is carefully controlled. .